

NOSC

NOSC TR 565

NOSC TR 565

Technical Report 565

HIGH-PRESSURE VIEWPORTS FOR INFRARED SYSTEMS

Phase 1 — Germanium

Jerry D. Stachiw

September 1980

Final Report for Period
October 1979 — September 1980

Prepared for
Naval Material Command
Director of Naval Laboratories
Washington, DC 20360

Under NOSC IR/IED Technical Project F61512

Approved for public release; distribution unlimited.

NAVAL OCEAN SYSTEMS CENTER
SAN DIEGO, CALIFORNIA 92152

NAVAL LIBRARY (DAYSIDE)
NAVAL OCEAN SYSTEMS CENTER
SAN DIEGO, CA 92152

10947
Be1



NAVAL OCEAN SYSTEMS CENTER, SAN DIEGO, CA 92152

A N A C T I V I T Y O F T H E N A V A L M A T E R I A L C O M M A N D

SL GUILLE, CAPT, USN

Commander

HL BLOOD

Technical Director

ADMINISTRATIVE INFORMATION

Work was performed under direction of the Naval Material Command, Director of Naval Laboratories, as part of NOSC IR/IED technical project F61512 by members of the Ocean Technology Department. This report covers work from October 1979 to September 1980.

CONTENTS

PROBLEM . . .	page 1
RESULTS . . .	1
RECOMMENDATION . . .	1
INTRODUCTION . . .	3
BACKGROUND DISCUSSION . . .	4
Atmospheric Transmission . . .	4
Thermal Imagers . . .	4
Thermal Imagers in Marine Environment . . .	11
MATERIALS CONSIDERATIONS FOR IR WINDOWS . . .	12
Materials . . .	12
Germanium . . .	15
Coatings . . .	20
Prevention of Ice Formation . . .	29
Window Design Considerations . . .	31
STUDY PLAN . . .	35
VIEWPORT DESIGN . . .	35
Viewport Components . . .	35
Mechanical Properties of Germanium . . .	36
FABRICATION PROCESS . . .	47
Windows . . .	47
Mounting . . .	52
Gaskets . . .	52
Test Specimens . . .	58
EXPERIMENTAL EVALUATION . . .	58
Windows . . .	58
Material Test Specimens . . .	72
TEST RESULTS . . .	76
Windows . . .	76
Test Specimens . . .	76
DISCUSSION . . .	91
Physical Properties of Germanium . . .	91
Structural Performance of Germanium Windows . . .	107

DESIGN RECOMMENDATIONS . . . 108

- Design Stresses . . . 108
- Window Design . . . 109
- Mountings . . . 109
- Sealing . . . 111

CONCLUSION . . . 111

ILLUSTRATIONS

- 1 Atmospheric transmission of 1000-ft horizontal air path at sea level; 5.7-mm precipitable water, 79°F . . . page 5
- 2 Black body spectral emittance at various temperatures . . . 6
- 3 Basic components of a thermal imager utilizing a single cryogenically cooled photon detector and a dual-axis mechanical scanner . . . 7
- 4 Basic components of a thermal imager utilizing an electrically scanned, mechanically chopped, pyroelectric vidicon . . . 7
- 5 Techniques for dissecting the scene with arrays of discrete detectors . . . 8
- 6 Transmission region of optical materials, 2 mm thick . . . 13
- 7 Typical sizes and shapes of germanium windows and lenses . . . 22
- 8 Conductivity as a function of temperature for single-crystal germanium in the intrinsic range . . . 23
- 9 Thermal conductivity of germanium from 300°K to 1020°K, as determined by the radiant heat flow method; n-type, polycrystalline, with $\rho = 30$ ohm-cm . . . 24
- 10 Transmittance of uncoated and AR-coated (both faces) polycrystalline germanium . . . 25
- 11 Transmittance of AR-coated polycrystalline germanium as a function of temperature . . . 26
- 12 Refractive index as a function of temperature for single-crystal doped n-type germanium. Sample resistivity at 300°K is 1.2 ohm-cm . . . 27
- 13 Standard shapes for pressure-resistant windows . . . 32
- 14 Plane germanium window with plane bearing surface for low-pressure applications (< 100 psig) . . . 33
- 15 Plane germanium window with twin-bevel bearing surfaces for moderate pressure applications (< 1000 psig) . . . 34
- 16 Spherical sector window design for high-pressure applications ($< 20\,000$ psig) . . . 37
- 17 Spherical sector window for 20 000-psi Cervit . . . 38
- 18 Compliant metallic window seat for spherical sectors . . . 39
- 19 Plastic mounting ring which allows the metallic seat to contract radially under pressure . . . 40
- 20 Gaskets for window seat . . . 41
- 21 Axial strains measured along a meridian on the spherical sector window fabricated from Cervit C-101 glass ceramic . . . 42
- 22 Circumferential strains measured on the same window as the axial strains on figure 21 . . . 43
- 23 Germanium test specimens used for determination of its structural properties . . . 45
- 24 Dimensions of test specimens shown in figure 23 . . . 46

ILLUSTRATIONS (Cont'd)

- 25 Germanium blank in the shape of spherical sector produced between matching male and female graphite molds . . . 48
- 26 Closeup of the as-cast surface on the germanium blank . . . 49
- 27 Exterior surface of the germanium sector after grinding and pitch polishing . . . 50
- 28 Interior surface of the germanium sector after grinding and pitch polishing . . . 51
- 29 Components of the spherical sector window assembly . . . 53
- 30 Spherical sector window assembly . . . 54
- 31 Cleaning and inspection of the window's bearing surface prior to bonding of Fairprene 5722A gasket . . . 57
- 32 Application of rubber contact cement to both the window bearing surface and the Fairprene 5722A gasket . . . 60
- 33 Trimming the end of the gasket for a perfect butt joint . . . 61
- 34 Inspecting the joint on the bonded gasket . . . 62
- 35 Placing the gasketed window on the window seat . . . 63
- 36 Centering the gasketed window on the seat . . . 64
- 37 Squeezing the O-ring between the edge of the window and the lip on the window seat . . . 65
- 38 Placing the window retainer on top of the window . . . 66
- 39 Fastening the window retainer to the window seat with screws . . . 67
- 40 Completed window test assembly . . . 68
- 41 Window test assembly attached to a heavy steel bulkhead, which in turn is suspended by a pipe from the pressure vessel end closure . . . 69
- 42 Framework for securing the window test assembly during dynamic pressure testing . . . 71
- 43 Test fixture for applying three-point bending moment to the germanium test specimens . . . 73
- 44 Test fixture for applying compressive load to the germanium test specimens . . . 74
- 45 Test fixture for long-term flexure testing of germanium test specimens . . . 75
- 46 Fairprene 5722A bearing gasket after 100 pressure cycles; 0 to 13 500 psi, 8-hour cycle length . . . 77
- 47 Same gasket as in figure 46 . . . 78
- 48 Composite bearing gasket (Fairprene 5722A bonded to KEVLAR-49 cloth-reinforced epoxy) after 100 pressure cycles; 0 to 20 000 psi, 8-hour cycle length . . . 79
- 49 Same gasket as in figure 48 . . . 80
- 50 Acoustic emissions recorded during pressure cycling of the germanium spherical sector from 0 to 4500 psi . . . 81
- 51 Germanium spherical sector after exposure to dynamic pressure pulse with 2250-psi peak pressure . . . 82
- 52 Closeup of the germanium spherical sector in figure 51 . . . 83
- 53 Spalling of the exterior surface on germanium test cylinders that occurred at approximately 70 percent of the ultimate load . . . 84
- 54 Spalling observed after 24-hour-long application of 61,538-psi compression stress . . . 89
- 55 Typical fracture surface on specimens subjected to short-term flexure loading . . . 90
- 56 Static fatigue life of germanium . . . 93
- 57 Uncoated germanium window prior to immersion in San Diego Bay . . . 99

58a	Uncoated germanium window after 4-month-long submersion in San Diego Bay . . .	100
58b	Closeup of the etched germanium surface . . .	101
59a	Typical monolayer AR coating after 4 months of submersion . . .	103
59b	Closeup of the pitted surface on coated germanium . . .	104
60	Transmittance of solid AMTIR-1 chalcogenide glass; 0.25 inch thick, uncoated . . .	105
61	Transmittance of 0.25-inch-thick germanium window, coated on a single surface with 0.001-inch-thick AMTIR 1 chalcogenide glass . . .	106
62	Compliant mounting design for brittle windows of hyperhemispherical shape . . .	112
63	Hyperhemispherical window in a compliant mounting . . .	113
64	Distribution of stresses on the interior surface of the hyperhemisphere shown in figure 62 under short-term pressurization of 2 000 pounds per square inch (13.7 mPa) at ambient room temperature . . .	114

TABLES

1	Comparison of physical and optical properties of optical-grade germanium and chalcogenide glass . . .	page 15
2	Minerals containing germanium . . .	16
3	Listing of primary germanium producers, zinc smelters, and mine sources . . .	17
4	Production of germanium from byproducts of the zinc ore reduction process . . .	18
5	Typical published physical properties of germanium . . .	19
6	The refractive index of germanium at 27° C . . .	21
7	Resistance of germanium sector windows to underwater explosions . . .	85
8	Mechanical properties of optical-grade polycrystalline germanium (Boule #1.) . . .	86
9	Mechanical properties of optical-grade polycrystalline germanium (Boule #2.) . . .	87
10	Mechanical properties of optical grade polycrystalline germanium (Boule #3.) . . .	88
11	Static fatigue of optical-grade polycrystalline germanium in flexure . . .	92
12	Mechanical strength of optical-grade polycrystalline germanium . . .	94
13	Mechanical strength of optical-grade germanium in various lots . . .	95
14	Effect of temperature on the flexural strength of optical-grade polycrystalline germanium . . .	96
15	Mechanical strength of optical-grade polycrystalline germanium . . .	98

PROBLEM

Infrared imaging and/or tracking systems mounted on undersea vehicles require for their successful operation pressure resistant windows which not only transmit infrared energy when the vehicle surfaces but also protect the electro-optical receiver from incursion of sea water when the vehicle is submerged. This requires the selection of (1) material which is transparent to IR energy, (2) window shape which is resistant to pressure, (3) mounting which holds the window securely in place without generation of stress concentrations, (4) seals that provide a leakproof joint between the mounting and the window, and (5) optical coating which decreases the reflection of IR energy from both surfaces, but at the same time protects the exterior surface from chemical and galvanic corrosion by sea water.

The problem of finding a workable solution to the requirement for a pressure resistant window transparent to IR energy increases in difficulty with the operational depth of the vehicle as the increasing hydrostatic pressure demands an optimized structural design where the distribution and magnitude of stresses in the window are equalized and minimized, respectively.

RESULTS

Germanium spherical sector windows set in compliant mountings have been found to perform satisfactorily in marine environment from above to below the ocean surface. Spherical sector windows with $t/R_1 = 0.333$ and included spherical angle $\alpha = 150^\circ$, when fabricated from optical grade polycrystalline germanium and mounted in Monel K-500 seats on elastomeric gaskets, have withstood without fracturing static pressurizations in the 0-to-20 000-psi and dynamic impulses in the 0-to-1000-psi range.

Although seawater corrosion decreases the effective transmission of IR energy through germanium windows to zero in less than 3000 hours, special coatings have been either discovered or developed which, when applied to the window, guarantee transmission in excess of 70 percent even after 6000 hours of continuous or intermittent submersion in sea water.

The two coatings which provide the germanium windows with long term protection against sea water corrosion are (1) a soft, thick chalcogenide glass coating and (2) a thin, hard, multilayer antireflective coating. The transmission through a germanium window coated on both faces with the thin, hard AR multilayer coating is in the 90-to-95-percent range, while the transmission through a window coated on the inner face with a hard monolayer AR coating and on the outside with the protective chalcogenide coating is in the 70-to-75-percent range. After submersions of 4000 hours, the transmissions through both windows decreased by only 2 to 5 percent.

RECOMMENDATION

Germanium windows in the shape of spherical sectors whose surfaces are protected by either a hard, multilayer AR coating, or a soft chalcogenide glass coating serve as a cost-effective solution to operational requirements posed by IR electro-optical systems on undersea vehicles.



INTRODUCTION

The sense of vision has served man well in the exploration of land and sea. Electro-optical systems operating in the 0.3-to-0.8- μm wavelength range have augmented the sense of vision by allowing man to view objects at illumination levels which are below the threshold of unaided vision. The same electro-optical systems also extend man's presence to locations which are either inaccessible (eg, surface of remote planet); hazardous (eg, high radiation level); or too small for human occupancy (eg, interior of drone aircraft). Still, these systems are limited by the same environmental parameters that limit unaided human vision. Thus in total darkness, haze, or fog, the man- and electro-optical systems operating in the visual spectrum of light are hindered.

Furthermore, even if sufficient illumination is present and the atmospheric conditions allow good visibility, the information provided to the viewer will be limited. Thus he will be able to discern differences in reflectivity of surfaces (ie, colors and/or shades of gray), and his ability to differentiate between observed objects and background will depend primarily on intensity of illumination and difference in reflectivity of objects and background. Unless the objects are well illuminated and the reflectivity of their surfaces differs sufficiently from the background, they will probably blend with the background and escape detection.

There are, however, approaches for detection and classification of objects at a distance that do not rely on reflection and reflectivity differences of surfaces in the visual spectrum. There are ranging and detection techniques which use high-frequency radio waves (radar) and high-frequency sound waves (sonar). These rely on the reflection and reflectivity differences of surfaces to radio or sound waves. Both of these approaches are active, since the objects to be "viewed" must be first illuminated by either radio or soundwaves of the appropriate frequency. There is a third approach, however, that does not require any illumination for detection and classification of objects because it only processes signals emitted by the objects and converts them into visual images. This approach relies on thermal self-emission and emissivity differences of objects which produce thermal images in the viewing system.

The thermal imaging system relies for its operation on thermal energy patterns generated by all objects whose temperature is above absolute zero. The differences in radiated thermal energy are defined for thermal imaging work in terms of effective scene temperatures rather than in radiometric terms. These effective temperatures represent the contributions made by scene temperature, reflectivity, and emissivity together. Thus the effective temperature at a point can be conceived as that temperature of a black-body radiator which would produce the measured irradiance at that point. Similarly, the irradiance measure through an attenuating atmosphere can be conceived as having been produced by an apparent temperature which is less than the effective temperature of a point on the object.

The differences in effective temperatures of a thermal scene correspond in a large degree to the reflectivity differences in a visual scene and thus allow the transfer of visual concepts to thermally imaged scenes. The mechanical scanning devices which convert thermal radiation to visible radiation in real time for presentation on a television screen are defined as FLIRs (Forward Looking InfraRed).¹ This paper focuses primarily on design considerations and materials for FLIRs operating in a marine environment.

¹ Naval Air Development Center, Report of Action Group JAG-1, State of the Art of Airborne Forward Looking Infrared (FLIR) Technology, vol 1, ed by PM Moser, August 1976.

BACKGROUND DISCUSSION

ATMOSPHERIC TRANSMISSION

The major applications of FLIRs have been, to date, in the military arena where they have been used for target acquisition, fire control, surveillance, intelligence gathering, and navigation.¹ But, as the cost of FLIRs decreases because of mass production for the military, they will become attractive for nonmilitary uses. The nonmilitary applications, just to mention a few, include thermal pollution surveys, forest fire detection and fighting, preventive maintenance, inspection of machinery, crime prevention, aircraft navigation, aircraft landing aids, and air-sea rescue. The reason for the popularity of thermal imaging systems over passive electro-optic imaging devices operating in the visible light spectrum lies in the ability of the thermal imagers to provide superior images over a wider range of atmospheric and illumination conditions. Thus, while image intensifiers and low-light television systems require some illumination and good atmospheric visibility, the thermal imagers will perform equally well during day and night even under very marginal atmospheric visibility conditions (eg, haze and light fog).

There are two processes that affect the passage of thermal radiation through the terrestrial atmosphere (fig 1).² These processes are absorption and scattering by gas molecules, molecular clusters, rain, snow and suspensions such as smoke, fog, haze, and smog.³ The most significant absorbers are water (2.7, 3.2, and 6.3 μm in wavelength), carbon dioxide (2.7, 4.3, and 15 μm), ozone (4.8, 9.6, 14.2 μm), nitrous oxide (4.7, 7.8 μm), and methane (3.2, 7.8 μm). The water and carbon dioxide absorption bands in effect limit the thermal radiation through terrestrial atmosphere to two windows in the 2-to-20- μm spectral range. The two windows available for transmission of radiant energy through terrestrial atmosphere are the 3.5-to-5 and 8-to-14- μm wavelength bands.

There are several reasons why the 8-to-14- μm wavelength window in atmospheric transmission is preferred by FLIR designers over the 3.5-to-5- μm wavelength window. Haze attenuates the 3-to-5- μm band more than the 8-to-12- μm band, the ratio of thermal sensitivity of a system to transmission is higher in this band, and the peaks of radiant energy emitted by objects at ambient terrestrial temperature are centered in this band (fig 2).²

THERMAL IMAGERS

Thermal imagers can be divided into many classes on the basis of detectors, scene dissection procedures, scanning mechanisms, and processing of preamplified detector signals for video presentation. To date, two successful approaches have been developed for converting incoming infrared signals to visual images in thermal imaging systems. The approach yielding the best performance relies on a mechanically scanning discrete photon detector in a technique analogous to television systems (fig 3), while the approach yielding visual images of lesser quality relies upon an electrically scanned pyroelectric vidicon (fig 4).³

There is a basic distinction between scene dissection procedures. This distinction is based on whether the scene is dissected serially or in parallel (fig 5). As fig 5b shows, the parallel scene dissection utilizes an array of discrete detectors oriented perpendicularly to

² Lloyd, JM, Thermal Imaging System, Plenum Press, New York-London, 1975.

³ Infrared Information and Analysis Center, Environmental Research Institute of Michigan, Ann Arbor, The Infrared Handbook, ed by WL Wolfe and GJ Zissis, 1979.

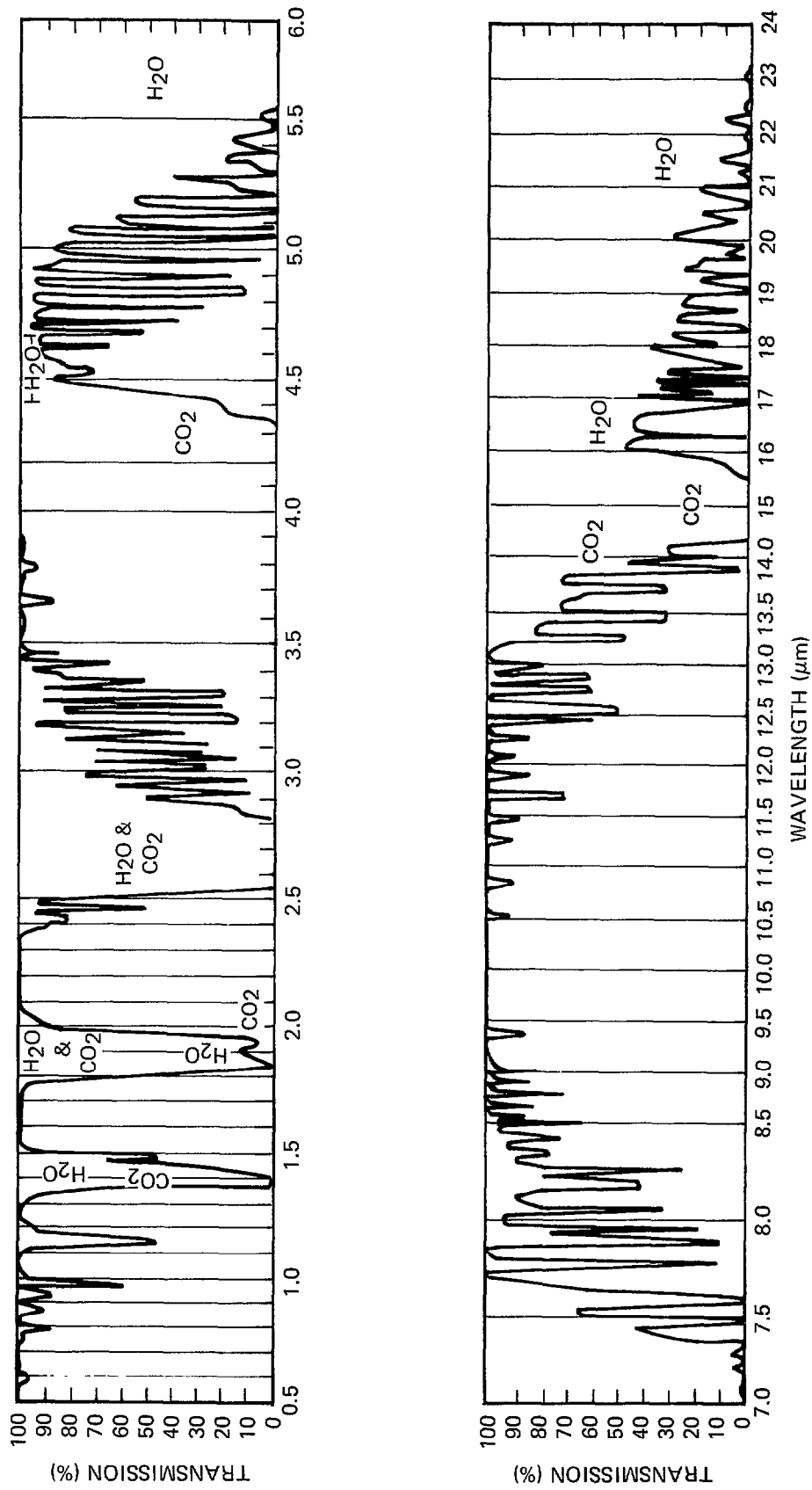


Figure 1. Atmospheric transmission of 1000-ft horizontal air path at sea level; 5.7-mm precipitable water, 79°F.

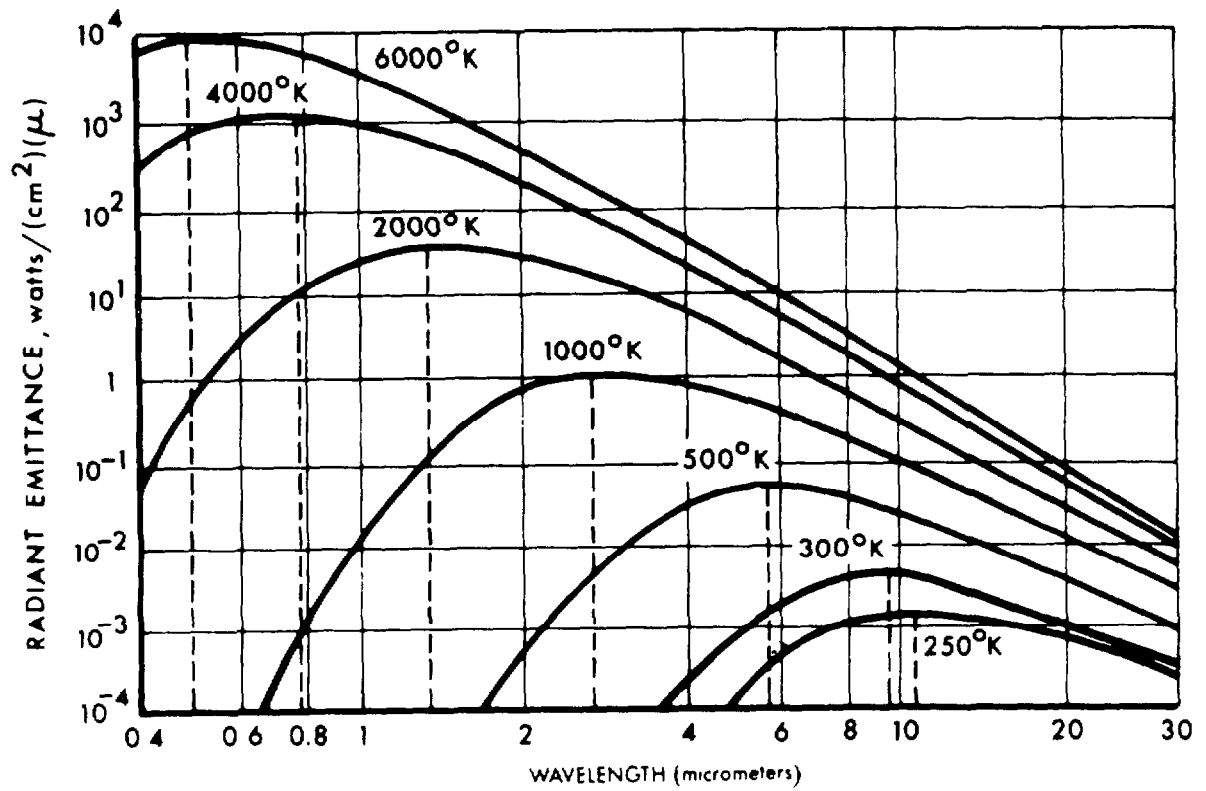


Figure 2. Black body spectral emittance at various temperatures.

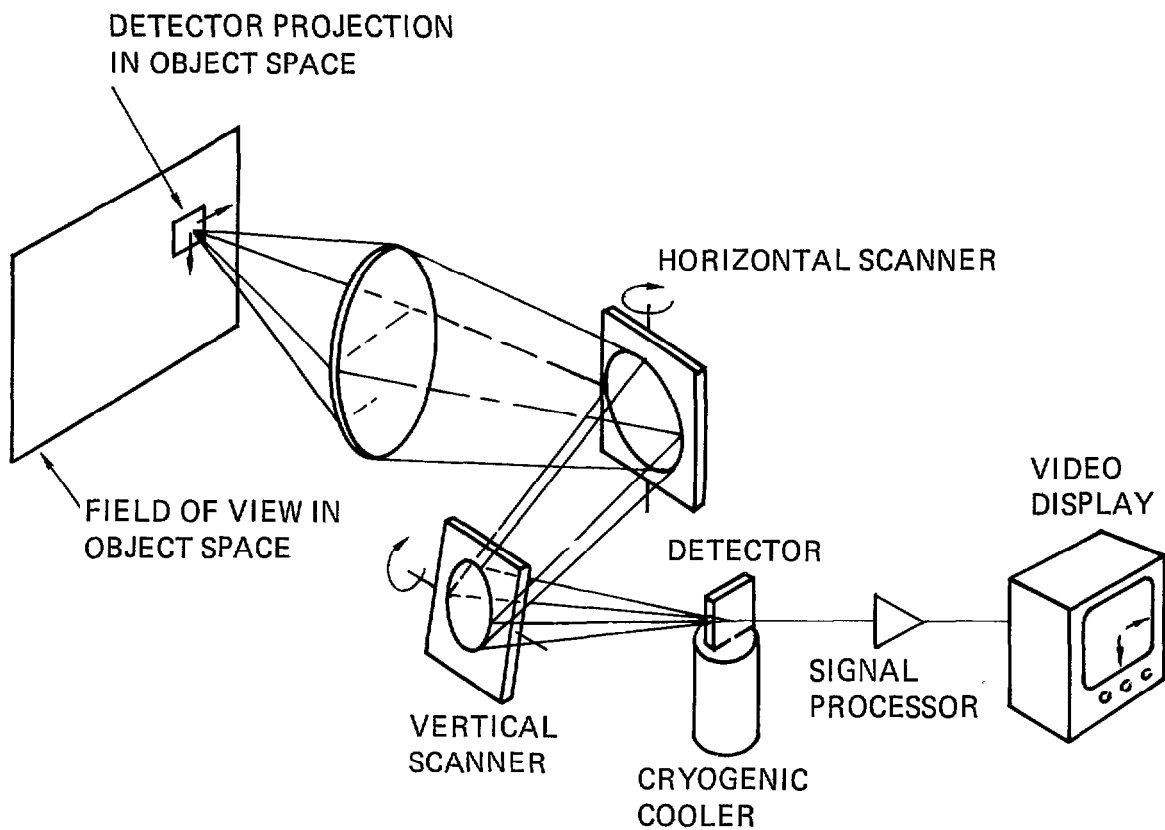


Figure 3. Basic components of a thermal imager utilizing a single cryogenically cooled photon detector and a dual-axis mechanical scanner.

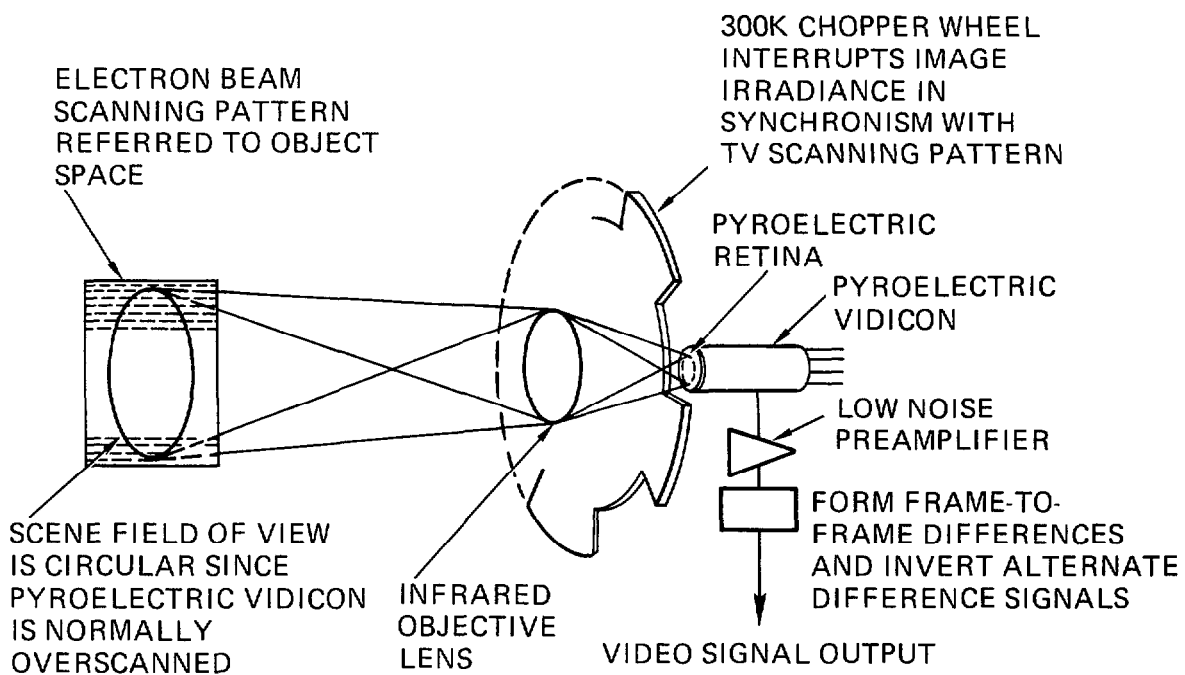
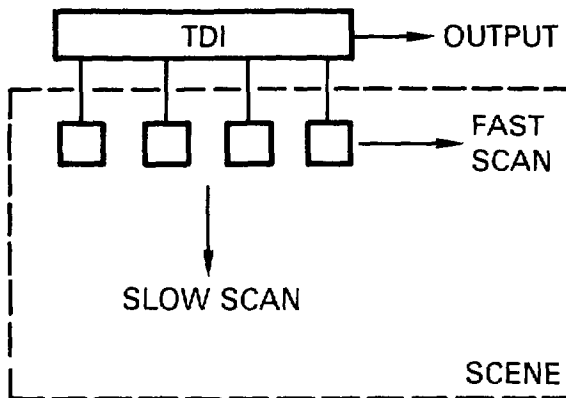
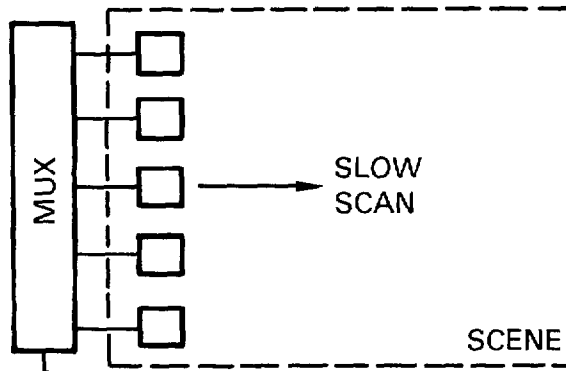


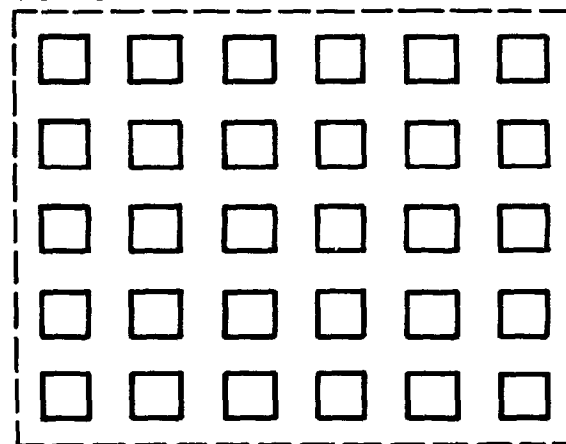
Figure 4. Basic components of a thermal imager utilizing an electrically scanned, mechanically chopped, pyroelectric vidicon.



a. SERIAL SCAN



b. PARALLEL SCAN



c. STARING (NO SCAN) MOSAIC

Figure 5. Techniques for dissecting the scene with arrays of discrete detectors.

the primary scan axis. The resulting electrical signals from each detector are individually amplified, processed, and displayed on a CRT screen simultaneously or in parallel. Serial scene dissection, on the other hand (fig 5a), utilizes an array of detectors oriented in parallel to the primary scan axis which serially scans each point of the thermal image. The resulting electrical signals from each detector are, as a rule, delayed and summed by an electrical integrating delay line.

Although both dissection procedures have their own advantages and disadvantages, the serial scan is considered to be superior to the parallel scan. Its superiority lies in the fact that nonuniformities of individual detectors are eliminated by the integrating delay line which superimposes the outputs of all detectors, thus simulating a single scanning detector. Its disadvantage lies in the fact that it requires rather complex optics. The major advantage of parallel scanning is that the optics are much less complex because it utilizes a sensor where the detector and the display are scanning off the same mirror. The major disadvantage of parallel scanning lies in variations of individually processed signals from each detector.

The mechanical scanning mechanisms for FLIRs vary from one design to another, depending on the scene dissection procedure used, type of application, cost ceiling, space limitations, etc. The most common ones utilize an oscillating plane mirror, rotating polygonal mirror, rotating reflective carousel, rotating refractive prism, revolving lenses, rotating V-mirror, or other means. The rotation, or oscillation, of these mechanical components must be accomplished at high velocities to scan the whole scene and generate a picture of TV quality on the picture tube. One obvious technique for elimination of these costly and complex mechanical scanning mechanisms would be to place in the focal plane a mosaic array of detectors covering the whole field of view (fig 5c). The signals from all detectors would be individually amplified and displayed on the picture tube. This approach, in principle, promises to eliminate complex mechanisms and, as a result, lower the cost, reduce mechanical failures, and increase optical performance. It has, to date, failed to achieve these objectives. Future advances in detector technology may, however, drastically revise the current position of staring (nonscanned) mosaic detector arrays.

So far, the discussion has only covered those FLIRs which use discrete, solid-state photon detectors and are operated at cryogenic temperatures, since these are the detectors that to date have provided military FLIRs with resolution capabilities of ≤ 0.0002 radian at $\leq 0.2^\circ\text{C}$. These detectors are cooled to cryogenic temperature to reduce thermally generated background noise to acceptable levels so that the electrical signals generated in the detectors represent a suitable signal-to-noise ratio.

Although the optical performance of the cryogenically cooled, mechanically scanned, solid-state photon detectors is excellent, there is a strong desire to eliminate the costly and failure-prone cryogenic coolers and mechanical scanners in FLIRs. This is feasible with a class of detectors that change their electrical characteristics (eg, resistance, magnetic orientation, or potential) only when the impinging electromagnetic radiation in the visible and infrared spectrum induces in them a temperature change. Thermistors, thermocouples, and pyroelectric detectors make it possible to detect infrared radiation without cumbersome cryogenic cooling because these devices are capable of operating at ambient room temperatures. Furthermore, they respond to both visible and IR radiation, which makes them useful under a very wide range of atmospheric conditions. Unfortunately, they have two very serious disadvantages: slower response time and lower sensitivity relative to the cryogenically cooled photon detectors. Only the pyroelectric detector appears to have a response time (nanoseconds) comparable to the cryogenically cooled photon detectors. Because of

considerable interest in pyroelectric detectors, several thermal imaging systems have been built around these detectors and are available for commercial applications.⁴

The heart of these systems is the pyroelectric vidicon tube (PEV) which has a pyroelectric crystal material as its active target element (fig 4). When the temperature of a point on the pyroelectric target is disturbed by incident thermal radiation, the permanent microscopic dipole domain undergoes spontaneous polarization which results in the buildup of charge on the opposite surface of the target. The electric charges on the target represent the electrical analog of the imaged thermal scene and are read by a scanning electron beam. The current variation in the beam as it discharges the charge pattern is the desired video signal.

The resolution and sensitivity typically achievable with the state-of-the-art pyroelectric vidicon are 0.0006 radian at $0.5^{\circ}\text{C } \Delta T$, still short of the performance level (0.0002 radian at $0.2^{\circ}\text{C } \Delta T$) achievable by mechanically serial-scanned, cryogenically cooled photon detectors in top-of-the-line military FLIRs. It compares, however, rather well with the optical performance of commercial FLIRs utilizing mechanical scanning and cryogenic cooling techniques. There are strong indications that, with continued development of pyroelectric vidicons, their resolution can be improved significantly.

The discussion so far has brought out two important advantages of PEV thermal imagers: absence of requirement for cryogenic cooling of detectors at ambient temperatures and electron-beam scanning. As a result, the PEV thermal imagers are an order of magnitude less complex, and therefore less expensive. There is one serious drawback, however, to PEV thermal imagers; the detector responds only to changes in temperature. As a result, a thermally static scene does not generate any images in the PEV thermal imager. This is acceptable where the PEV thermal imager is used for intruder surveillance. In this case, only the image of the intruder appears on the otherwise blank screen.

For applications where a thermally static scene is to be observed, the required changes in detector temperature are introduced artificially. This is typically accomplished either by panning the camera across the viewed scene or by mechanically chopping the camera's view of the scene. Of the two approaches, chopping at approximately 16 Hz has resulted in optimum image detail with a minimum of chopper-induced flicker. The use of a rotary mechanical chopper in front of the PEV window introduces some complexity to the thermal imaging system which otherwise has no other moving mechanical components. However, because the chopper is not a part of the optical train in the PEV thermal imaging system, it contributes very little to the overall cost of the system. This is in contrast to the mechanically driven optical scanner in the FLIR system with cryogenically cooled photon detectors, where the cost of the precision-made scanner components is the major contributor to the high cost of the FLIR.

The preceding discussion can be summarized by saying that although there are many feasible approaches to the design of thermal imagers, experience has shown that only two of them provide cost-effective solutions to thermal imaging requirements. Where the operational requirements call for thermal imagers with real-time maximum sensitivity and resolution capability, the expensive, serially scanned, cryogenically cooled array of photon detectors has been found to provide the best visual analog of the thermal image on the television tube. On the other hand, where the requirements call for real-time thermal imagers with medium sensitivity and resolution capability, the inexpensive, electronically scanned pyroelectric vidicons provide a satisfactory visual analog of the thermal image on the television tube at

⁴ Levitt, RS, and T Conklin, Infrared Imaging, Heating Up, Industrial Research, July 1977.

much lower prices. As a result, the user has a clear choice between expensive thermal imagers with excellent resolution and inexpensive thermal imagers with mediocre resolution. Thus a major user can, by specifying only the inexpensive, low-performance PEV thermal imagers for applications where their performance is acceptable, save enough money to acquire at least one serially scanned, cryogenically cooled, high-performance FLIR imager for applications requiring maximum optical performance.

THERMAL IMAGERS IN MARINE ENVIRONMENT

There are many potential applications of thermal imagers in the marine environment, both military and civilian. Typical military applications are detection and classification of surface and airborne targets from ships, submarines, and aircraft equipped with thermal imagers. Because of optimized sensitivity and resolution, the detection range of thermal imagers with cryogenically cooled, serially scanned photon detectors is essentially horizon-limited, while their classification range is in excess of several miles. The exact detection and classification ranges will, of course, vary with the size and thermal intensity of the target, atmospheric conditions, diameter of the objective's lens entrance aperture, and experience of the observer.

Besides allowing the observer to detect and classify the target in total darkness and/or haze, the thermoelectric imager provides him with information unique to thermal imagers. The observer can, for example, determine from the image on the TV monitor whether a ship's power plant is cold (ie, dead), or hot (ie, operational), whether the vessel is propelled by a fossil-burning or nuclear power plant, and whether there are any other power plants operating on deck (ie, idling engines in aircraft, deck-mounted generators, compressors, or winches). In addition, thermal imagers can be employed in fire control of conventional weapons and in guidance of smart bombs or rockets.

The civilian applications for thermal imagers are just as numerous and varied as for the military. Their performance in search and rescue at sea has surpassed radar and visual observation from low or high-flying aircraft. The reason for this is that the thermal emission contrast between inflatable liferafts with their occupants and the surrounding sea surface is significantly higher than the visual contrast, or the contrast in radar return. Thermal imagers also allow firefighters to see the source of fire through smoke and thus they can evaluate the extent and location of fire on ships and offshore platforms. Because current high-resolution imagers are bulky, their application in firefighting has been limited, to date, to aircraft and ships serving as firefighting control centers. As the PEV or photon detector technology shrinks the thermal imagers to the size of transistor radios, firefighters may be equipped with helmet-mounted thermal imagers that will restore to them their sense of vision in smoke-filled ship compartments.

Thermal imagers also serve successfully as detectors of potential trouble in industrial equipment. By continually surveying failure-prone equipment aboard an offshore platform or ship, incipient failure can be detected before it turns into catastrophic failure. Typical examples of such equipment are pumps, electric motors and generators, and hydraulic and mechanical transmissions. With the help of thermal imagers, it is also feasible to check periodically the level of fluids in bare or insulated storage tanks with great accuracy. Thermal imagers are also excellent tools for detecting leakage of thermal and chemical pollutants into the sea as the thermal emission of warm or oil-covered water is significantly different from unpolluted seawater at ambient temperature.

In addition to industrial applications, thermal imagers can serve during periods of minimum visibility for perimeter surveillance, visitor identification and control, floating

debris and iceberg avoidance, and navigation among anchored or permanent platforms. Because these applications are very similar to the military uses, all of the technology and operational experience gained by the defense establishment are directly transferable to industry for those applications that do not compromise the security classifications imposed by Department of Defense on some of the critical areas of technology.

In general, one can state that the utilization of thermal imagers in the marine environment will have the same impact on at-sea operations as radar and sonar had several decades ago. It is hard to conceive today how in the past ships, submarines, offshore platforms, and aircraft operated solely on the basis of unaided vision. Several decades from now it will be hard to conceive of how they ever operated without the aid of thermal imagers. It is hoped that this report will in some small measure aid prospective users and designers in selecting the right kind of housing design and construction materials for thermal imagers compatible with the intended service in the marine environment.

MATERIALS CONSIDERATIONS FOR IR WINDOWS

MATERIALS

Of primary concern to the designer of an IR imaging system for the marine environment is selection of the window material. This selection must be based on an evaluation of both optical and mechanical characteristics. Because the imaging system is primarily an optical system, the window must satisfy optical lens criteria, such as transmissivity to the proper wavelengths of IR emissions, suitable index of refraction, and stability of optical properties with variations in temperature. In addition, the window must protect the fragile and sensitive imager components from a hostile external environment. Thus it must possess acceptable mechanical strength, hardness, scratch and fracture resistance, and thermal shock resistance as well as be insoluble in seawater and resistant to corrosion.

The principal selection criterion must be the ability to transmit IR radiation with a minimum of absorption. Figure 6 illustrates the transmission regions for a variety of IR window materials (ref 3). As mentioned earlier in this paper, transmission in the 8-to-12-micron wavelength range is the most desirable for marine applications because the peaks of ambient energy emitted by objects at ambient terrestrial temperatures are centered in this band (fig 2). Another desirable optical characteristic is a high refractive index that does not change with temperature nor with wavelength (zero dispersion). The high refractive index is necessary to minimize lens curvature and thickness. The low thermal coefficient for refractive index prevents aberration unbalancing and changes in focal length as the temperature changes. Low dispersion will minimize chromatic aberration.

There are several mechanical properties that directly affect the optical performance of an IR window. There should be a low coefficient of thermal expansion so that the window shape and dimensions do not change with changes in temperature. This will prevent aberration unbalancing and changes in the focal length. In addition, it will minimize the magnitude of stresses generated in the window by differences in thermal expansion between the window and the metallic mounting. The material surface must be compatible with antireflective coatings (ie, good adherence) so that the surface reflection losses can be minimized. The window material should also have a high surface hardness and scratch resistance to prevent degradation of the lens surface. Insolubility in seawater and corrosion resistance are also important for preventing degradation in marine environments.

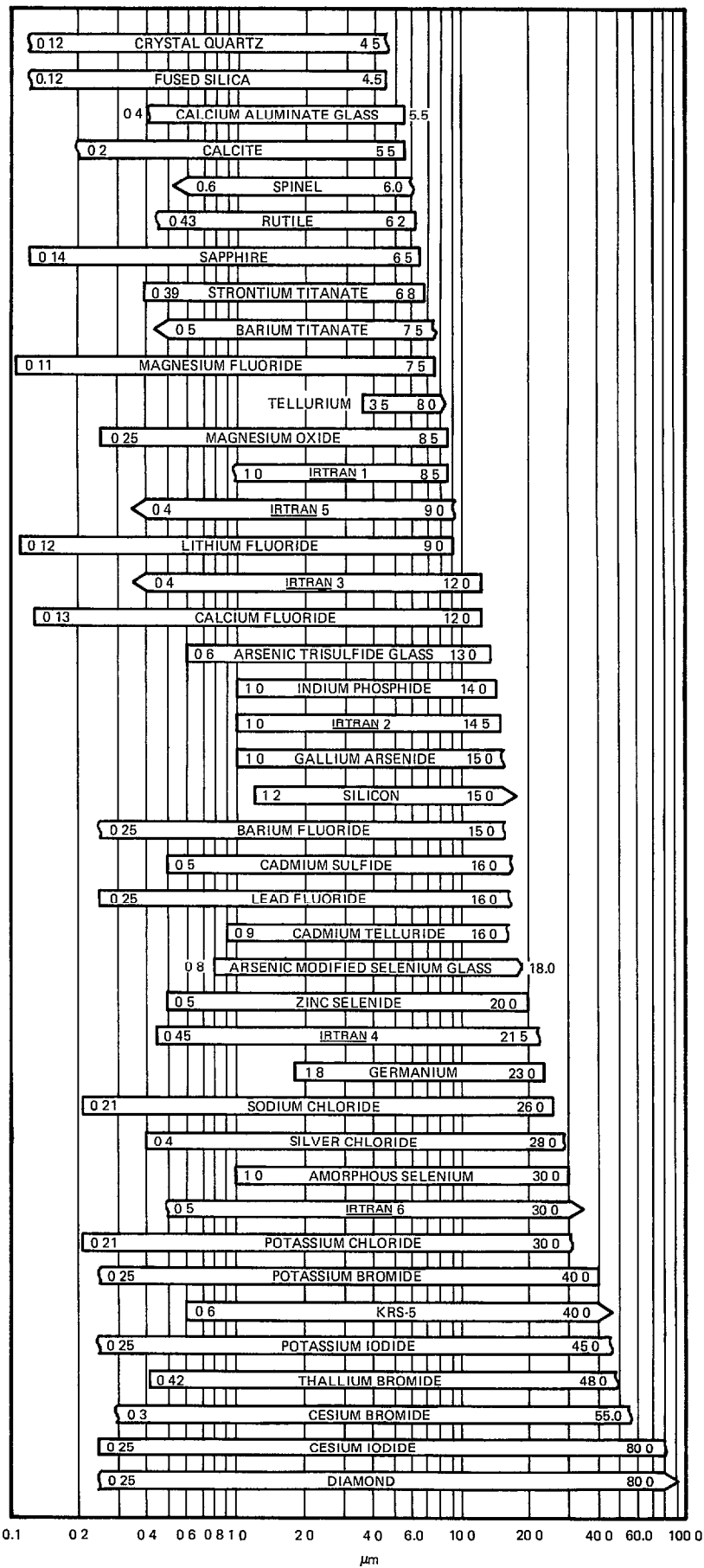


Figure 6. Transmission region of optical materials, 2 mm thick.

The structural integrity of the housing that contains the thermal imaging system depends on the structural integrity of the window. It must have high mechanical strength, especially for those windows exposed to hydrostatic pressure. High mechanical strength also allows the window to be relatively thin and therefore more transmissive to infrared radiation. Corrosion resistance, in addition to preventing optical degradation of the external surface, is of importance in maintaining the sealing of the internal components from seawater. Scratch resistance is important because most IR materials are quite brittle and notch-sensitive. Tensile strength can be reduced by as much as 75% by a surface scratch. Finally, the window must be capable of withstanding thermal shocks, such as submersion in cold seawater after exposure to elevated air temperatures, without fracturing or the onset of cracking.

Having compiled such a long list of required features, it is now necessary to say that no ideal material has yet been found which satisfies all of them (ref 2). The four principal classes of materials which are used as thermal imaging windows are: (1) semiconductors, both silicon and germanium (single-crystal or polycrystalline); (2) hot-pressed polycrystalline II-IV compounds such as the various IRTRANS; (3) chemical vapor-deposited zinc selenide and zinc sulfide; and (4) the chalcogenide glasses such as TI-1173 and AMTIR-1. Because marine applications require primarily high structural strength and corrosion resistance, the two principal materials which should be considered for the 8-to-12- μ m wavelength are polycrystalline germanium and the amorphous chalcogenide glasses. ZnSe is considered to be inappropriate for this application as the bulk transmission of this material decreases significantly after periodic submersions in seawater and its structural properties do not measure up to those of germanium. The optical and mechanical properties of germanium and one of the chalcogenide glasses, AMTIR-1 (germanium-arsenic-selenium glass), are compared in table 1 (see ref 5). The principal structural differences involve the presence of crystalline structure in germanium while the chalcogenide glasses represent a supercooled liquid structure with no inner surface structure. They are therefore termed amorphous.

In comparing the mechanical properties of these two classes of materials, the germanium is seen to be stronger, harder, more thermally conductive, and hence more resistant to fracture than the glasses. The advantages of chalcogenide glass include a more thermally stable index of refraction. In addition, the constituent elements in the glass can be carefully tailored to produce color correction. Finally, it has been determined experimentally that uncoated germanium corrodes in seawater while chalcogenide glass AMTIR-1 exhibits excellent corrosion resistance (ref 6).

A major advantage to the use of germanium in windows is that manufacturers have had nearly 20 years' experience in fabricating lenses for thermal imaging systems from this material. Optical-grade germanium is readily available in virtually any size and shape at more competitive prices than many of the other IR materials. Grinding and polishing techniques developed over the years for germanium optical lenses also apply to germanium windows. Windows as large as 26 inches diagonal have been made and by no means represent the maximum attainable size (ref 7). Partial spheres and hyperhemispheres are examples of the complex shapes achievable in germanium with state-of-the-art grinding and polishing equipment (fig 7).

⁵ Hilton, A Ray, Infrared Transmitting Glasses as Optical Materials in Passive Systems, Society of Photo Optical Instrumentation Engineers, Proceedings, vol 131, 1978.

⁶ Naval Ocean Systems Center TR 421, Resistance of Coated and Uncoated IR Windows to Seawater Corrosion, by JD Stachiw and SL Bertic, August 1979.

⁷ Stachiw, JD, Design Parameters for Germanium Windows Under Uniform Pressure Loading, Society of Photo-Optical Instrumentation Engineers, Proceedings, vol 131, January 1978.

<u>Property</u>	<u>Germanium</u>	<u>AMTIR-1</u>
Composition	Ge	Ge ₃₃ As ₁₂ Se ₅₅
Transmission range	2-18 μm	1-15 μm
Refractive index (10 μm)	4.0025	2.4975
$\Delta N/\Delta T^\circ \times 10^{-6}$	400	72
Hardness (Knoop)	850	170
Thermal expansion	$6 \times 10^{-6}/^\circ\text{C}$	$13 \times 10^{-6}/^\circ\text{C}$
Thermal conductivity, cal/s cm°C	1.4×10^{-2}	5.5×10^{-4}
Specific heat, cal/gm $^\circ\text{C}$	7.4×10^{-2}	7.2×10^{-2}
Density, gm/cm ³	5.33	4.40
Modulus of rupture, annealed (psi)	8000	2500
Glass transition temperature, T _g $^\circ\text{C}$	937 $^\circ\text{C}$ (MP)	405
Upper use temperature, $^\circ\text{C}$	200	310
Dispersion		
3.5 μm	102	192
8-12 μm	970	127
Reflectivity	36%	18.3%
Transmission maximum (uncoated)	53%	69%
Absorption @ 10.6 $\mu\text{m cm}^{-1}$	0.02	0.02
Poisson's ratio	0.25	0.27
Compressive strength (psi)	30 000	30 000
Modulus of elasticity (psi)	1.49×10^7	0.319×10^7

Table 1. Comparison of physical and optical properties of optical grade germanium and chalcogenide glass.

GERMANIUM

Sources of Germanium

Germanium does not occur in nature as a native element, but as a component in rare minerals and certain metallic ores (ref 8). No known ore deposits exist in which germanium would be the principal product sought or recovered. As a rule, germanium is found in the lattice of base metal ores, or in minerals associated with a base metal ore, like ores of zinc, lead, or copper (table 2).

Although the germanium content of sphalerite is quite low, it serves as the primary source of germanium in the United States, where it is retrieved as a byproduct from production of zinc in the tristate area of Oklahoma, Kansas, and Missouri. In other parts of the world, particularly Africa, germanium is found in the rich germanite, renierite, and argyrodite minerals that occur together with base metal ores (table 3).

The production of germanium from germanium-rich residues associated with the zinc smelting process takes place in three steps: (1) processing of zinc sulfide ores to obtain

⁸ Piedmont, JR, and JR Riordan, The Supply of Germanium for Future United States Demands, Society of Photoinstrumentation Engineers, vol 131, Practical Infrared Optics Seminar, 1978.

Germanium Minerals

<u>Name</u>	<u>Composition</u>	<u>Approximate Germanium Content (%)</u>
Stottita	FeGe(OH) ₆	29
Schaurteite	Ca ₃ Ge(SO ₄) ₂ (OH) ₆ ·3H ₂ O	14
Briarite	Cu ₂ (FeZn)GeS ₄	13-17
Germanite	Cu ₃ (GeFe)S ₄	6-11
Renierite	(CuFeGeZn) (SiAs)	6-9
Argyrodite	Ag ₈ GeS ₆	7
Fleischerite	Pb ₃ Ge(SO ₄) ₂ (OH) ₆ ·3H ₂ O	6.7

<u>Other Minerals</u>		<u>Approximate PPM</u>
Sphalerite	ZnS	100-1850
Chalcopyrite	CuFeS ₂	10-40
Enargite	Cu ₃ AsS ₄	10-80
Cassiterite	SnO ₂	10

Table 2. Minerals containing germanium.

zinc oxide and germanium-rich residue; (2) processing germanium-rich residues to obtain germanium dioxide; and (3) processing germanium dioxide to obtain pure germanium (table 4). Additional zone refinery steps are required to convert this germanium into an optical grade n-type polycrystalline germanium with resistivity in the 5-to-50-ohm/cm range.

Properties of Germanium

Physical properties of germanium place it in the group of metalloids (table 5). Its specific heat is less than that of copper, but higher than that of molybdenum. The thermal conductivity at room temperature is similar to that of nickel. The coefficient of expansion is lower than that of titanium but higher than that of molybdenum. The specific gravity and modulus of elasticity are close to those of titanium. Germanium differs significantly, however, from other metals in the area of electrical conductivity. While most metals are relatively good conductors of electricity, germanium is not. Thus, when the electrical conductivity of germanium is compared to that of iron, it is found that iron conducts electricity better by approximately a factor of 10⁶. In addition, while the electrical conductivity of metals decreases moderately with increasing temperature, that of germanium increases very significantly (figure 8). Thermal conductivity, on the other hand, decreases significantly with increasing temperature (figure 9).

Structurally, mono- and polycrystalline germanium resembles brittle ceramics. It is very sensitive to crack initiators in the form of chips and scratches and to stress risers in the form of point loadings. Its compressive strength is an order of magnitude higher than its tensile strength, and there is a total absence of yielding prior to failure. The structural

<u>Germanium Producers/Country</u>	<u>Smelters/Country</u>	<u>Raw Material Source/Country</u>
Hoboken-Overpelt/Belgium	Hoboken/Olen, Belgium Vieille Montagne/France New Jersey Zinc/USA	Kipushi/Zaire Salatossa/Italy Sardinia/Italy Tenn Valley/USA
Japan Electronic Metal/Japan Tokyo Electric Company/Japan Sumitomo/Japan Hitachi/Japan	USSR, Belgium W Germany & Canada	USSR, Zaire Italy and Canada
Eagle-Picher/USA Kawecki Berylco/USA	Eagle-Picher/USA New Jersey Zinc/USA	Tri-State/USA Illinois/USA Tenn Valley/USA
Pertusola/Italy	Penarroya/France Pertusola/Italy	Salatossa/Italy Malines/France Largentiere/France
Leninogorsk/USSR USTJ-Kamenogorsk/USSR Konstantinovsk/USSR Penarroya/France	Leninogorsk/USSR Kamenogorsk/USSR Konstantinovsk/USSR Penarroya/France	Kazakhstan/USSR Urals/USSR Ukraine/USSR Malines/France Largentiere/France Saint Salvy/France
Comeca/France Vieille Montagne/France		
Otavi/West Germany Preussag-Weser/West Germany Miasteczko/Poland	Otavi/West Germany Preussag/West Germany Miasteczko/Poland	Tsumeb/Namibia Orzel/Poland Boleslaw/Poland Trzebionka/Poland Matylda/Poland

Table 3. Listing of primary germanium producers, zinc smelters, and mine sources.

properties are isotropic in polycrystalline material and nonisotropic in single-crystal material. Since most of the large germanium castings are of polycrystalline nature, the discussion on design of germanium viewports shall be oriented in this direction.

Optically, germanium is transparent to electromagnetic radiation in the infrared spectrum (2 to 23 micrometers). Optimum transmission occurs in the 6-to-14-micrometer range. Because of the high index of refraction in air (table 6), the reflection losses are severe, amounting to 53% for two parallel polished surfaces. To decrease the reflectivity and improve the transmissivity, multilayer antireflective coatings are applied to the surfaces. With the aid of proper AR coatings, the transmissivity of germanium can be raised to more than 90 percent in the 6-to-11-micrometer range (figure 10). Since the intrinsic transmissivity of germanium is inversely related to its temperature, a significant rise in germanium temperature is always accompanied by a significant decrease in optical transmissivity (figure 11). Thus at 80°C the transmissivity of coated germanium at 10-micrometer wavelength has already decreased to 50 percent. Furthermore, the increase in temperature is accompanied

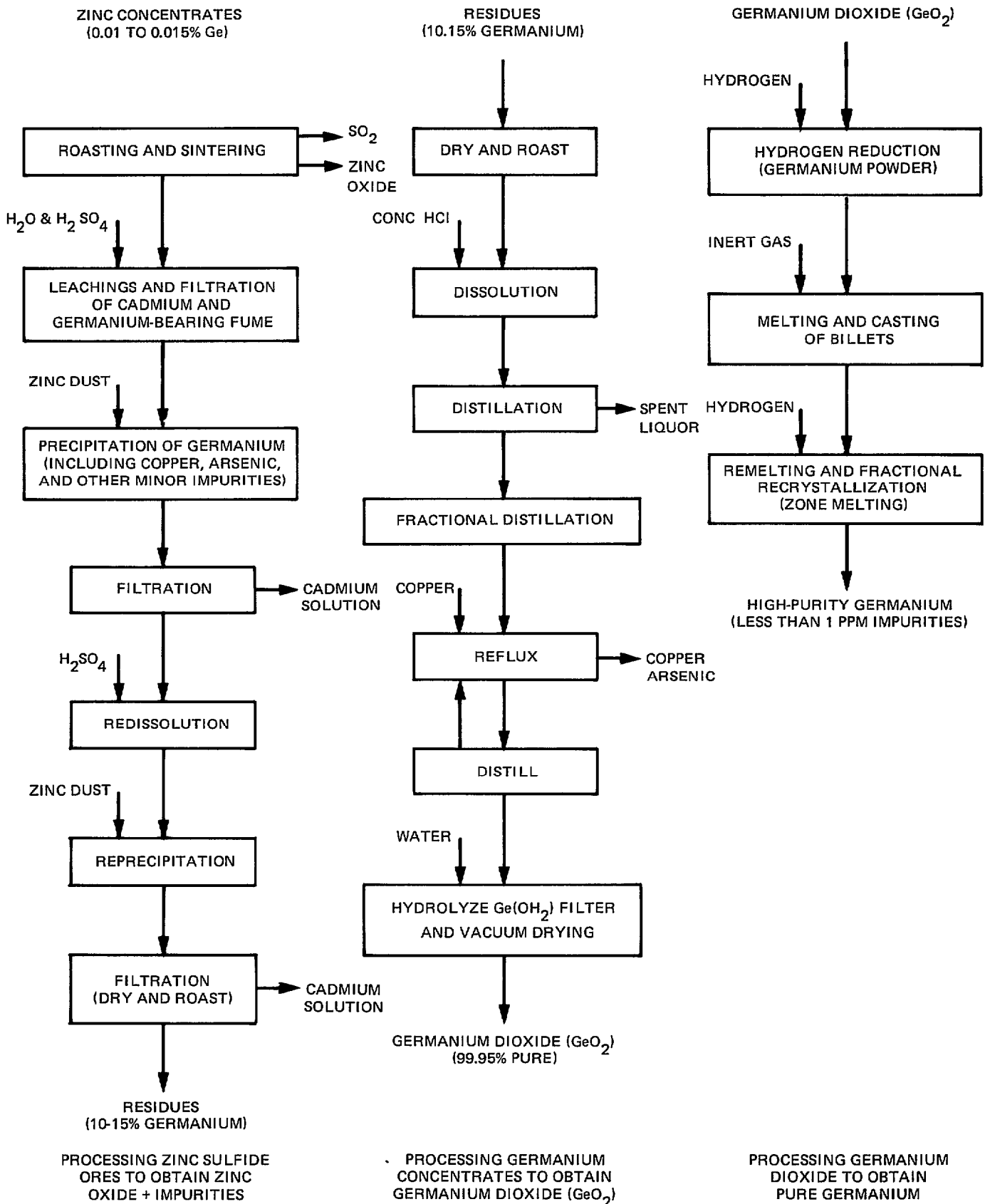


Table 4. Production of germanium from byproducts of the zinc ore reduction process.

Germanium (Ge)

Composition

Single crystal, synthetic; atomic number 32. The energy gap is approximately 0.7 eV

Atomic Weight

72.60 (GL Pearson, and WH Brattain, Proc IRE, vol 43, p 1794-1806, 1955)

Specific Gravity

5.327 at 25°C (A Smakula and V Sils, Phys Rev, vol 99, p 1744-1746, 1955)

Crystal Class

Cubic, diamond structure

Transmission

Long wavelength limit 23.0 μ

Short wavelength limit 1.8 μ

Reflection Loss

52.9% for two surfaces at a wavelength of 10 μ

Refractive Index

Values of refractive index at 27°C, for the wavelength range 2 to 16 μ , are given; the data are those of CD Salzberg and JJ Villa, J Opt Soc Am, vol 48, p 579, 1958. The resistivity of the germanium sample is about 50 ohm-cm. (These data are about 5 parts in the third decimal place lower than those reported by HB Briggs, Phys Rev, vol 77, p 287, 1950.) The authors report corrections to their original measurements (J Opt Soc Am, vol 47, p 244-246, 1957) and also report refractive indices of polycrystalline germanium which differ from those of the single crystal by only a few parts in the fourth decimal place

Dispersion

Dielectric Constant

16.6 at a frequency of 9.37×10^9 cps for a sample that has a resistivity of 9.0 ohm-cm. (University of Pennsylvania, Quarterly Progress Report Number 4, Contract AF 33(616)-78, June 1953)

Melting Temperature

936°C (Pearson and Brattain, above ref) 942°C (A Smakula, private communication)

Thermal Conductivity

0.14 cal/(cm s C°) at 20°C (KA McCarthy and SS Ballard, Phys Rev vol 99, p 1104, 1955)

Thermal Expansion

$5.5 \times 10^{-6}/C^\circ$ at 25°C (ME Fine, J Appl Phys, vol 24, pp 338-340, 1953)

$6.1 \times 10^{-6}/C^\circ$ at 25°C (Pearson and Brattain, above ref)

Specific Heat

0.074 in a temperature range from 0°C to 100°C (Pearson and Brattain, above ref)

Hardness

Solubility

Insoluble in water, soluble in hot sulfuric acid and aqua regia, etched in CP-4 (HCP, p 531)

Table 5. Typical published physical properties of germanium (continues overleaf).

Elastic Moduli

Young's modulus, 1.49×10^7 psi. Calculated from elastic coefficients
Modulus of rigidity, 9.73×10^9 psi. Calculated from elastic coefficients
Bulk modulus, 1.12×10^7 psi. (Pearson and Brattain, above ref)

Elastic coefficients at 20°C

c_{11} 1.29×10^{12} dyne/cm²
 c_{12} 4.83×10^{11} dyne/cm²
 c_{14} 6.71×10^{11} dyne/cm²

(HJ McSkimin, J Appl Phys, vol 24, pp 988-997, 1953)

Anisotropy factor, 1.66

Notes

Germanium can be used as an optical material both as a single crystal and in polycrystalline form. It is hard and brittle at room temperature and tends to fracture during fabrication. Its chemical inertness makes it useful for optical applications although its electrical properties are affected by moisture, etc. It should have a purity corresponding to 16-30 ohm-cm to be useful. It can be coated with silicon monoxide in the region out to about 5 μ , and zinc sulfide for the 8- to 13- μ region. There is usually an absorption band observed at 11.6 μ ; this is due to Ge-O stretching superimposed on a weak lattice band vibration. Germanium becomes opaque at about 125°C.

Table 5. Continued

by an increase in the index of refraction (figure 12). Therefore steps must be taken during the design of electro-optical imaging systems utilizing germanium lenses to keep the temperatures of lenses below 40°C.

COATINGS

There are two classes of coatings which must be considered for IR windows, anti-reflection (AR) coatings and anticorrosion coatings. The AR coatings are required because the high index of refraction which was advantageous for minimizing lens curvature and thickness also results in a large percentage of thermal radiation being reflected away from each window surface. At the exterior and interior surfaces of the optical elements, the amount of incident radiation which is transmitted through to the detectors will be reduced, decreasing the system sensitivity. At the interior surface, thermal self-radiation from the imaging system itself can be reflected into the optical path, increasing the thermal self-noise level. As can be seen in table 1, the reflectivity of a single germanium surface is around 36% and that of AMTIR-1 is around 18%. For a germanium window, 36% of the incident thermal radiation will be reflected when it enters the window and 36% of the remaining radiation will be reflected into the interior of the germanium when it exits the window. Therefore, an antireflection coating must be applied to both surfaces of a germanium window. Figure 10 illustrates typical transmittances of uncoated and AR-coated germanium as a function of wavelength. Since chalcogenide glass reflects only 18% of incident radiation per surface, antireflection coating could be omitted from the exterior window surface with only minor loss of thermal imager performance. This would decrease the cost of glass windows and extend the interval between window replacements as the bare chalcogenide glass is significantly more corrosion-resistant than currently available AR coatings.

Antireflection coatings can be either a single-layer coating or a multiple-layer coating. These are usually vapor-deposited onto the window surface (substrate) under vacuum and at elevated temperature. The optimum temperature depends on the substrate material. Some

Wavelength (μ)	Refractive Index (η)	Wavelength (μ)	Refractive Index (η)
2.0581	4.1016	4.866	4.0170
2.1526	4.0919	6.238	4.0094
2.3126	4.0785	8.66	4.0043
2.4374	4.0708	9.72	4.0034
2.577	4.0609	11.04	4.0026
2.7144	4.0552	12.20	4.0023
2.998	4.0452	13.02	4.0021
3.3033	4.0369	14.21	4.0015*
3.4188	4.0334	15.08	4.0014*
4.258	4.0216	16.00	4.0012*

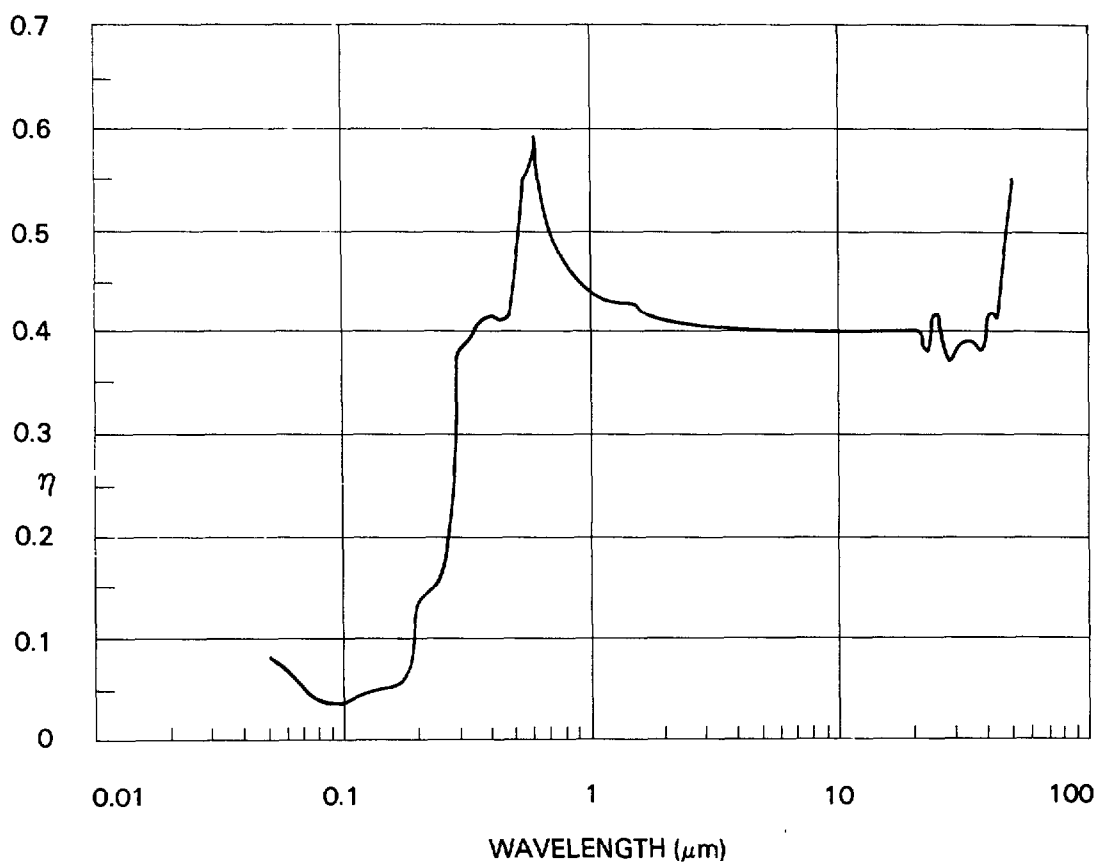


Table 6. The refractive index of germanium at 27°C.



Figure 7. Typical sizes and shapes of germanium windows and lenses.

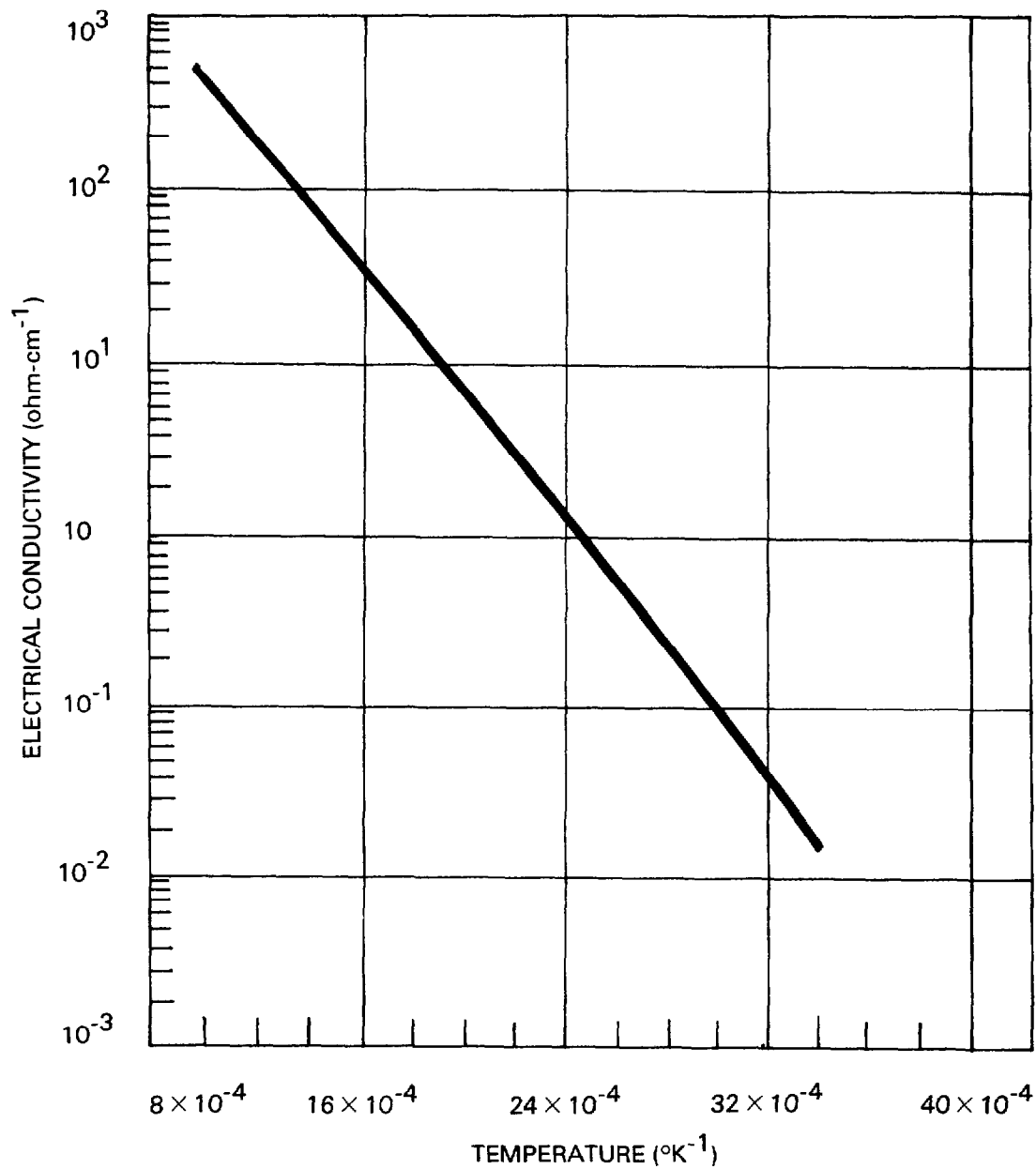


Figure 8. Conductivity as a function of temperature for single-crystal germanium in the intrinsic range.

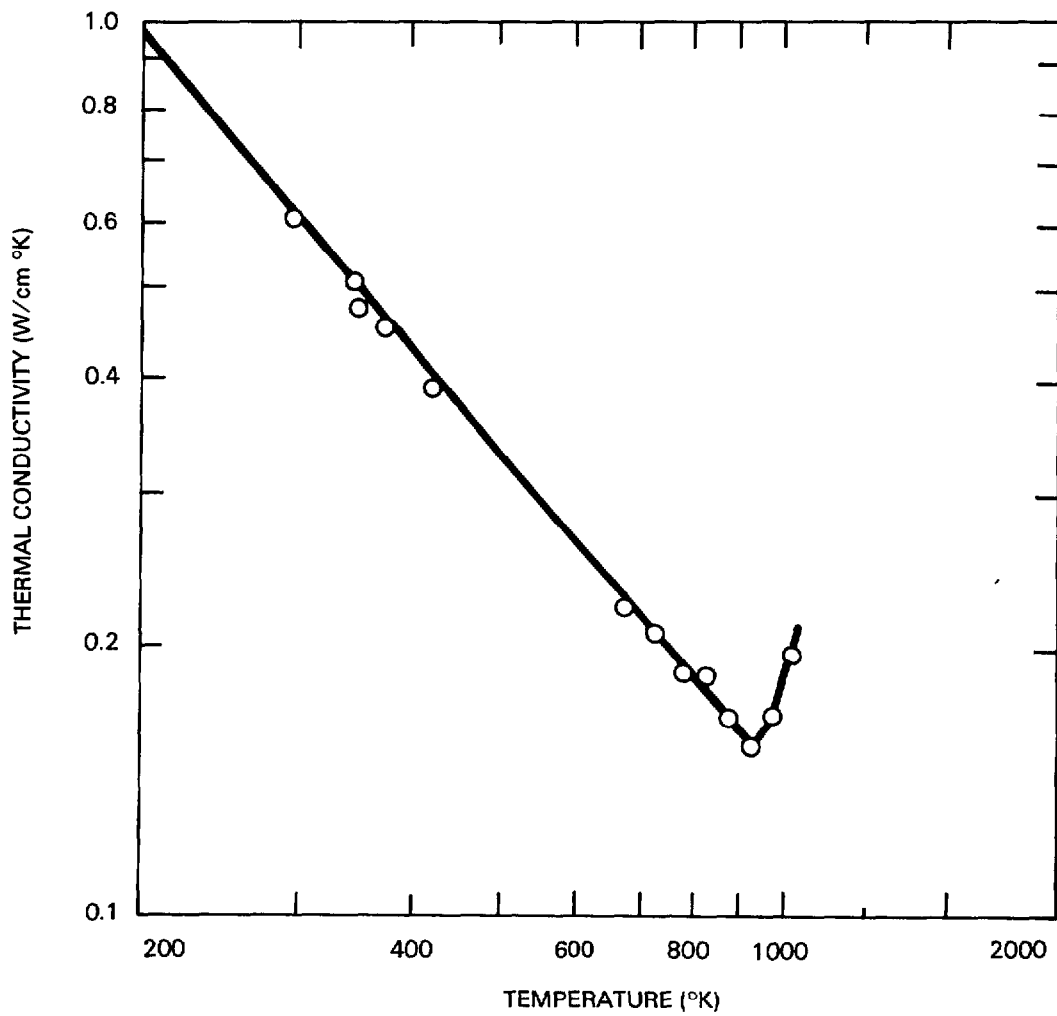


Figure 9. Thermal conductivity of germanium from 300°K to 1020°K, as determined by the radiant heat flow method; n-type, polycrystalline, with $p = 30$ ohm-cm.

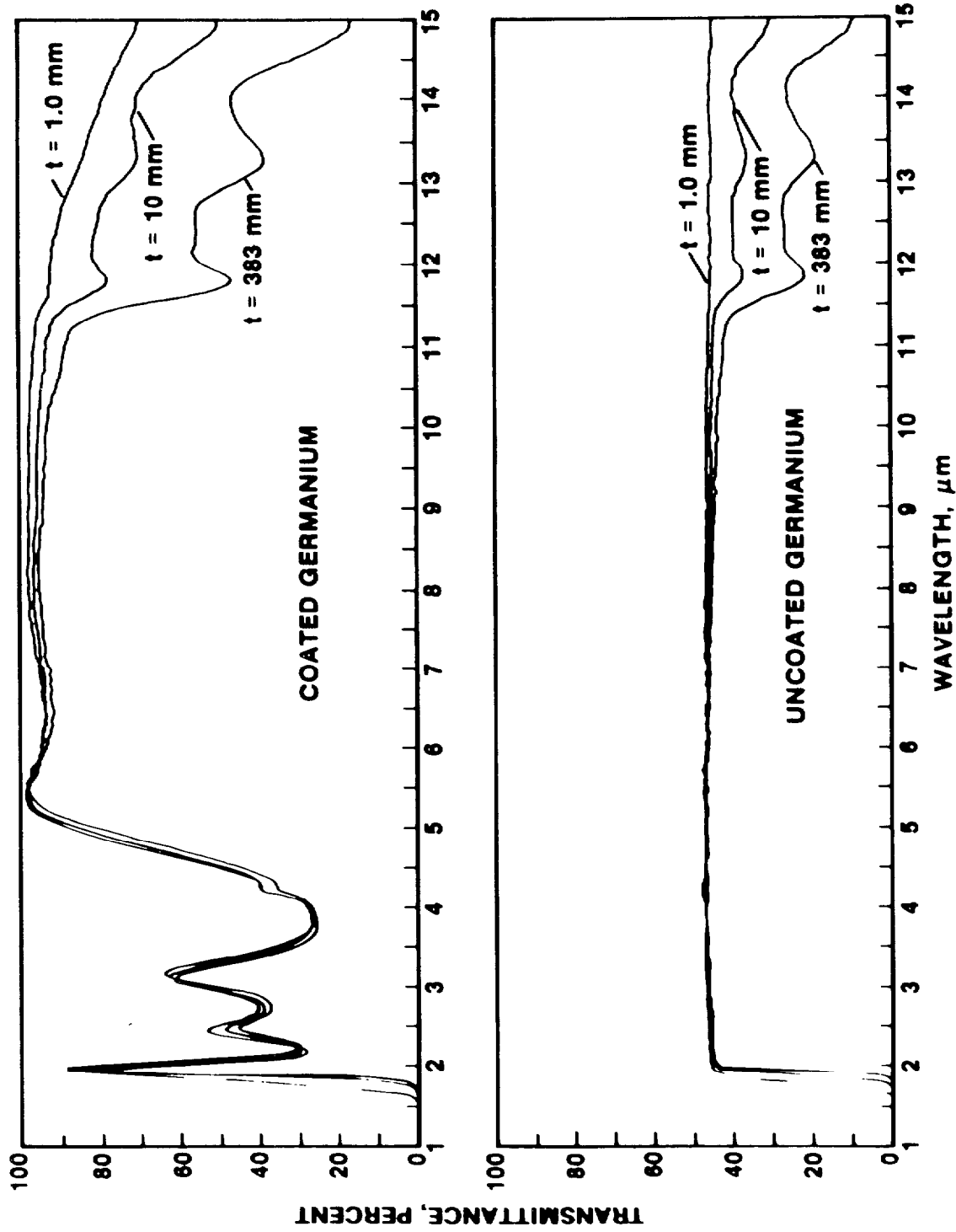


Figure 10. Transmittance of uncoated and AR-coated (both faces) polycrystalline germanium.

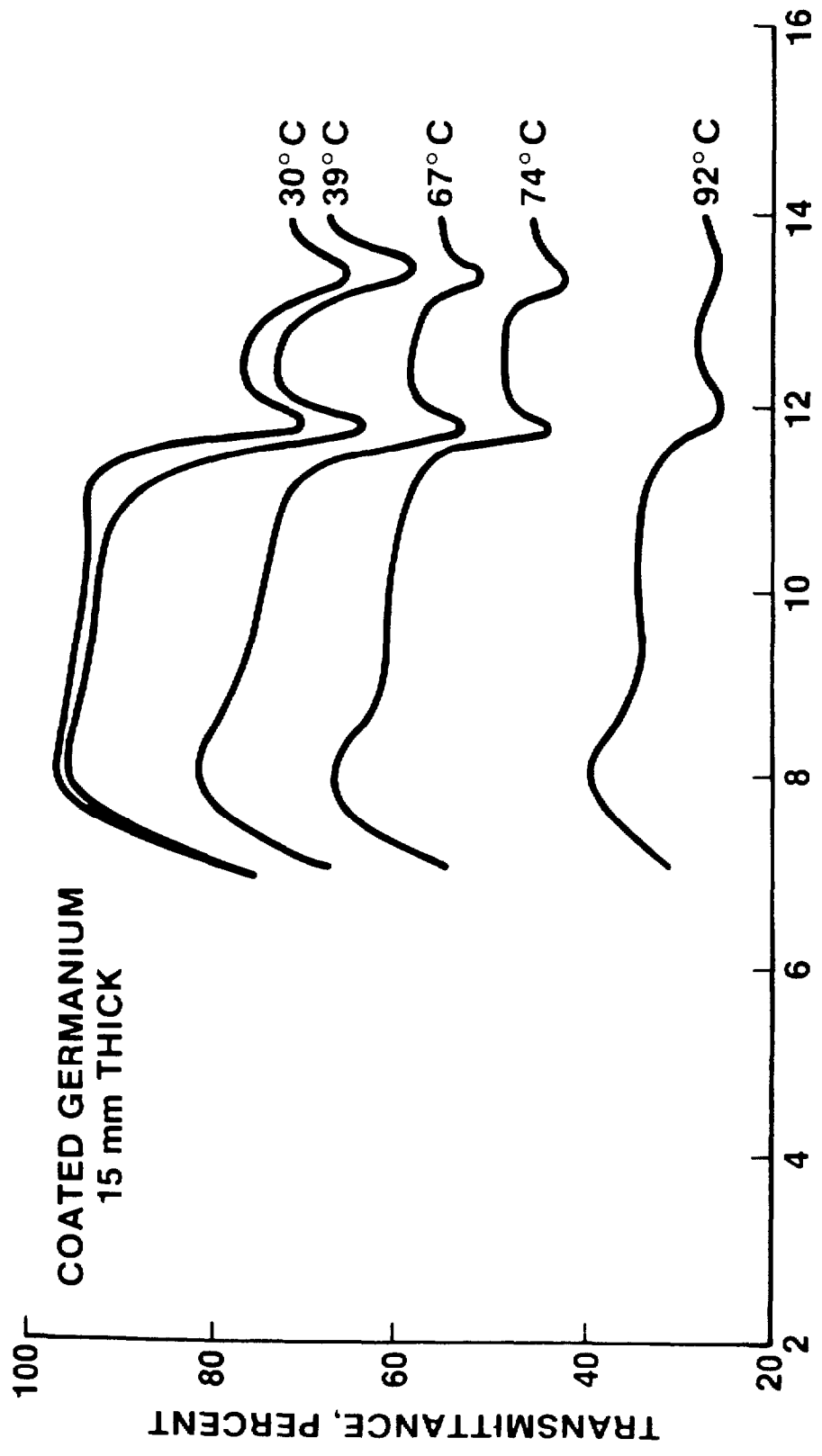


Figure 11. Transmittance of AR-coated polycrystalline germanium as a function of temperature.

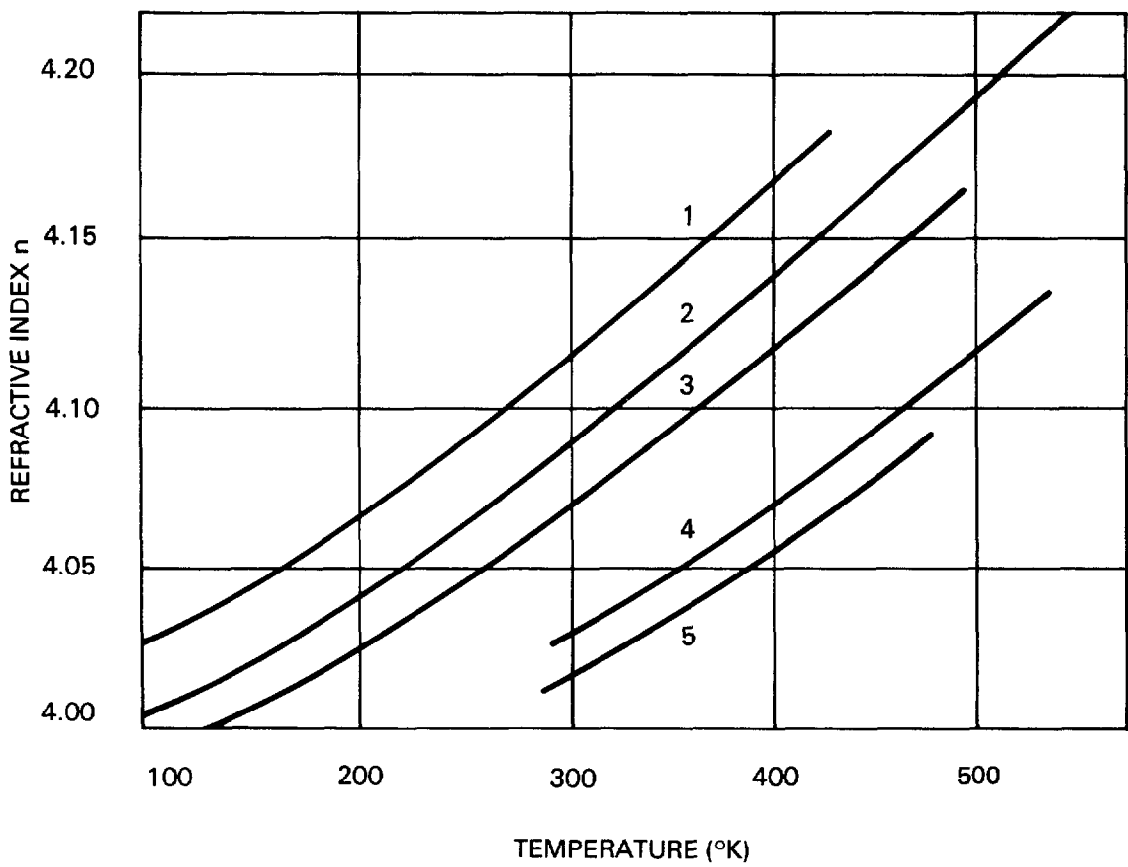


Figure 12. Refractive index as a function of temperature for single-crystal doped n-type germanium. Sample resistivity at 300°K is 1.2 ohm-cm.

researchers have found that the use of an ultrahigh vacuum (UHV) provides more consistency in the optical characteristics of the coating and better adhesion in some material combinations of coating and substrate (ref 9).

A single-layer coating can be selected to produce zero reflectance at a single wavelength. The material selected must have a refractive index which is the geometric mean of the substrate index and the index of the incidence medium (air on the external side). That is $\eta_1 = (\eta_0 \eta_s)^{1/2}$ where η_1 is the coating index, η_0 is the medium index, and η_s is the substrate index. At normal incidence, the coating thickness should be an odd number of quarter wavelengths for the wavelength selected for zero reflectance. Two materials which have been used for single-layer AR coatings are silicon monoxide and thorium oxyfluoride (ref 10).

Double-layer and triple-layer coatings have been developed to enable reflectance to be reduced over a range, or bandwidth, of infrared wavelengths. They are also employed to reduce the total coating thickness, since single-layer coatings must be relatively thick to satisfy the fractional wavelength requirements. A three (or more)-layer coating has a typical optical thickness of 1/4 or 1/2 wavelength (0.0001 inch–0.0002 inch for a 10-micrometer wavelength). For a three-layer coating, there are three refractive indices and three thicknesses which can be varied to achieve the desired performance. The principal design limitation is the availability of coating materials with sufficiently high refractive indices. Typical multiple-layer coating materials include ThF_4 , ZnS , As_2S_3 , ZnSe , and Ge (ref 9). The choice of the particular coatings is based on design criteria such as minimizing absorption and minimizing differential strains that might cause poor adhesion.

In addition to their optical function, AR coatings provide lenses serving as windows with partial corrosion protection. Tests conducted in San Diego Bay have shown that germanium windows covered with single or multiple-layer AR coatings withstood a 4-month continuous submersion in seawater with only minor surface deterioration and less than 5-percent loss in IR transmission (ref 6). The transmission through unprotected germanium windows, on the other hand, decreased in the same time period by 100 percent as the result of an increase in surface roughness and the formation of germanium oxides on the wetted window surface.

Thus, at the present time, selected single and multilayer AR coatings appear to provide fair corrosion resistance for germanium, as well as to perform adequately to reduce reflective losses through that material.

A phenomenon related to corrosion for windows submerged in seawater for extended periods of time is marine fouling. Resulting from the growth of small organisms, fouling can reduce transmission of infrared radiation directly and accelerate corrosion of the window surface. Effective antifouling coatings have not been found to date which are transparent to IR signals. Techniques using forced circulation of seawater over the window surfaces have had mixed success (ref 6). Fouling can be reduced substantially but the impinging water has the tendency to erode AR coatings. The most reliable technique for the prevention of fouling discovered to date is to wash the windows daily with tap water and expose

⁹ Rome Air Development Center Technical Report 77-40, Laser Window Surface Finishing and Coating Science, by M Braunstein et al 1977.

¹⁰ Kingslake, R, Applied Optics and Optical Engineering, vol 1, Academic Press, New York, 1965.

them, at least briefly, to ultraviolet radiation (eg, sunlight). This daily exposure to sunlight and air appears to be so effective that even without periodic washdowns with tap water, biofouling can be significantly reduced.

PREVENTION OF ICE FORMATION

Thermal imaging systems operating in marine environments at subfreezing ambient temperatures lose their operational effectiveness when the windows become coated with a layer of ice (ref 11). The operational value of these systems will decrease significantly unless a heating technique is developed that keeps the window ice-free without significant deterioration of window surfaces and without degradation of transmitted image quality. For effective performance in a polar environment, the IR window should be heated so as to prevent ice formation at temperatures as low as -40°F (-40°C) and wind velocities as high as 40 ft/s (12 m/s).

Four principal techniques have been considered for heating IR windows (ref 12). These are (1) intrinsic heating by passing electricity through the windows; (2) conductive heating by the attachment of resistive heaters; (3) convective heating by forcing heated air over the internal and/or external surface of the window; or (4) application of an electrically conductive coating to the interior surface of the window.

The first technique, intrinsic heating, is based on the conductive nature of the window material, particularly germanium, a semiconductor. This technique has been used for a number of years in aircraft-mounted IR systems. It is necessary to regulate electric current to the window precisely because of the characteristic property of resistivity decrease with temperature increase. That is, as the current is passed through the window (from one end to the other in flat windows), the window heats up, the resistivity decreases, more current is drawn, and a thermal runaway is experienced. Current regulation with temperature sensing and feedback is required to prevent this occurrence. A second characteristic of this heating technique is electrolytic corrosion at the crystal grain boundaries. Although a number of coating techniques have been tried, this corrosion has not been completely prevented in intrinsically heated airborne windows. Because of the conductivity of salt water, intrinsically heated windows in the marine environment experience accelerated electrolytic corrosion and window etching.

A second technique for preventing ice formation is to attach resistive heaters to the edges or surfaces of the IR window so as not to obstruct the field of view of the imaging system. Since germanium is electrically conductive, it is also a good thermal conductor. It has been determined experimentally that power densities on the order of 2 to 3 watts per square inch of exposed surface area will prevent ice formation on periodically submerged windows exposed to -40°F (-40°C) air at speeds of 40 ft/s (12 m/s). The heaters can be fabricated from a variety of materials. A design which allows attachment to complex window shapes is a laminate of silicone rubber reinforced with glass fibers sandwiched around conductive foil grids. This heater can be placed at the base of a spherical sector window, or incorporated into the bearing gasket clamped between the window and the seat.

¹¹ NOSC TR 191, Ice Formation on Germanium Windows in Marine Service, by JD Stachiw and DL Endicott, March 1978.

¹² NOSC TR 413, De-Icing Techniques for Germanium Windows in Marine Environments, by JD Stachiw and DL Endicott, 1979.

The third technique for preventing ice formation is to force preheated air over the window surface. This technique is most effective when the air can be directed at the exterior surface of the window so as to melt the ice directly. Directing heated air at the interior surface of an IR window requires large air flows and high temperatures to achieve elevated window temperatures. This air may also interfere with the optical components and detectors which usually must be cooled. The heated air technique is therefore more viable for arctic applications in the splash zone or for shore installations rather than for submersible systems, where external air ducts are not practical.

A fourth technique, which is only conceptual at this time, is to make use of an electrically conductive coating transparent to infrared radiation and applied to the interior window surface. This technique, which employs resistive films transparent to the visual spectrum, has been used on aircraft windows and some optical devices to prevent condensation and fogging. The primary advantage is an even distribution of heat over the interior surface of the window. Furthermore, since the conduction path between the heater and the ice is shorter than when the heat is applied at the edges, less time and less power are required to keep the lens ice-free.

For an electrically conductive coating to serve as a heating element requires that the window material be nonconductive electrically or that an electrically insulating layer be sandwiched between the germanium window and the conductive coating. To date, techniques and materials have not yet been developed for application of electrically conductive film to germanium windows. Some success has been reported, however with thin films of indium oxide deposited on chalcogenide glass test specimens (ref 13). Absorptances of 25% were observed for films of adequate resistivity. The principal limitation is in achieving a uniform thickness and composition. The largest samples uniformly coated were 3-inch X 3-inch X 3/8-inch flat windows. It is conceivable that a chalcogenide glass coating would be applied first to the germanium surface to insulate it from the electrically conductive coating. Since chalcogenide glass coating also imparts protection against corrosion by seawater, this arrangement may be found to be very effective (ref 14).

Although prevention of ice formation is necessary for the use of IR imaging systems in arctic applications, the heating techniques must also minimize degradation of the imagery. Despite the fact that only limited testing has been performed, it has been demonstrated that intrinsic heating, resistive heating, and heated air do not degrade the imagery if the window is kept below certain maximum threshold temperatures which affect the transmissivity. Because the windows are not in the focal plane of the viewed scene, the window temperatures can be substantially higher than the scene temperature. Although the maximum temperature threshold is a function of the window material and the sensor characteristics, loss of resolution and gray scale were not observed with pyroelectric vidicon systems at germanium temperatures below 102° F (50° C), whereas window temperatures of only 40° F (5° C) were required to prevent ice formation.

¹³ Air Force Avionics Laboratory, Wright-Patterson AFB, Technical Report AFAL-TR-73-340, Development of Deicing Methods for Chalcogenide Windows for Reconnaissance and Weapon Delivery, by SN Rea and RS Wriston, August 1973.

¹⁴ Stachiw, JD, and DL Endicott, Material and Design Considerations for Thermal Imager Windows in Marine Service, Proceedings of Oceans 1979, Institute of Electronic and Electrical Engineers Publication 79CH 1478-70EC.

WINDOW DESIGN CONSIDERATIONS

Windows for pressure-resistant viewports can be made in any shape desired by the designer. However, through experience and tradition, several shapes have come to be considered as standard. Those shapes are plane disc, plane beveled disc, plane twin-beveled disc, spherical sector, hemisphere, and hyperhemisphere (figure 13). Of these shapes, only the latter three are suited for high-pressure viewports utilizing windows fabricated from brittle materials like glass, germanium, or ceramics.

The reason for the suitability of the spherical sector, hemisphere, and hyper-hemisphere shapes for high-pressure windows is their spherical curvature, which places the body of the window into compression. In this respect, those three window shapes differ from the plane disc, plane beveled disc, and the plane twin-beveled disc shapes for which the low-pressure faces of the windows are placed in tension under the action of pressure on the high-pressure face. Since most optical materials are stronger in compression than in tension, the use of spherical curvature allows the windows to withstand higher stresses than they would under action of tensile stresses. Still, for applications where the external pressure is low to moderate, the plane windows hold certain advantages, like the ability to be fabricated in large shapes; low cost; and ease of mounting. Where external pressures are not too extreme, plane windows have been used with success (figures 14 and 15).

Where external pressures are high, only windows with spherical curvature can be utilized efficiently since the use of plane shapes would require extreme thickness of windows to keep the tensile stress below acceptable limits. On the basis of this engineering approach, spherical windows fabricated from acrylic plastic, glass, and ceramic have already been utilized successfully under external hydrostatic pressures in excess of 1000 psi (see references 15 through 21). What has been lacking is a proven viewport design with a germanium window for pressures in excess of 10 000 psi.

It was thought that a design for high pressure could be readily arrived at if the existing principles from already proven viewport designs were incorporated without many changes into the viewport containing a germanium window for high-pressure service. The applicability of principles based on design of glass windows for high pressure to design of high-pressure germanium windows would be validated in a study utilizing experimental evaluation procedures. This report summarizes the results of this study.

-
- 15 Stachiw, JD, Transparent Structural Materials for Underwater Research and Exploration, Industries Atomique et Spatiales, vol 18, no 3, pp 71-94, 1974.
 - 16 Stachiw, JD, Glass or Ceramic Spherical Shell Window Assembly for 20,000 psi Operational Pressure, Journal of Engineering for Industry/ASME Transactions, vol 97, no 3, 1975.
 - 17 Gray, KO, and JD Stachiw, Glass Housing for Hydrospace Lights and Instruments, Journal of Engineering for Industry/ASME Transactions, vol 92, no 1, 1970.
 - 18 Stachiw, JD, Glass and Ceramics for Underwater Structures, Ceramic Age, vol 80, no 6, July 1964.
 - 19 Stachiw, JD, and RF Snyder, The Design and Fabrication of Glass and Ceramic Deep-Submergence, Free-Diving Instrumentation capsules with Capabilities of 3500 Fathoms, American Society of Mechanical Engineers paper 65-UnT-1, 1965.
 - 20 Naval Undersea Center TP 393, Glass or Ceramic Spherical-Shell Window Assembly for 20,000 psi Operational Pressure, by JD Stachiw, May 1974.
 - 21 Stachiw, JD, Hyperhemispherical Viewports for Undersea Applications, Journal of Engineering for Industry/ASME Transactions, vol 101, no 3, 1979.

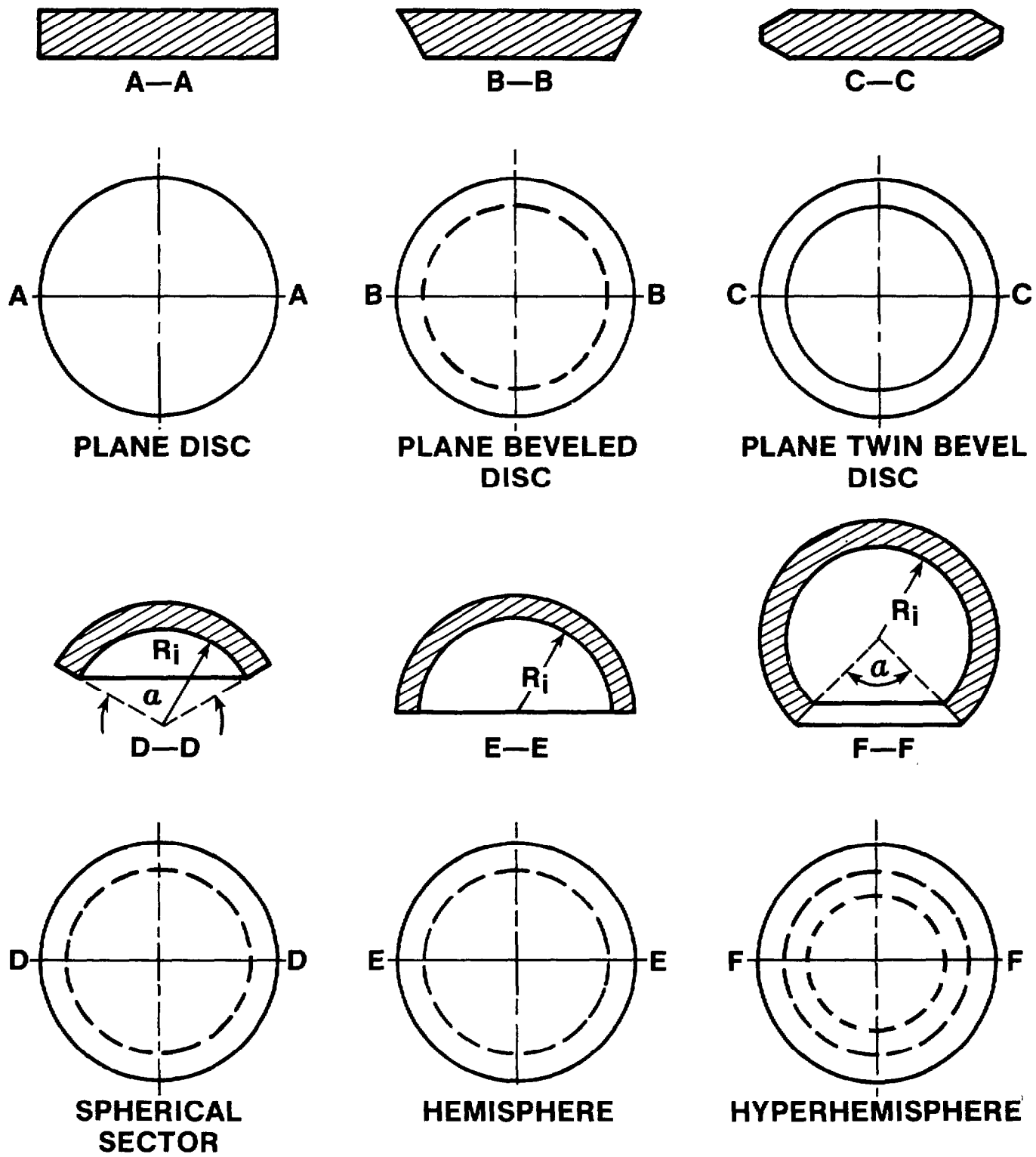


Figure 13. Standard shapes for pressure-resistant windows.

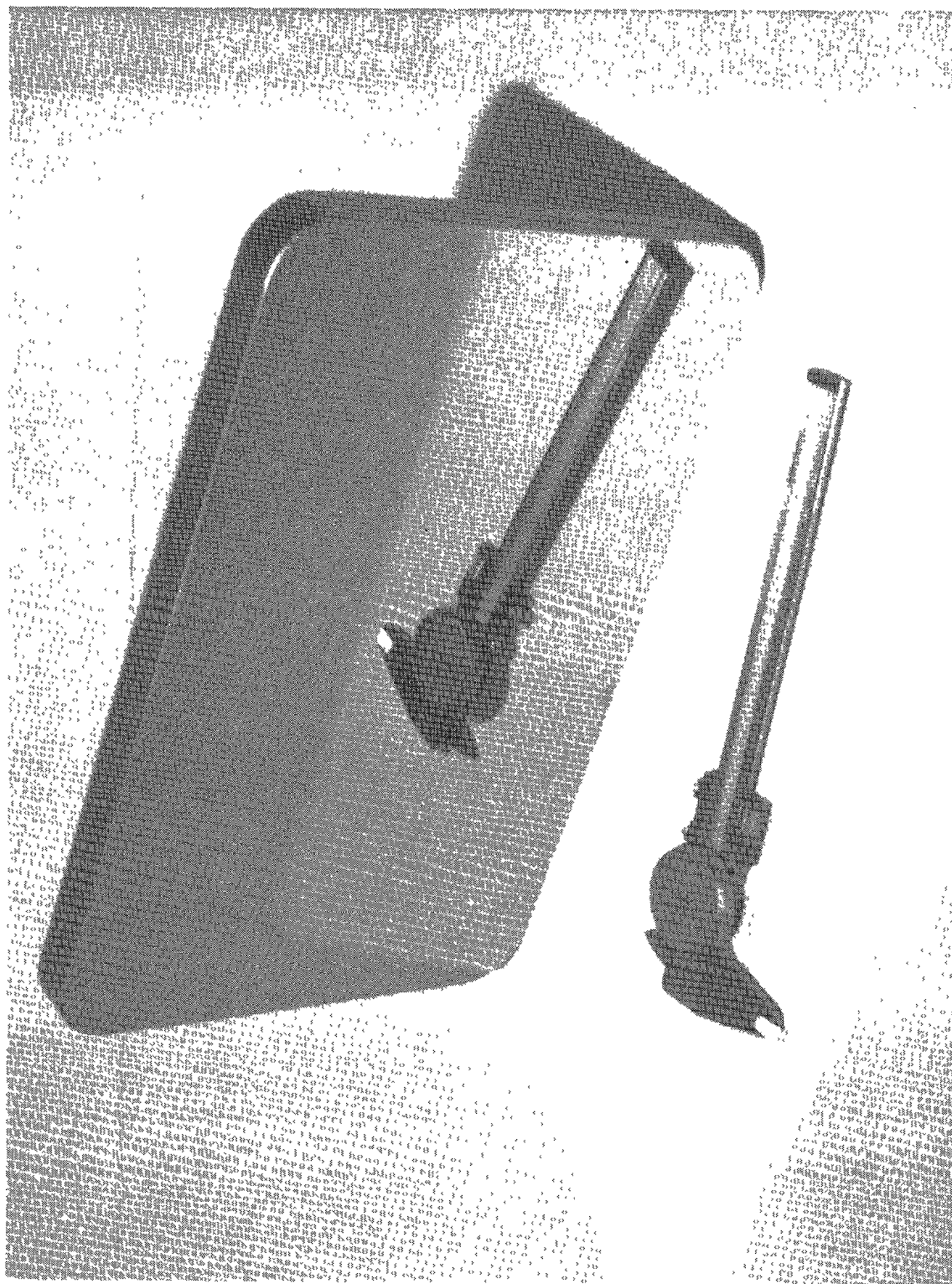
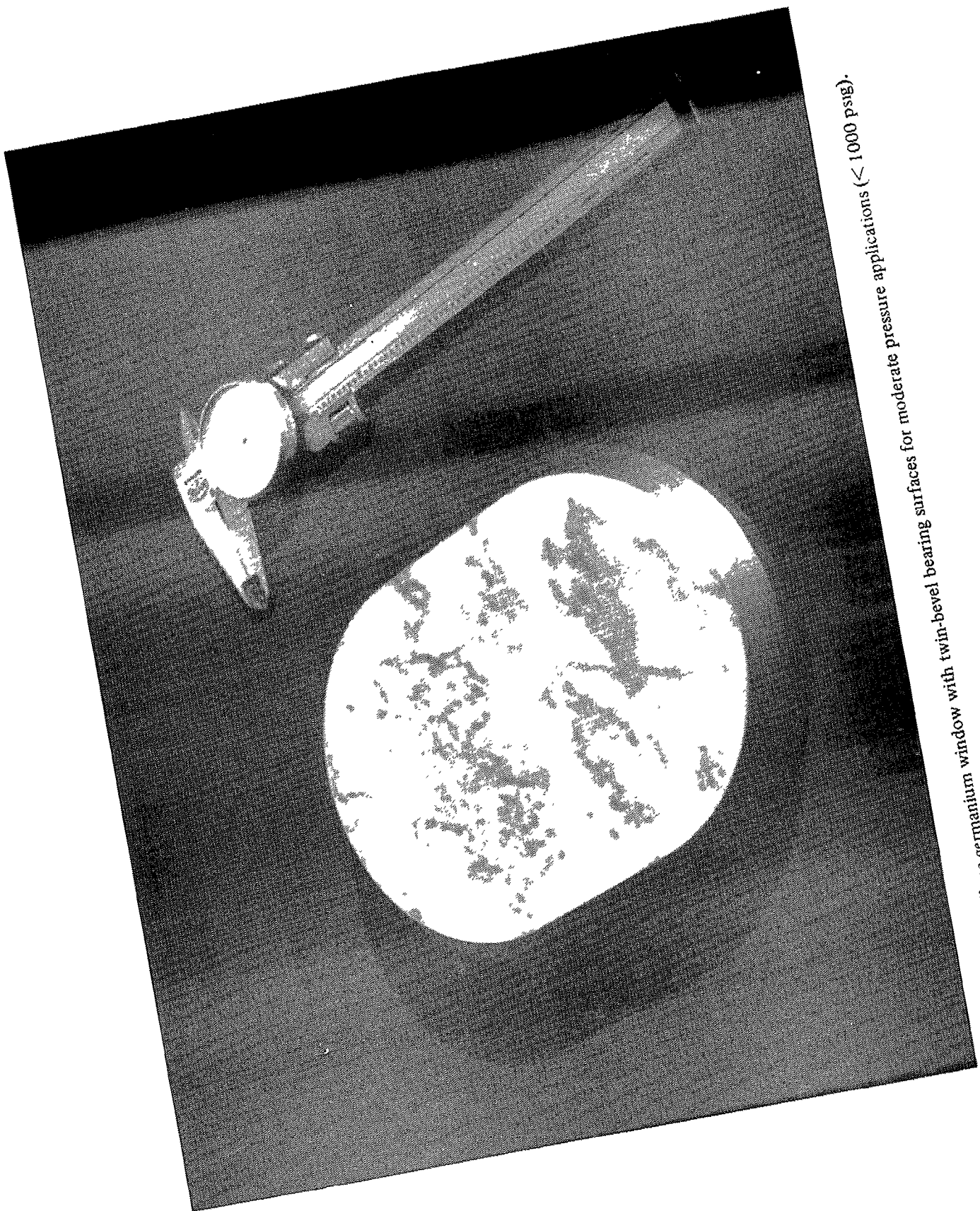


Figure 14. Plane germanium window with plane bearing surface for low-pressure applications (< 100 psig).



15. Plane germanium window with twin-bevel bearing surfaces for moderate pressure applications (< 1000 psig).

STUDY PLAN

The objective of the study was to show that an optical viewport for abyssal depths or land-based high-pressure chambers can be successfully designed and fabricated from germanium.

The scope of the study was limited to a single-viewport design and a total of five window test specimens.

The approach to the study was experimental in nature and relied in a large measure on previous experimental and analytical work conducted with viewports utilizing acrylic plastic, glass, ceramic, and germanium windows.

As test specimens, 1-inch-thick germanium 150° spherical sectors with 4-inch outside radius, mounted in K-500 monel alloy seats, were used. The germanium in the spherical sector windows was n-type polycrystalline material with optical properties.

The test procedure consisted of pressurizing the 150° spherical viewport test assemblies to various levels of external pressure under static, cyclic, and dynamic conditions inside the deep ocean simulators at the Southwest Research Institute.

Instrumentation consisted of electrical resistance straingages for measurement of strains in the viewport components, piezoelectric pressure transducers for measurement of dynamic pressure peaks, and piezoelectric accelerometers for measurement of acoustic events inside the window body.

VIEWPORT DESIGN

VIEWPORT COMPONENTS

The viewport design selected for evaluation in this study was based on the following principles validated in other studies during the design of viewports with glass or ceramic windows for high-pressure service:

1. Spherical sectors see only compressive stresses under external pressure loading and are thus the best-suited shape for windows made of materials with low tensile but high compressive strength (ref 15).
2. A spherical sector with 150° included spherical angle appears to generate the least number of shear cracks in the conical bearing surface of the sector under a given bearing stress.
3. A plane conical bearing surface on a spherical sector window generates the least amount of stress concentrations in the window mated to a seat whose radial and angular displacements differ from that of the window.
4. The included angles of the window and seat must match within 1 to 2 minutes of arc.
5. Bearing gaskets made of compliant elastic material must be interposed between the mating bearing surfaces of the window and the seat (refs 17 and 20).
6. Ideal bearing gasket construction for high bearing stresses consists of two layers of epoxy-impregnated KEVLAR-49 cloth bonded to a single layer of Neoprene-impregnated nylon cloth (refs 16 and 20).

7. The radial and angular displacements of the window seat should match as closely as possible the radial and angular displacements of the window.

8. The retaining ring should generate only compressive stresses inside the window.

9. The bearing surface on the window must be either pitch-polished or finished with an 8-to-10-micrometer grinding compound.

10. The edges of the bearing surface on the window must be provided with a 0.010 to 0.020-inch chamfer whose finish matches that of the bearing surface. No chips are to be allowed on the chamfered surfaces. Chips of up to 0.020 inch can be removed with a stone of appropriate roughness.

Based on the above proven criteria, a 150° spherical sector viewport was designed and fabricated. The dimensions chosen for this viewport were the same as those of the successful Naval Undersea Center (NUC) spherical deep-submergence glass window assembly which was evaluated in 1976 (figures 16 through 20; see also ref 20). The reason for choosing the proven glass window dimensions for the germanium window was that by making the dimensions of the germanium window identical, the structural performance of both materials could be directly compared and conclusions reached on the structural adequacy of germanium. Furthermore, since the performance of the Monel seat and glass window had been found satisfactory during the previous window test program, no need existed for a stress analysis prior to sizing of the viewport components. As a matter of fact, the distribution and magnitude of stresses measured previously in the viewport assembly with a Cervit 201 window are the same as in the identical viewport assembly with a germanium window because the modulus of elasticity for both materials is approximately the same (figures 21 and 22).

MECHANICAL PROPERTIES OF GERMANIUM

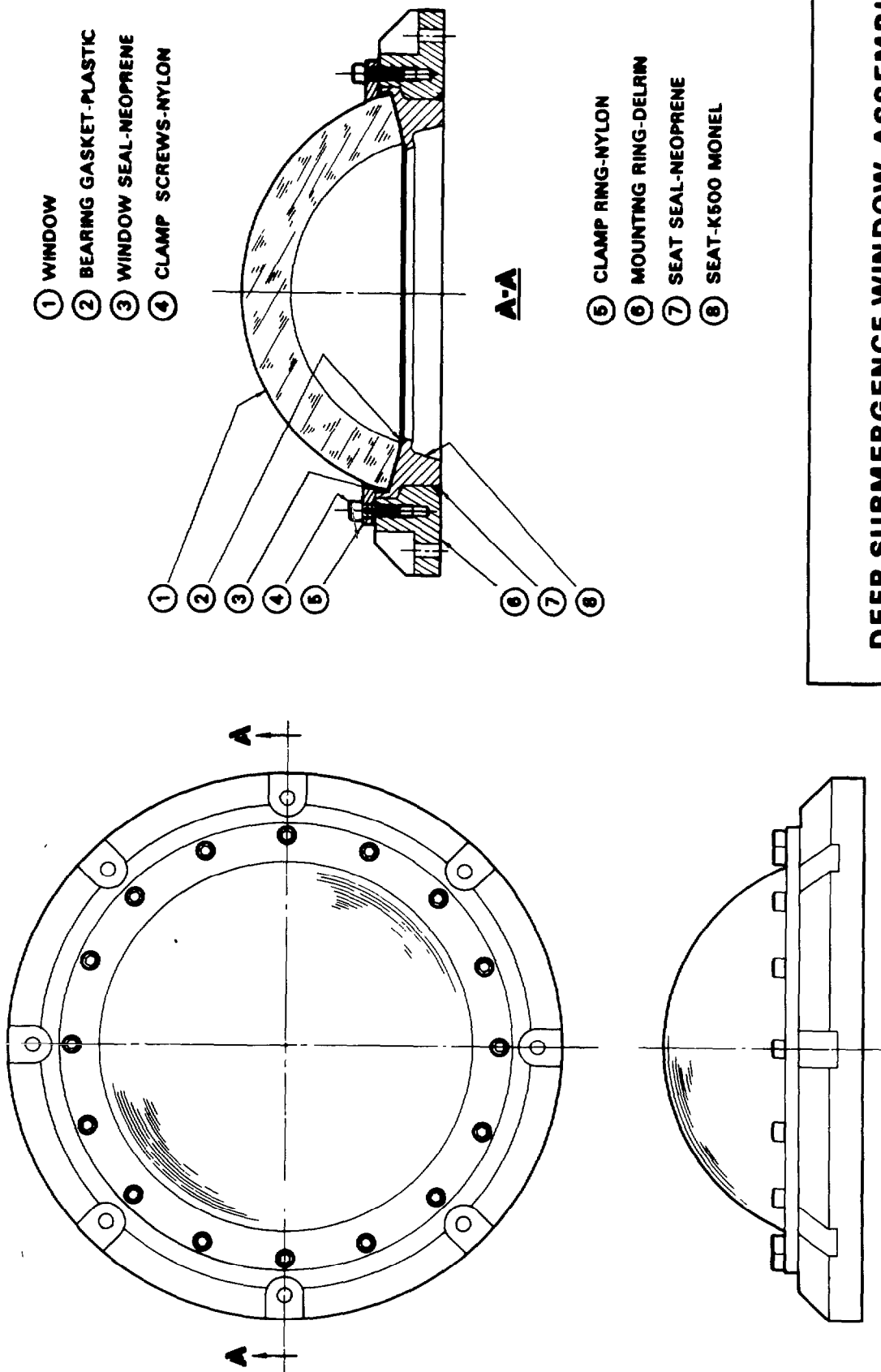
Although no need existed to repeat the earlier stress analysis of viewport components (ref 20), there was a definite requirement for establishing the mechanical properties of germanium prior to fabrication of the windows to the same dimensions as the glass and ceramic windows of the past study. If the tensile and compressive strength of germanium were found to be substantially lower than that of glass, the test pressures in the evaluation program would have to be lowered accordingly, so that the window would not fail on first pressurization and thus terminate the test program prematurely.

A review of technical literature failed to discover sufficient test data for an engineering judgment on the mechanical properties of germanium. In response to this lack of published data, a two-pronged approach to obtaining data was launched. On one hand, a concerted effort was made to ferret out unpublished data generated by fabricators of germanium optics; at the same time, a germanium test program was initiated at the Naval Ocean Systems Center.

The objectives of the material study were to provide the following important items of information for the designer of germanium windows:

1. Average and guaranteed minimum flexural strength, and the effect of surface finish on that strength.

2. Average and guaranteed minimum compressive strength and the effect of surface finish on that strength.



- ① WINDOW
- ② BEARING GASKET-PLASTIC
- ③ WINDOW SEAL-NEOPRENE
- ④ CLAMP SCREWS-NYLON

- ⑤ CLAMP RING-NYLON
- ⑥ MOUNTING RING-DELRIN
- ⑦ SEAT SEAL-NEOPRENE
- ⑧ SEAT-K500 MONEL

DEEP SUBMERGENCE WINDOW ASSEMBLY
150° SPHERICAL SHELL DESIGN

Figure 16. Spherical sector window design for high-pressure applications (< 20 000 psig). This window assembly is designed to be bolted to any penetration reinforcing ring with a plane sealing surface. The assembly will tolerate radial contraction and angular rotation of the reinforcing ring without breakage of the window.

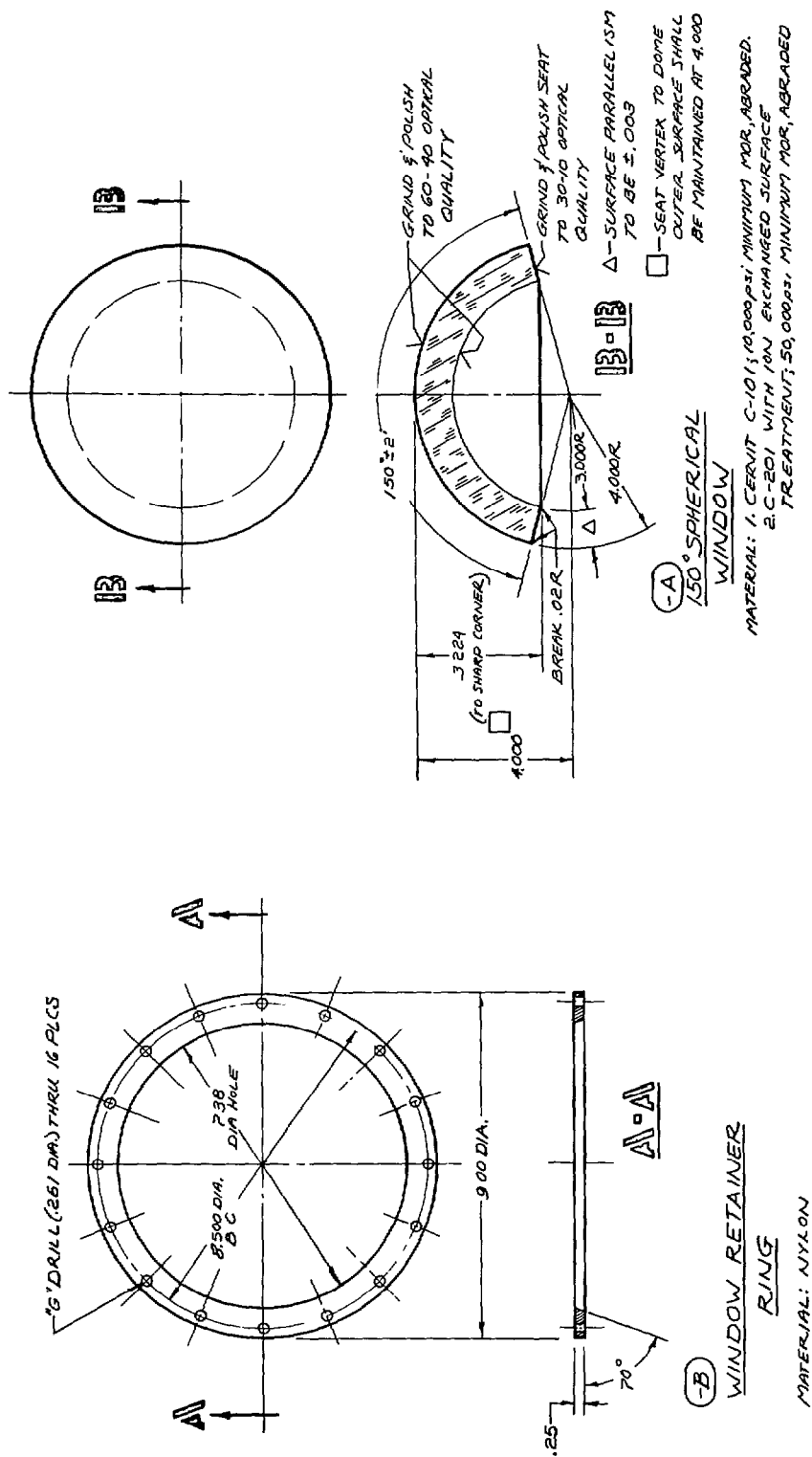
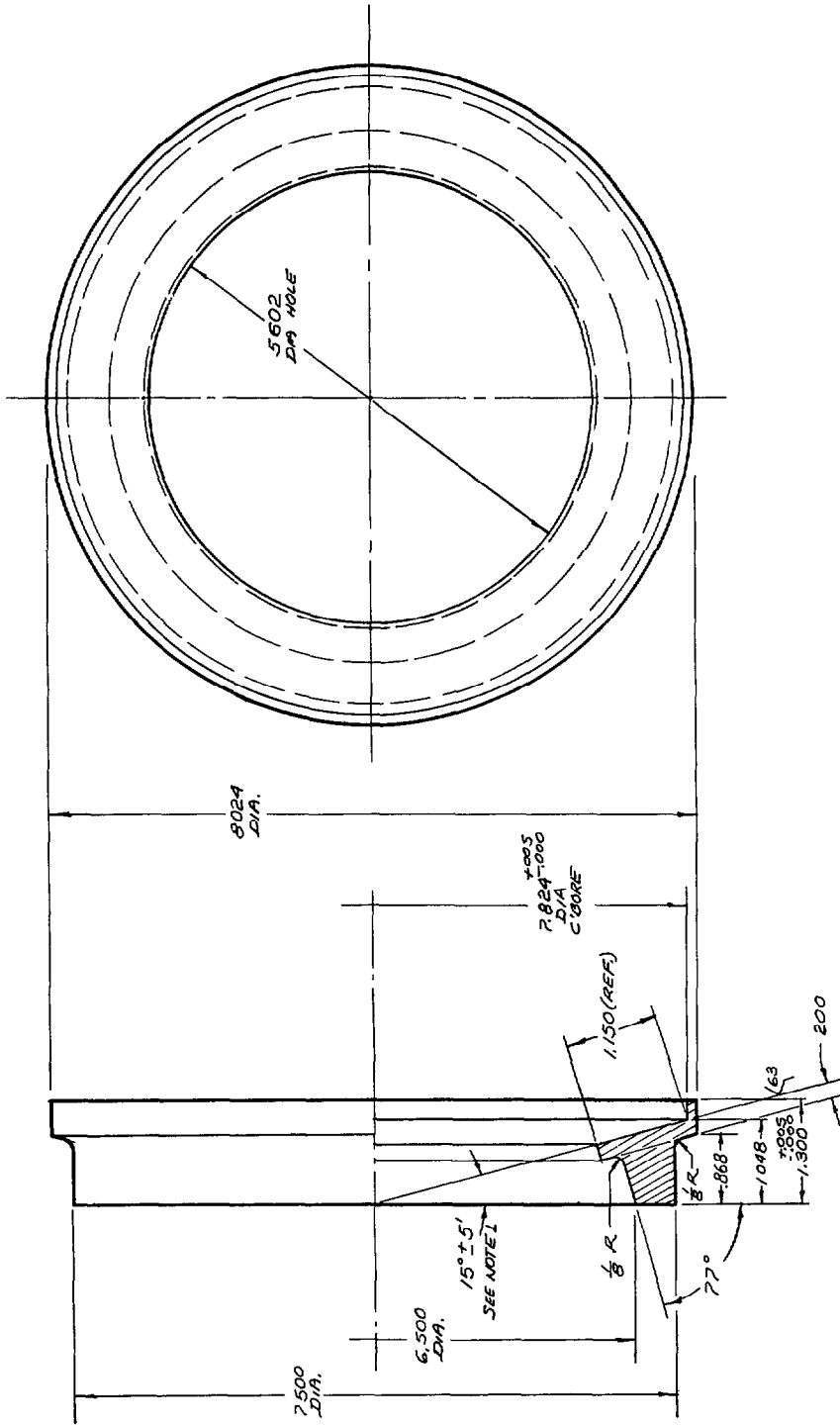


Figure 17. Spherical sector window for 20 000-psi Cervit glass. Glass ceramic and germanium windows have been built to this design.



NOTE: MATERIAL - MONEL K-500,
HEAT TREATED TO ROCKWELL
C-30 HARDNESS, MINIMUM
REQUIRED YIELD IS 100,000 psi.

Figure 18. Compliant metallic window seat for spherical sectors.

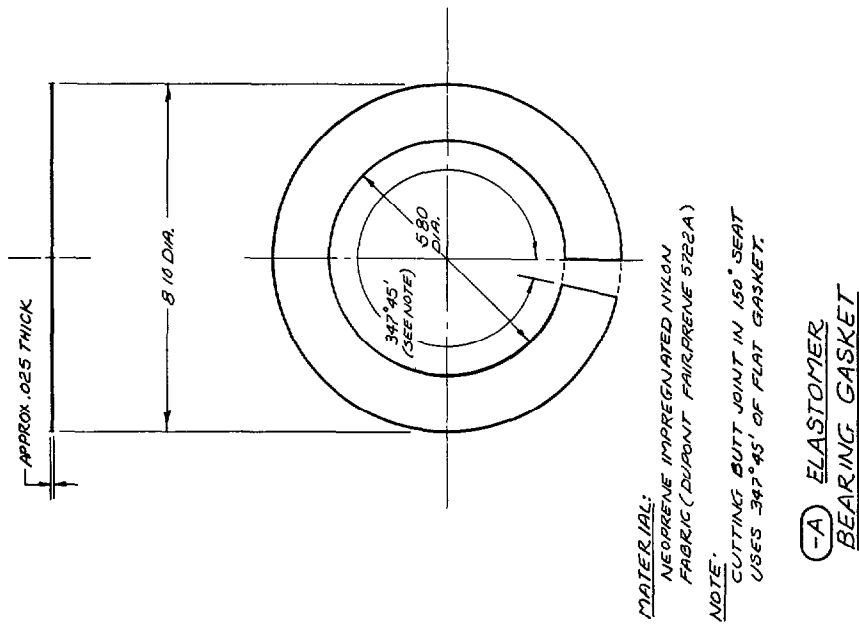
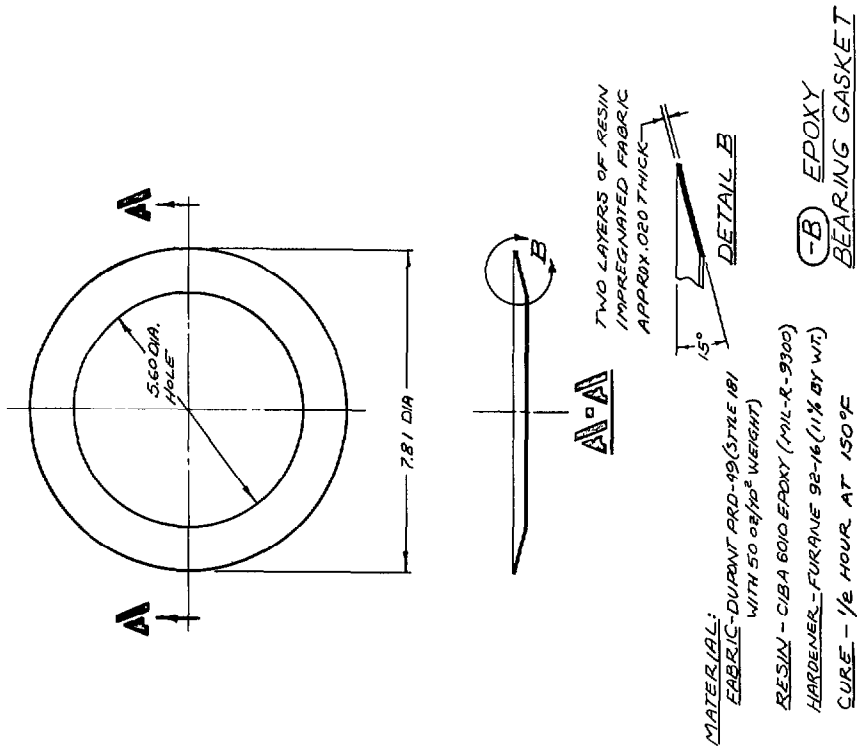


Figure 20. Gaskets for window seat.

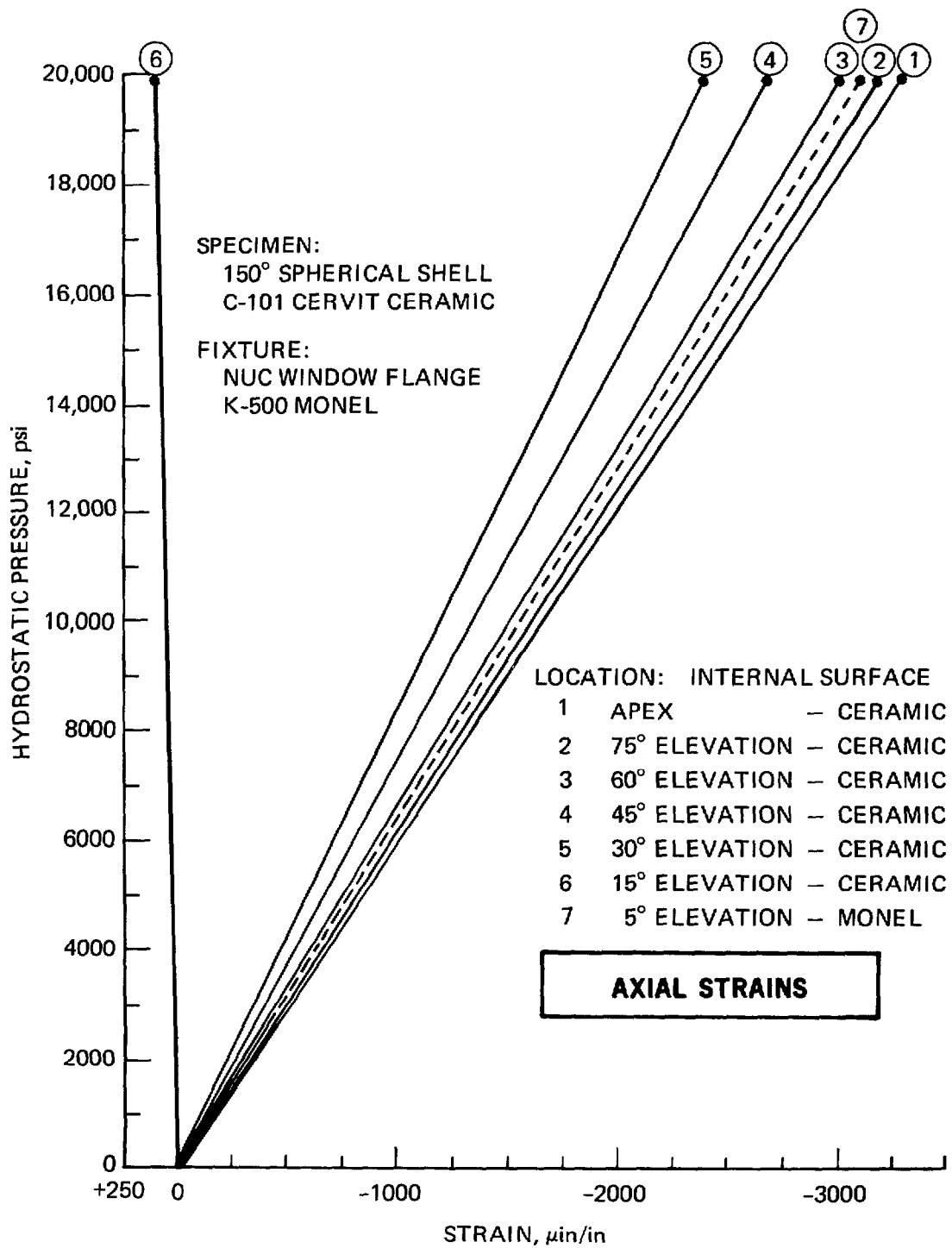


Figure 21. Axial strains measured along a meridian on the spherical sector window fabricated from Cervit C-101 glass ceramic. Note that the minimum value of the axial strain occurs on the concave surface near the edge of the window.

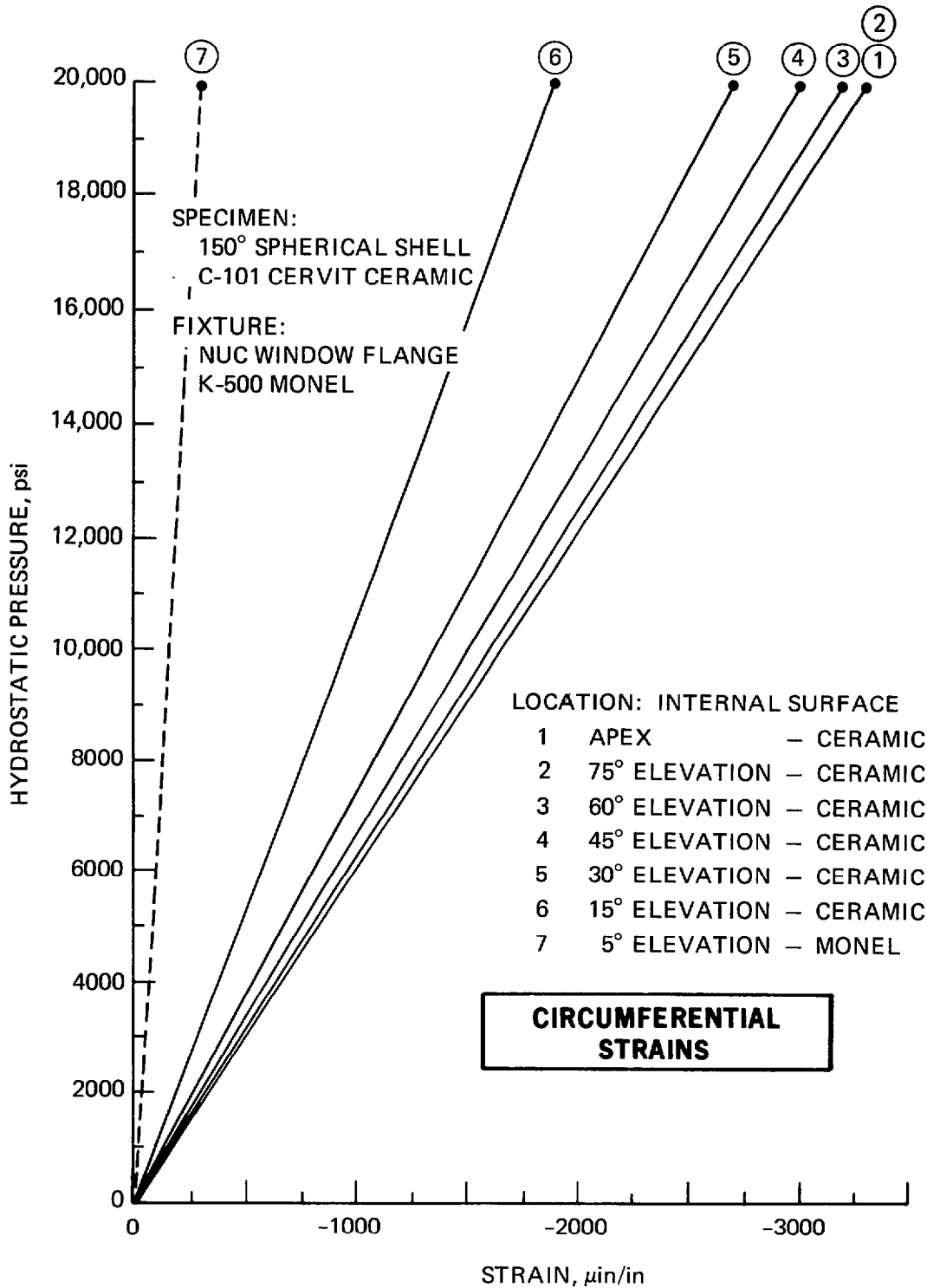


Figure 22. Circumferential strains measured on the same window as the axial strains on figure 21. Note that the window has a larger radial contraction than the window seat, resulting in sliding of the window upon the window seat.

3. Magnitude of size effect in germanium under compressive loading.
4. Stress corrosion threshold for germanium under long-term flexure loading.
5. Magnitude of Kaiser effect in germanium.

The first three items were of primary interest in the current study, while the fourth would be of extreme usefulness in the design of plane windows that are primarily subjected to flexure stresses. The last item would be of particular value in quality control, as it would permit the use of acoustic stress-wave emission techniques for determining the structural integrity of germanium windows prior to placement in service.

The average and guaranteed minimum flexural strengths were to be established by testing specimens to failure under short-term loading and comparing their ultimate stress values to those generated by other researchers. Because past experience has shown that the experimental values are heavily influenced by finish and dimensional tolerances on test specimens, steps were taken to ensure good finish and adherence to tight dimensional control (figures 23 and 24). This meant that in compressive test specimens the ends were chamfered, flat, at right angles to the axis of the cylinders, and parallel to each other. In flexure specimens, particular attention was paid to surface finish, absence of chips on the edges, and parallelism of all surfaces to the long axis of specimens. Although a pitch-polish finish could have been specified for the surfaces of flexure specimens to attain higher moduli of rupture, a ground finish corresponds closer to the finish found on bearing surfaces of germanium windows and, in addition, represents a conservative simulation of highly polished viewing surfaces on windows.

The stress corrosion threshold was to be established with flexure specimens subjected to different levels of long-term flexure in seawater. Identical test specimens subjected to the same flexure stress levels but in the absence of seawater would serve as control. Comparison of time intervals to failure for specimens in and out of water would give a fair indication of the stress corrosion effect.

The size effect in germanium under compressive loading would be measured by comparing the compressive stresses at moment of failure in large and small-diameter compressive specimens (1 and 0.5-inch diameters, and 2 and 1.5-inch lengths). Although the volumes of the two sizes of compressive test specimens varied only by a factor of approximately 5, this difference in volumes was considered to be adequate for establishing the presence or absence of the size effect in germanium. The presence of this effect has been established for brittle materials like concrete, rock, and glass and it was thought that there was a very high probability for its existence in germanium since it also is a very brittle material whose tensile or shear failure under compression could be triggered by the presence of internal flaws in the material. If the presence of the size effect were determined, the ultimate strength values determined with small test specimens would have to be discounted in proportion to the size of the germanium window for whose design they were to be utilized. On the other hand, the absence of size effect would allow the use of strength values established with small test specimens without any discounting for the design of large germanium windows.

The presence or absence of Kaiser effect would be established by pressurizing the germanium window several times to the same pressure level while the number of acoustic stress wave emission events was counted. If the number of events dropped off by at least an order of magnitude between the first and following pressurizations, it would be assumed that the Kaiser effect was present. If the effect were found to be present, it could be used

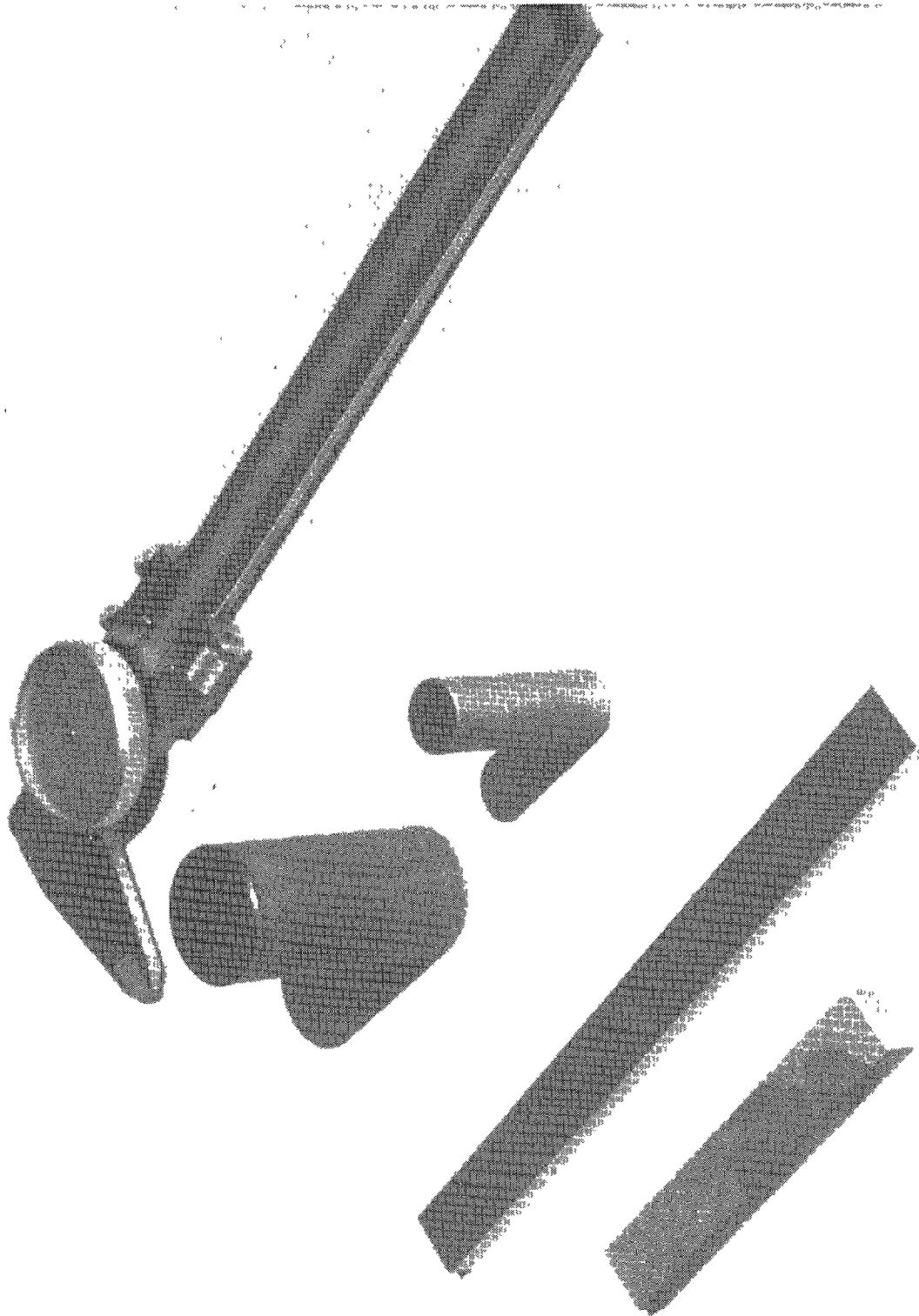


Figure 23. Germanium test specimens used for determination of its structural properties

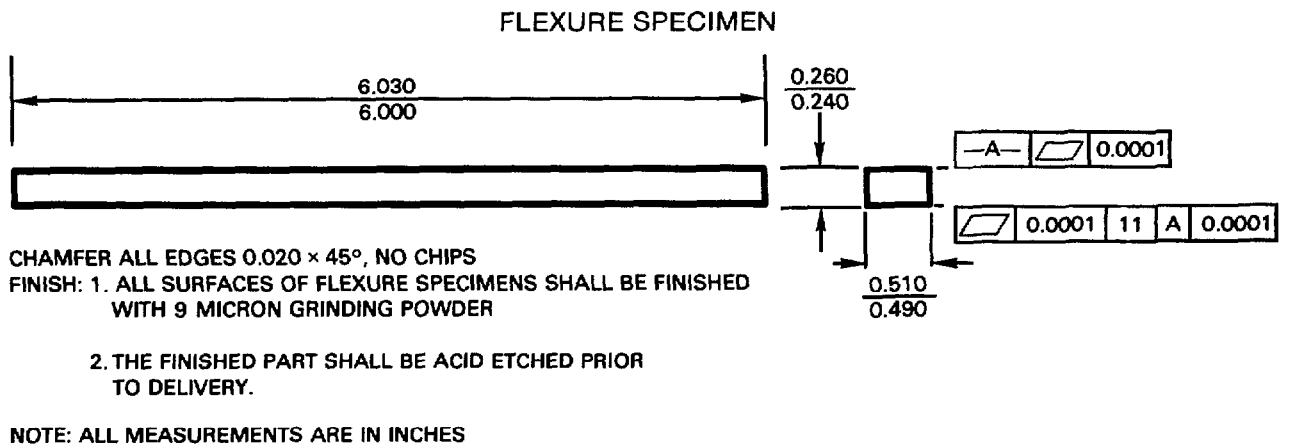
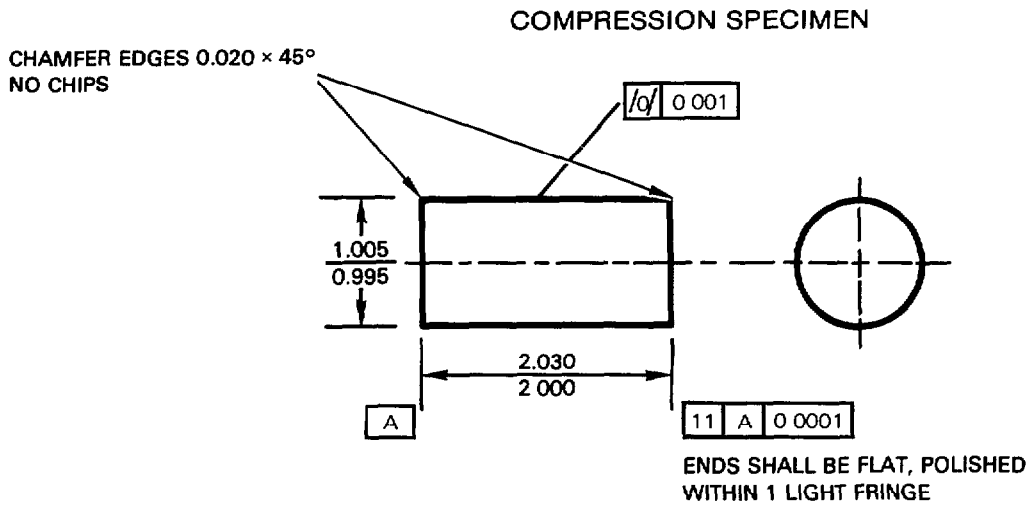


Figure 24. Dimensions of test specimens shown in figure 23.

very effectively as one of the nondestructive tests in a quality-assurance program during the procurement of new windows and subsequently during the periodic inspection of overhauled windows prior to return to service.

FABRICATION PROCESS

WINDOWS

Germanium windows were cast by Exotic Materials Inc. in the shape of spherical sectors in a graphite mold assembly. This approach minimized the amount of germanium which subsequently would have to be removed by grinding. For this reason, the convex and concave surfaces of the rough spherical sector conformed closely to the dimensions specified for the finished window (figure 25). The surfaces of the rough spherical sector had a finish of approximately $\sqrt{125}$, representing the mirror image of the machined surfaces on the graphite molds (figure 26).

To preclude the possibility of fracture during subsequent grinding and polishing, the cast spherical sectors were stress-relieved at 500°C for 24 hours in an argon atmosphere immediately followed by a 5-hour cool-down period. Although no quantitative measurements exist on the magnitude of residual stresses after such a stress-relief procedure, it is the consensus of germanium lens producers that the magnitude of remaining residual stress is not high enough to initiate fracture of the material in the presence of large microcracks generated by rough grinding.

Less than 0.10 inch had to be removed from the spherical surfaces of the germanium casting to meet the dimensional requirements specified for the finished window. Since the window was not to be used as an optical element but as a structural test specimen, no attempt was made to maintain optical figure on the convex and concave surfaces during polishing. The reason for polishing these surfaces was that such a surface aided in the visual detection of cracks generated during subsequent hydrostatic and hydrodynamic testing (figure 27).

Special attention was paid to the inclined bearing surface on the windows since the success of the spherical sector as a pressure-resistant window depended totally on the configuration and quality of finish on this surface. Since the magnitude of peak stresses in the bearing surface can be minimized only by elimination of point or line contacts with the seat on the metallic mounting, extra care was taken during fabrication and inspection to ensure that (1) the spherical angle of the bearing surface was within 2 minutes of specified value; (2) the profile of the bearing surface deviated less than 0.001 inch from a straight line; and (3) there were no chips present in the inner or outer chamfers. Furthermore, to minimize the presence of stress risers in the form of microcracks introduced into the surface of the window by grinding, the bearing surface was finished with progressively finer grinding powder until the last grinding operations were performed with a cast-iron lap and a slurry of 9-micron grinding powder (figure 28). Subsequently, the bearing surface was acid-etched by swabbing it with a mixture of hydrofluoric nitric and acetic acids. The objective of acid etching was to reduce further the magnitude of stress risers by reducing the depth-to-width ratio of microcracks not removed by grinding and lapping with the 9-micron grinding powder.

The convex and concave surfaces of the spherical sector were not subjected to acid etching as these surfaces would, during pressurization, see only compressive stresses, and thus acid etching would not contribute significantly to the structural performance of the

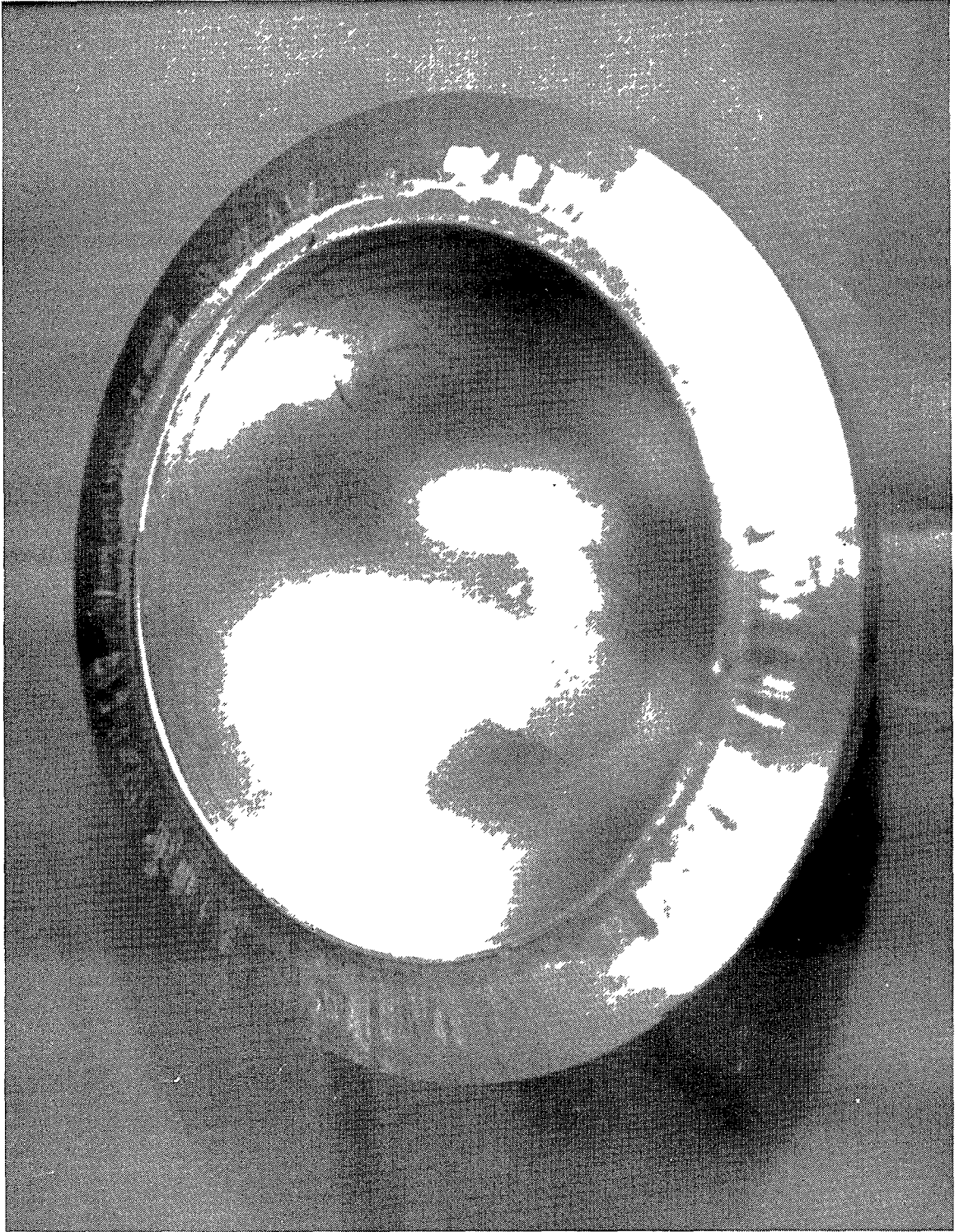


Figure 25. Germanium blank in the shape of spherical sector produced between matching male and female graphite molds.

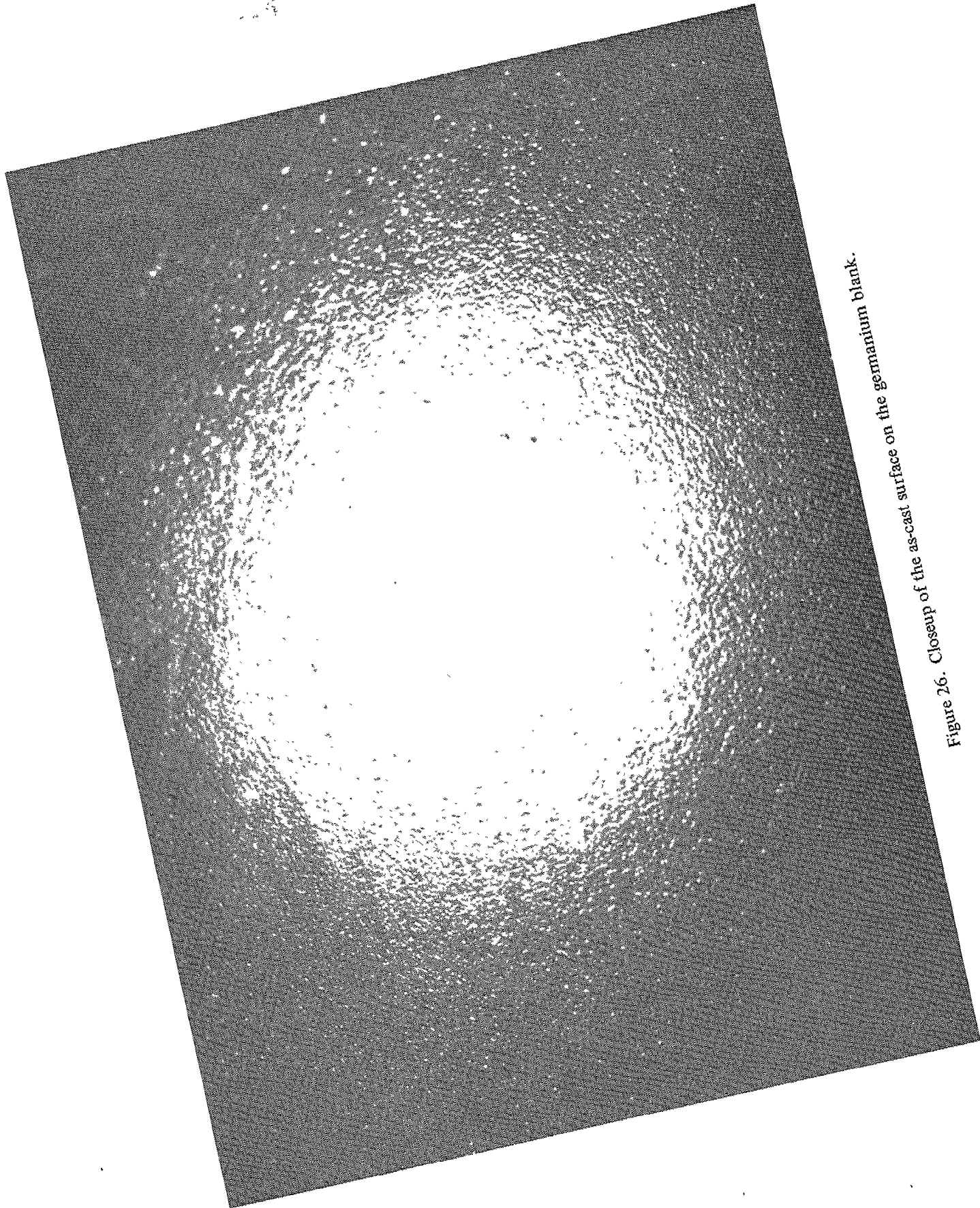


Figure 26. Closeup of the as-cast surface on the germanium blank.

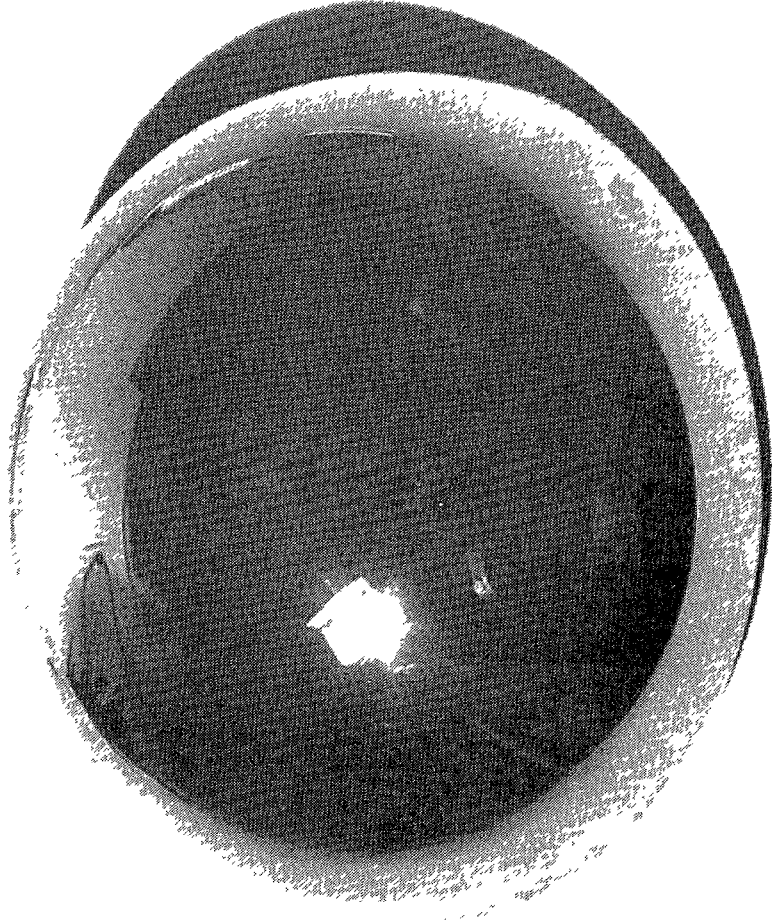


Figure 27. Exterior surface of the germanium sector after grinding and pitch polishing.

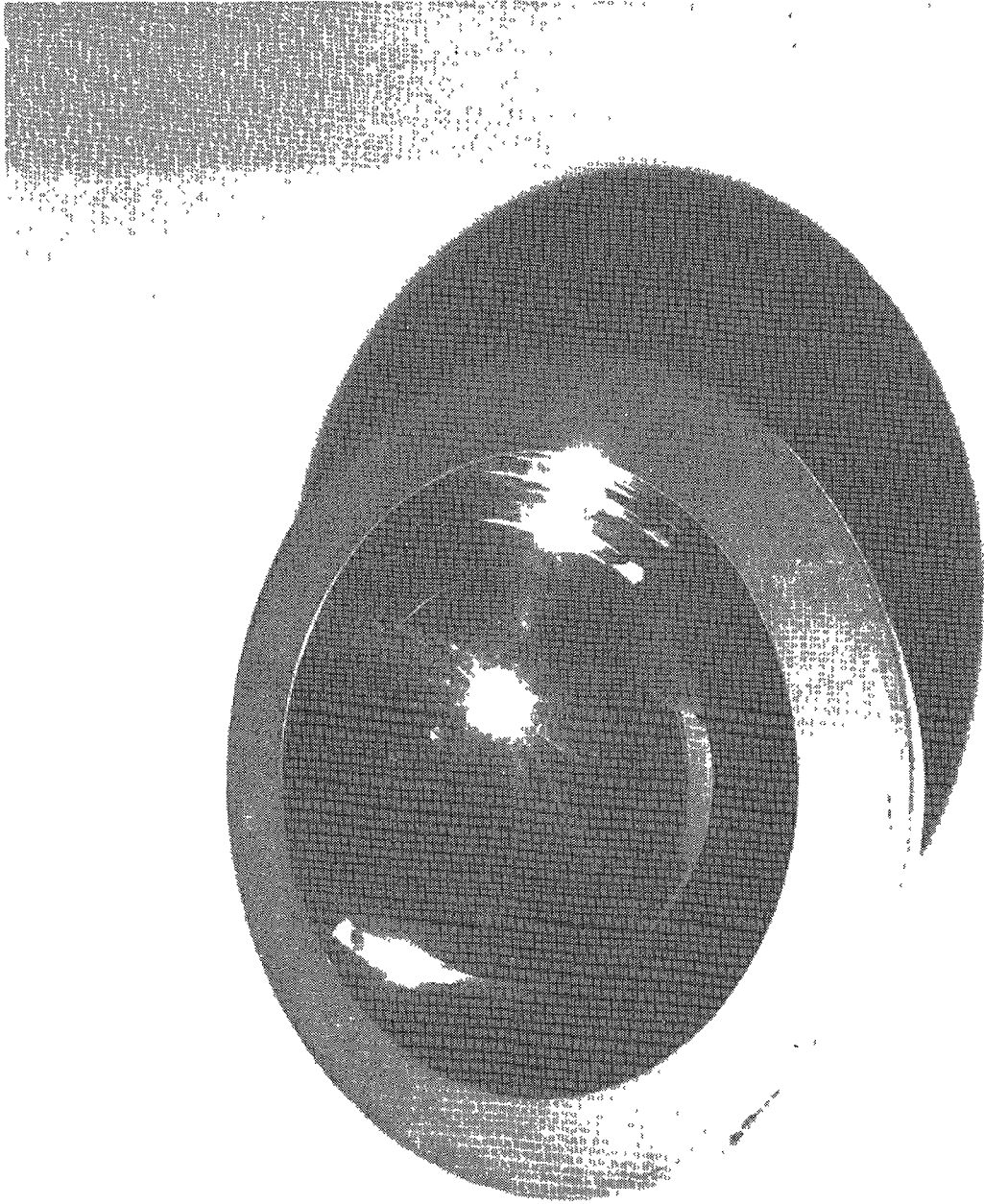


Figure 28. Interior surface of the germanium sector after grinding and pitch polishing.

sector. The case was different with the bearing surface, where besides compressive bearing stresses there were also some tensile stress components acting at right angles to the spherical surfaces of the sector. Although the magnitude of the nominal tensile stress is only a fraction of the compressive stress generated in the bearing surface by hydrostatic loading, the low tensile strength and brittle behavior of germanium make the peak stresses generated by tips of microcracks the probable source of fracture.

The sphericity and concentricity of the windows were measured to the nearest thousandth of an inch with a spherometer and dial indicator-equipped caliper, respectively. Both the sphericity and concentricity were found to be within dimensional tolerances called out on the drawing (figure 17). The conformance of the bearing surface to the specified angle was measured by placing the window on its cast-iron lap and establishing the magnitude of the gap between the mating surfaces of the window and the surface of the lap with a feeler gage. If the gap was less than 0.001 inch wide, the angle was considered to be within the specified angular tolerance. The profile of the bearing surface was measured by placing the edge of a brand-new razor blade across the width of the bearing surface and backlighting it with a 40-watt frosted lightbulb. If no light was visible underneath the edge of the razor blade, the surface flatness was considered to be acceptable.

MOUNTING

The mounting was fabricated by machining Monel K-500 ring forgings, heat-treated to Rockwell C-30 hardness. This material was chosen for its proven resistance to corrosion, tensile yield strength in excess of 100 000 psi, and a high modulus of elasticity which allowed matching the radial displacement of the compliant mounting to the radial displacement of the germanium sector over the whole pressure range from 0 to 20 000 psi without permanent deformation of the mounting (figures 18 and 29). To ensure proper fit with the sectors, the angle and the profile of the seat on the mounting were measured in the same manner as the bearing surface on the sector. Only if the seat passed the razor blade and feeler gage tests successfully was the mounting considered to be acceptable.

The plastic parts for the mounting assembly were made from Delrin and nylon, because of their proven resistance to seawater and weathering (figures 19 and 29). Plastics were chosen instead of metal for the nonload-bearing components of the assembly since their low modulus of elasticity would not impose any restraint on the window mounting during its radial and axial displacement when subjected to high hydrostatic pressure. The high radial compliance of the plastic mounting ring and of the window retainer ring made it possible for these plastic parts to maintain good fit with the metallic window mounting even when the metallic mounting had radially contracted under high hydrostatic pressure (figure 30).

GASKETS

Even though both the inclined bearing surface on the window and the inclined seat on the mounting were ground to very close angular and dimensional tolerances, a gasket had to be utilized which would preclude point or line contact between the two mating surfaces. Since the selection of the wrong gasket material would cause premature failure of the brittle germanium window, an extensive search was made of the technical literature on this subject. It became apparent very soon, however, that the choice is rather limited for applications where the bearing stresses are in the 40 000-to-50 000-psi range.

Past experience with gaskets for ceramic or glass windows supported by metallic seats has shown that the gasket must meet a very well defined set of physical requirements to

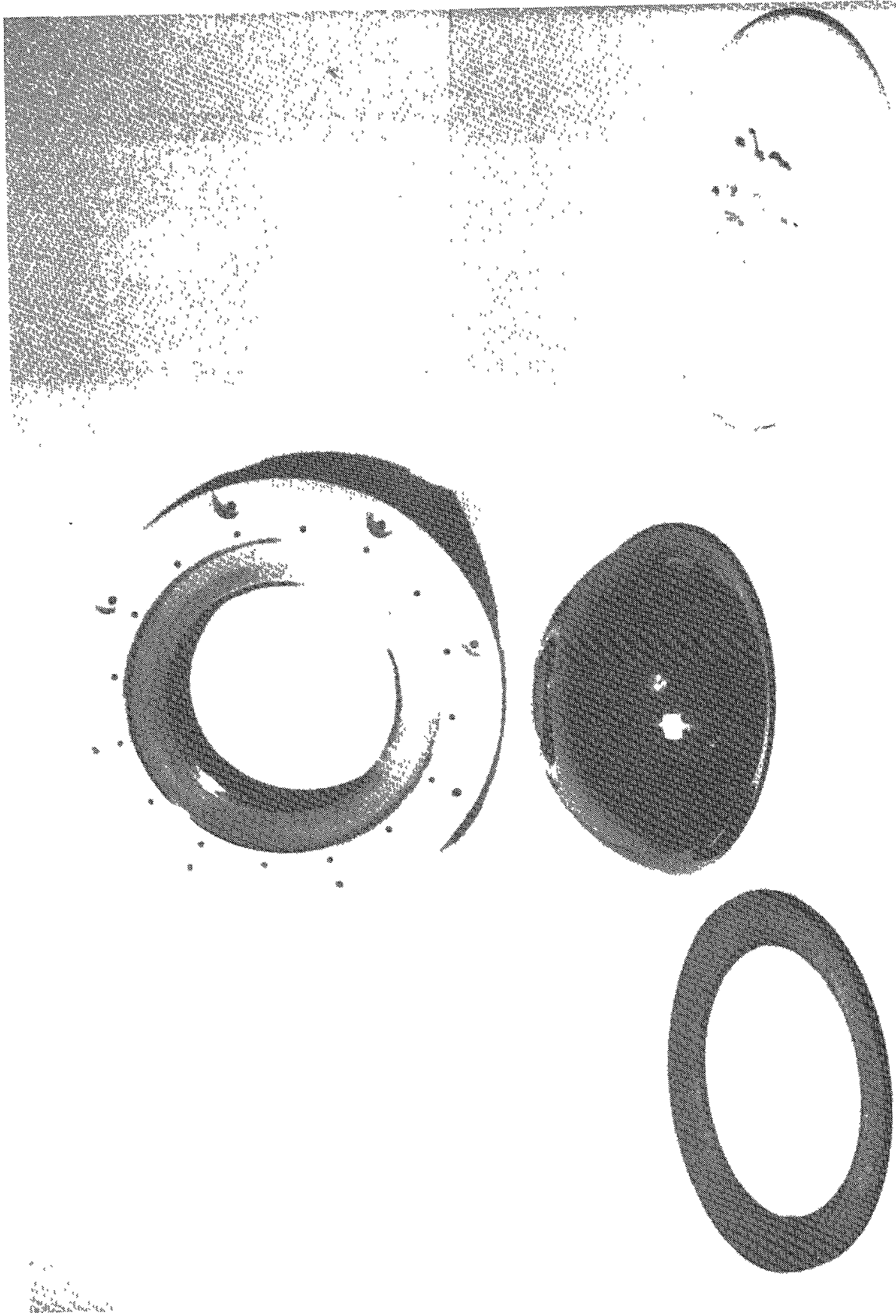


Figure 29. Components of the spherical sector window assembly.



Figure 30. Spherical sector window assembly.

preclude initiation of tensile fractures in the bearing surface of the dome (ref 2a). The physical requirements for a gasket under cyclic pressure may be summarized as follows.

1. The gasket shall not deform plastically under localized peak bearing stresses generated by point or line contact between the mating surfaces on the window and the seat.
2. The lateral movement of the gasket between mating bearing surfaces under design bearing pressure must be kept to a minimum.
3. The gasket shall accommodate local contacts between the mating bearing surfaces without generating peak stresses in the window's bearing surface in excess of the brittle material's compressive and tensile strengths.
4. The gasket shall resist wear and tear under repeated differential displacements between mating bearing surfaces.

These requirements eliminated metallic gaskets immediately since (a) if they were compliant enough to accommodate point contacts without generating high peak stresses in the mating surfaces, they also invariably deformed permanently, which made them unusable for cyclic applications (ie, lead, soft aluminum, copper, etc); or (b) if they were hard enough to withstand point contacts without permanent deformation, they also generated unacceptably high peak stresses in the hard, brittle bearing surface of the window (ie, hard aluminum, titanium, steel, etc).

A different problem presented itself with elastomers. Although they are very compliant, and will compress substantially under contact points between bearing surfaces without permanent deformation or generation of peak stresses in the high points on the bearing surface of the window, they will, because of their low modulus of elasticity, tend to squeeze out laterally from between the mating bearing surfaces. As a rule, the lateral strains become so large that the elastomeric material fails in tension between the mating surfaces and the two bearing surfaces come in contact. Similar problems exist with plastic gaskets, except that in this case the gasket deforms plastically before failing in tension because of the excessive magnitude of lateral strains.

The lateral displacement of the elastomeric or plastic gasket, besides contributing to the failure of the gasket, also amplifies the magnitude of tensile stress component in the bearing surface on the window. There are several approaches to minimizing the magnitude of lateral gasket displacement. These approaches are (1) decreasing the thickness of the gasket to absolute minimum (ie, 0.005 to 0.010 inch, depending on the magnitude of mismatch between the mating surfaces), so that the friction between the surfaces of the gasket and mating bearing surfaces will exert sufficient restraining force on the body of the gasket to keep it from squeezing out; (2) bonding the gasket to one of the bearing surfaces and in this manner augmenting the restraining friction force on the body of the gasket; and (3) a combination of approaches (1) and (2). All of these approaches work best when the radial contraction of the window matches that of the seat in which it is mounted

Obviously, the ideal gasket should be very compliant axially (for example, elastomers or plastics), at the same time remaining very still in the transverse direction. This can be accomplished by using a composite whose matrix is a compliant elastomer or plastic, while ensuring that the reinforcing fibers lying in the plane of the bearing surface are made up of a less compliant material. Through trial and error, it has been established in prior studies that

nylon cloth is an excellent reinforcing material for neoprene, while Kevlar-49 is ideally suited for epoxy plastic. To function properly, both the composite neoprene and epoxy gaskets must be less than 0.030 inch thick, with the reinforcing cloth inside the gasket being preferably one, and at the most two, layers thick.

The composite gasket of neoprene and nylon cloth is particularly suited for bearing surfaces with a weak modulus of rupture (flexural strength < 5000 psi) under bearing stresses in the 0-to-20 000-psi range. To function properly, the nylon cloth-reinforced neoprene gasket must (1) be the same width as the bearing surface on the window and (2) be bonded to the bearing surface on the window rather than the metallic seat, as otherwise the bow wave formed in the elastomeric gasket by the edge of the bearing surface on the window will act as a mechanical detent, causing the gasket to tear (figure 31). The gasket is generally fabricated by cutting a strip from commercially available nylon cloth-reinforced neoprene sheet and bonding it with a flexible contact cement to the bearing surface on the window.

The only major shortcoming of this composite gasket is its short cyclic fatigue life, particularly when the bearing stresses exceed 20 000 psi. Past studies show that under a bearing stress of 20 000 psi, the minimum cyclic fatigue life of the nylon cloth-reinforced gasket bonded to the brittle window and sliding upon a metallic seat with a finish of 32 rms is at least 300 cycles; at 40 000 psi, it is only 100 cycles.

The cyclic fatigue life of the gasket can be extended somewhat by polishing the surface on the metallic seat and coating it lightly with grease. This facilitates sliding of the gasket upon the metallic surface and thus minimizes the wear and tear on the gasket surface in contact with the metallic seat. The other surface of the gasket sees very little wear, as the adhesive prevents any relative displacement of the gasket with respect to the bearing surface on the window.

If the relative displacement between the window and the seat could be totally eliminated, there is no doubt that the cyclic fatigue life of the nylon-reinforced Neoprene gasket could be extended by at least a factor of 10. Since the relative radial displacement between the germanium sector and the Monel K-500 mounting in this study is the range of 0.001 and 0.010 inch, some wear was expected to take place on the neoprene gasket, particularly at bearing stress levels in excess of 20 000 psi.

The Kevlar-49 cloth-reinforced epoxy gasket is particularly well suited for windows fabricated from brittle material of medium strength ($5000 \leq \text{MOR} \leq 10\,000$ psi for ground finish) whose bearing surfaces are subjected to a bearing stress in the 30 000-to-60 000-psi range. To function properly, the Kevlar-49-reinforced epoxy gasket must (1) extend past the edges of the bearing surface on the window; (2) have smooth finish on both sides; and (3) be retained between mating bearing surfaces without bonding to either surface.

The requirements for polished surfaces on the gasket and absence of bonding are the result of the gasket's stiffness in both axial and hoop orientation. If such a gasket were bonded to the window, the radial force generated by radial movement of the window would shear the bond between the window and the gasket, damaging the bearing surface on the window, on the gasket, or both. The incorporation of smooth surfaces on the gasket circumvents this problem, as it facilitates the differential radial displacement between the window and the seat by allowing some of the sliding to take place on the upper, and some on the lower, surface of the gasket. The gasket is generally fabricated by placing one or two strips of Kevlar-49 cloth soaked in epoxy resin between male and female molds whose polished surfaces duplicate the configuration of the bearing surfaces on the window and the seat, and curing the composite under application of heat and axial compression. The resulting gasket is free of voids, is hard, and has very smooth surfaces.



Figure 31. Cleaning and inspection of the window's bearing surface prior to bonding of Fairprene 5722A gasket.

If some doubt exists on the ability of the hard gasket to accommodate large angular mismatches between the window and the seat without generation of excessively high peak stresses in the brittle window material, a nylon cloth-reinforced Neoprene gasket may be inserted between the Kevlar-49-epoxy composite gasket and the metallic seat. By placing the hard plastic gasket with smooth surfaces on top of the soft elastomeric gasket, the desirable attributes of both gaskets can be combined, which makes this assembly very attractive for mating surfaces under bearing stresses in the 20 000-to-40 000-psi range. By combining the two gaskets, the wear and tear on the elastomeric gasket will be decreased significantly since most of the differential displacement between the window and the seat takes place on the smooth upper surface of the stiff plastic gasket, while the soft elastomeric gasket, which is bonded to the lower surface of the plastic gasket, provides an elastic foundation for the significantly stiffer plastic gasket above. The application of the combined gaskets appears to be limited to bearing stresses below 40 000 psi, as at higher stress levels the edges of the window may shear the plastic gasket.

TEST SPECIMENS

The germanium test specimens were prepared by coring and sawing blanks from flat slabs, and subsequently grinding them to final dimensions. Since the surface finish on test specimens largely determines the test results obtained in flexure and compression testing, special care was taken in preparing the surfaces of test specimens.

Although it is known that pitch-polished surfaces on flexure specimens generate highest MOR (modulus of rupture) values for any brittle material, pitch polish was not utilized as (1) it contributes to wide dispersion of test data and (2) it is not representative of finishes on surfaces of windows which saw extensive service in the marine environment. Thus to decrease the dispersion of test values and to make them more representative of material strength in weathered windows, the surfaces on all test specimens were finish-ground with 9-micron grinding powder. Particular attention was paid to chamfers as past experience has shown that the presence of even fine chips on chamfers will significantly decrease the MOR of specimens even if all the other surfaces are polished.

The only departure from a fine ground finish was on the bearing surfaces of cylinders which were pitch-polished. Pitch-polishing these surfaces was not done in an attempt to increase the compressive strength of cylinders (particularly since a fine quality of finish on these surfaces does not contribute to an increase in test values), but to permit utilization of optical techniques for measurement of flatness and parallelism. Subsequent inspection of these surfaces with an optical flat showed less than one interference fringe over the total width of the bearing surface.

EXPERIMENTAL EVALUATION

WINDOWS

Instrumentation

Instrumentation for hydrostatic testing of windows consisted of two piezoelectric transducers bonded to the concave surface of the window at its center and near its edge. These transducers were connected to two amplifiers which provided a 60-dB amplification of the signal. The output of the amplifiers was connected to event counters.

Straingages were not used as strain data were available from prior tests in which straingaged Cervit C101 windows were tested in identical seats to 20 000-psi hydrostatic pressure (ref 20). Since the modulus of elasticity of Cervit C101 ceramic is similar to germanium, data generated by these tests can be also applied without any mathematical manipulation to germanium windows.

Assembly of Test Fixture

Each window was placed into a test fixture which simulated the operational window assembly mounted on an instrumentation housing. The major departures from an operational configuration (figure 30) consisted of two simple, inexpensive substitutions: (1) a mounting ring of PVC plastic for the Delrin mounting ring; and (2) a steel bulkhead for a large instrumentation housing. These substitutions allowed testing of the window assemblies in an inexpensive 10-inch-diameter pressure vessel instead of an expensive large-diameter vessel.

Two kinds of gaskets were utilized in the window assembly. For the cyclic pressure tests with a maximum pressure of $\leq 13\ 500$ psi, nylon cloth-reinforced neoprene gaskets of 0.020-inch thickness (Fairprene 5722A) were utilized. The assembly of the test fixture consisted of the following:

1. Cleaning the bearing surface on the window with acetone (figure 31).
2. Brushing on a coat of Pliobond contact adhesive on both the germanium bearing surface and one side of the gasket (figure 32).
3. Placing the gasket, tacky surface down, on the germanium bearing surface. Particular attention was paid to (a) centering of the gasket on the bearing surface and (b) elimination of any wrinkles in the gasket.
4. Cutting off surplus gasket length with a razor blade without nicking the bearing surface (figure 33). Great care was taken to cut the gasket in such a manner that the two ends of the bonded gasket butted together without an overlap or gap (figure 34).
5. Placing the gasketed window on its steel seat, which has been already inserted into the PVC mounting ring bolted to the top of the steel bulkhead (figures 35 and 36).
6. Inserting the O-ring seal into the annular space between the outside diameter of the window and the lip on the window seat (figure 37).
7. Placing the window retainer on top of the mounting ring (figure 38) and bolting it down securely with stainless steel screws to the mounting ring (figure 39). Torquing down the screws accomplishes two things: it secures the window in its seat and it compresses the O-ring for a secure seal (figure 40).
8. Attaching the window test fixture to the end closure of a pressure vessel by means of a threaded pipe that serves as a feedthrough for the instrumentation wires (figure 41).

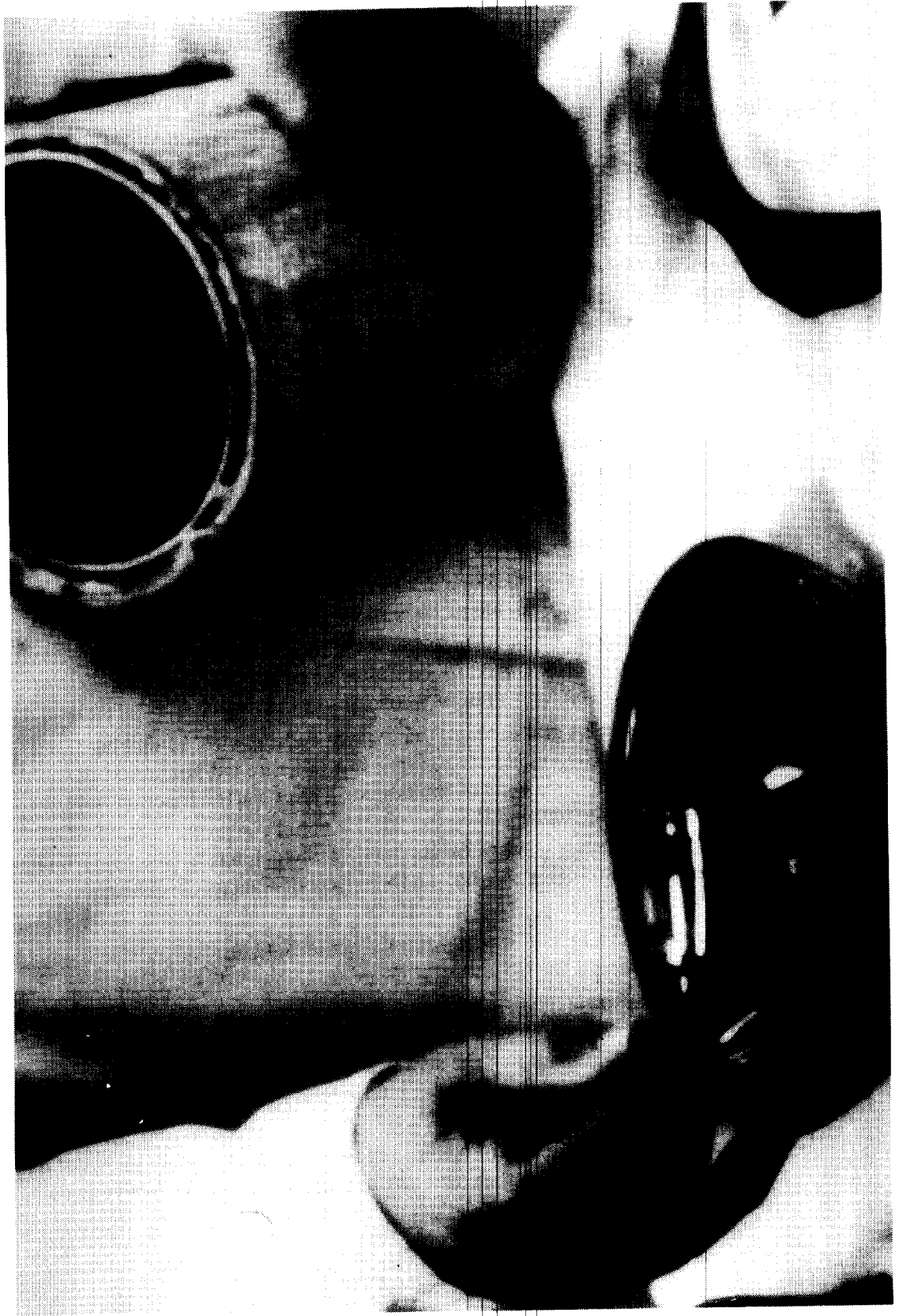


Figure 32. Application of rubber contact cement to both the window bearing surface and the Fairprene 5722A gasket.



Figure 33. Trimming the end of the gasket for a perfect butt joint.

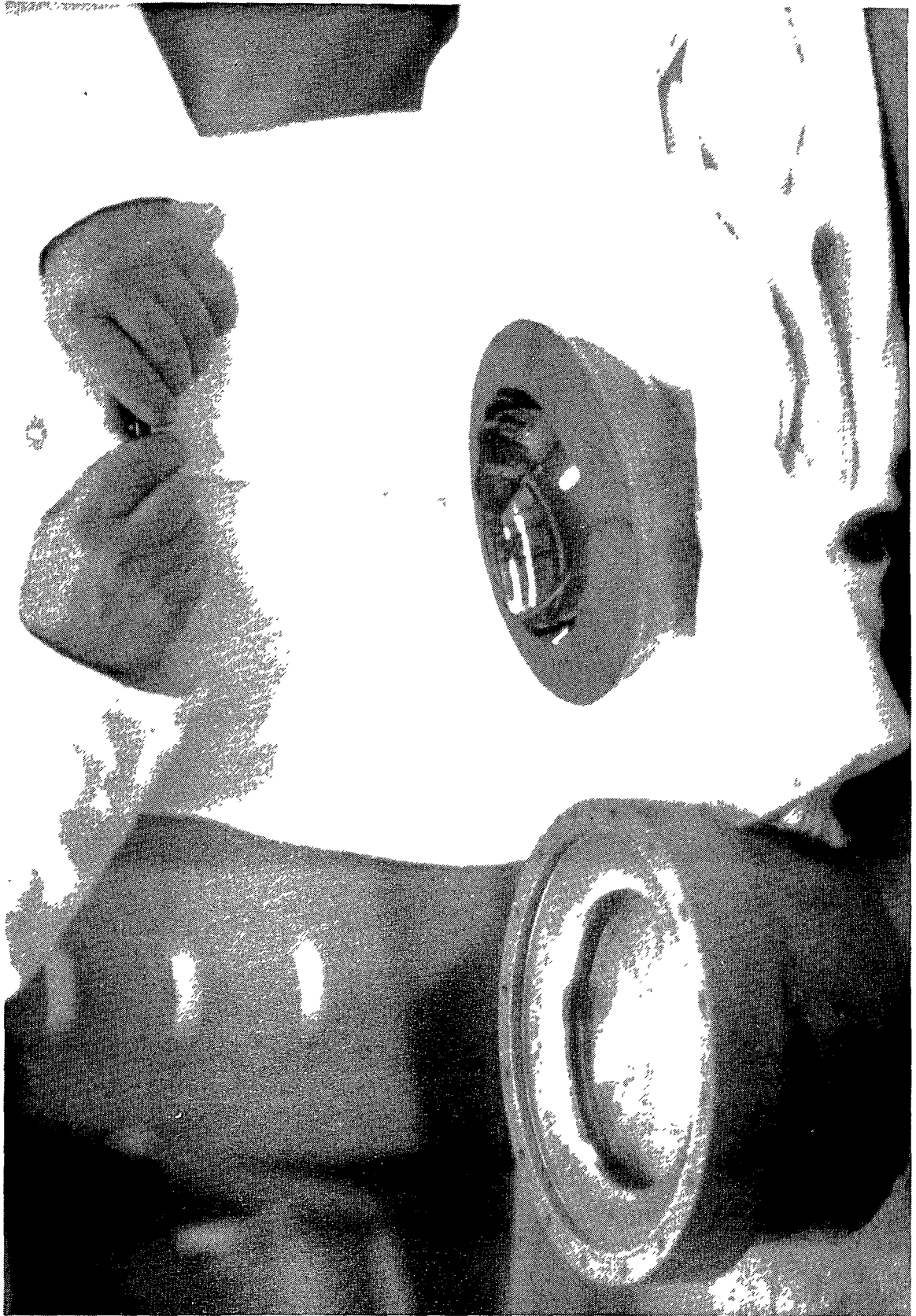


Figure 34. Inspecting the joint on the bonded gasket.

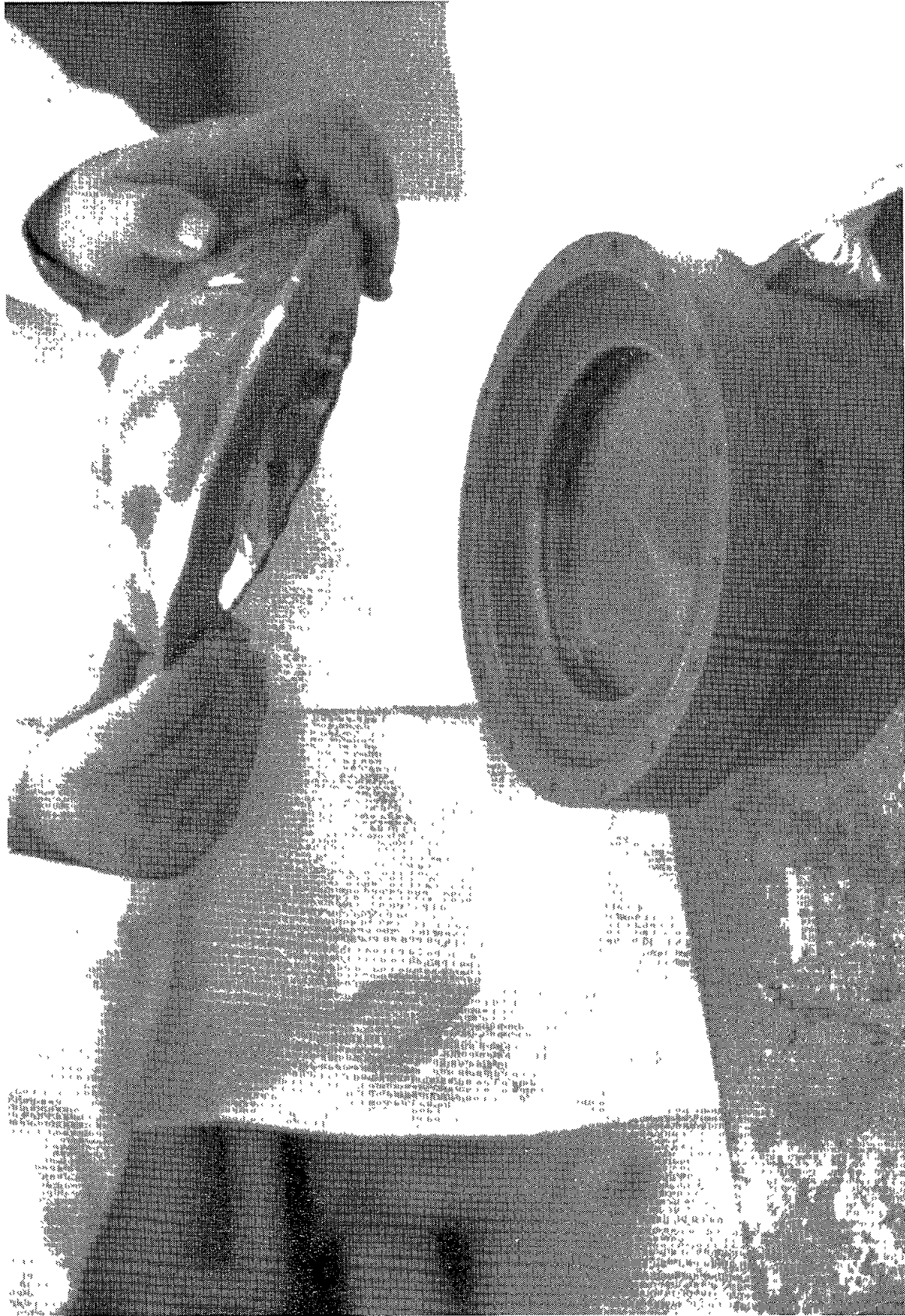


Figure 35. Placing the gasketed window on the window seat.

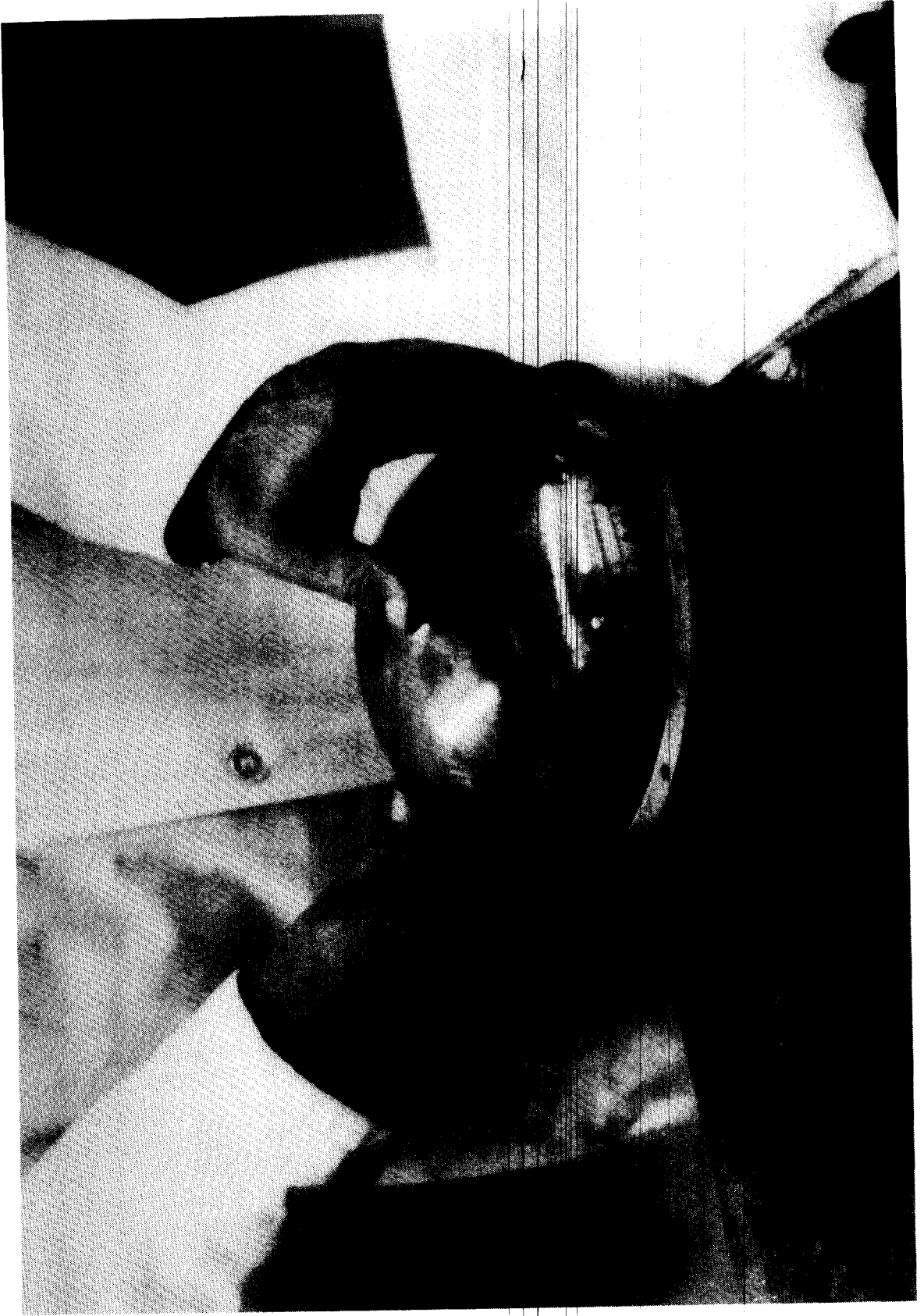


Figure 36. Centering the gasketed window on the seat.

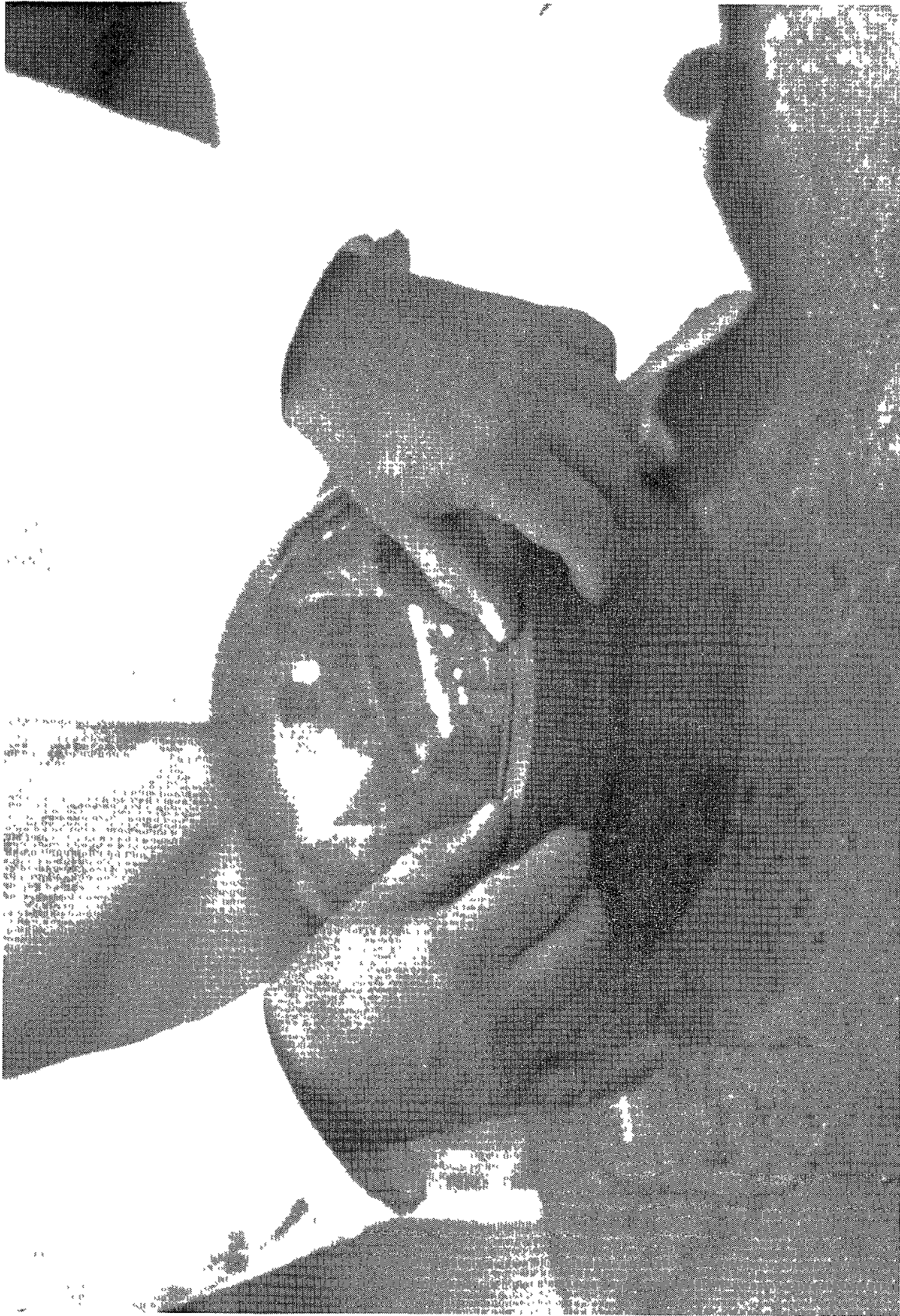


Figure 37. Squeezing the O-ring between the edge of the window and the lip on the window seat.

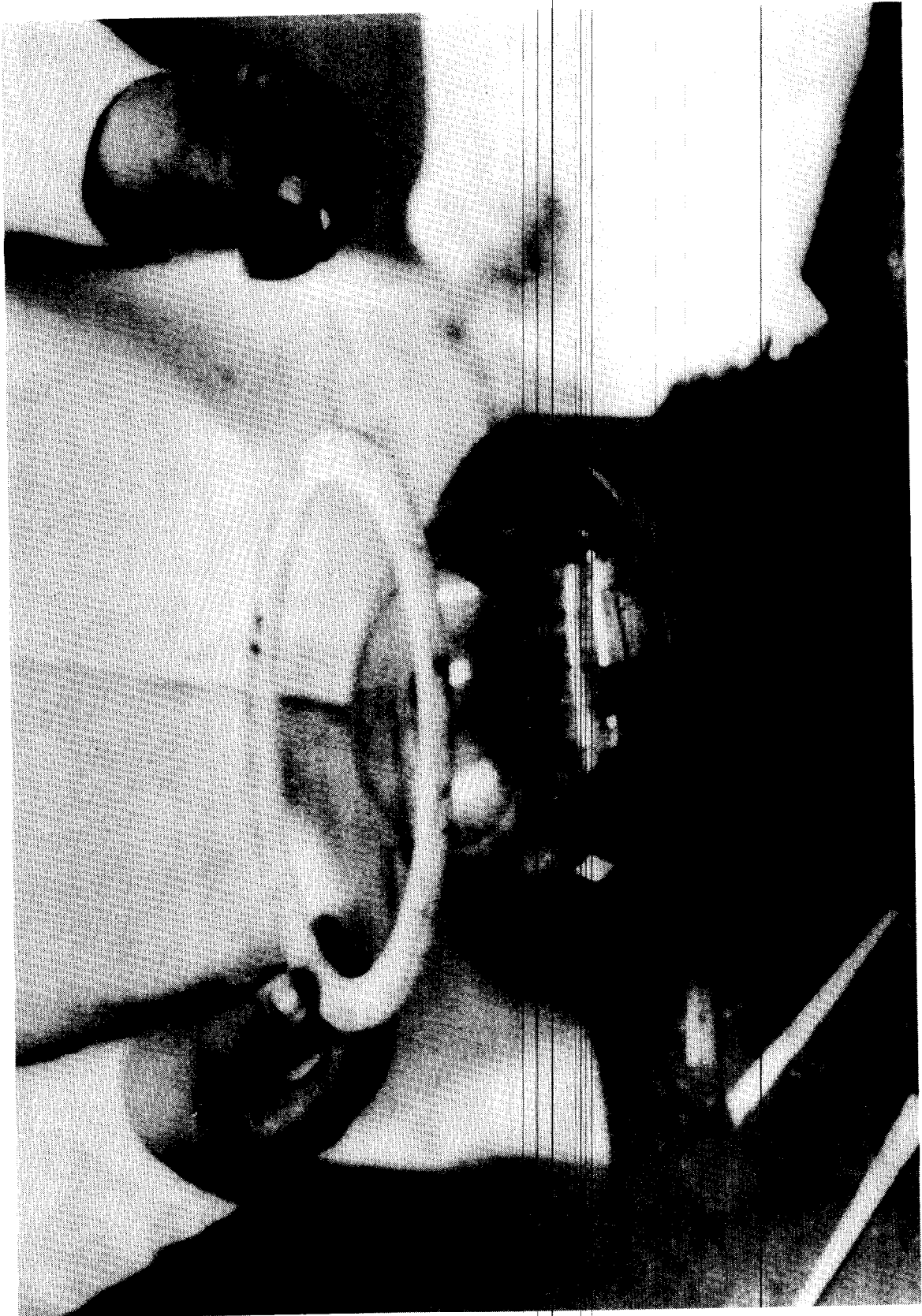


Figure 38. Placing the window retainer on top of the window.



Figure 39. Fastening the window retainer to the window seat with screws.



Figure 40. Completed window test assembly.

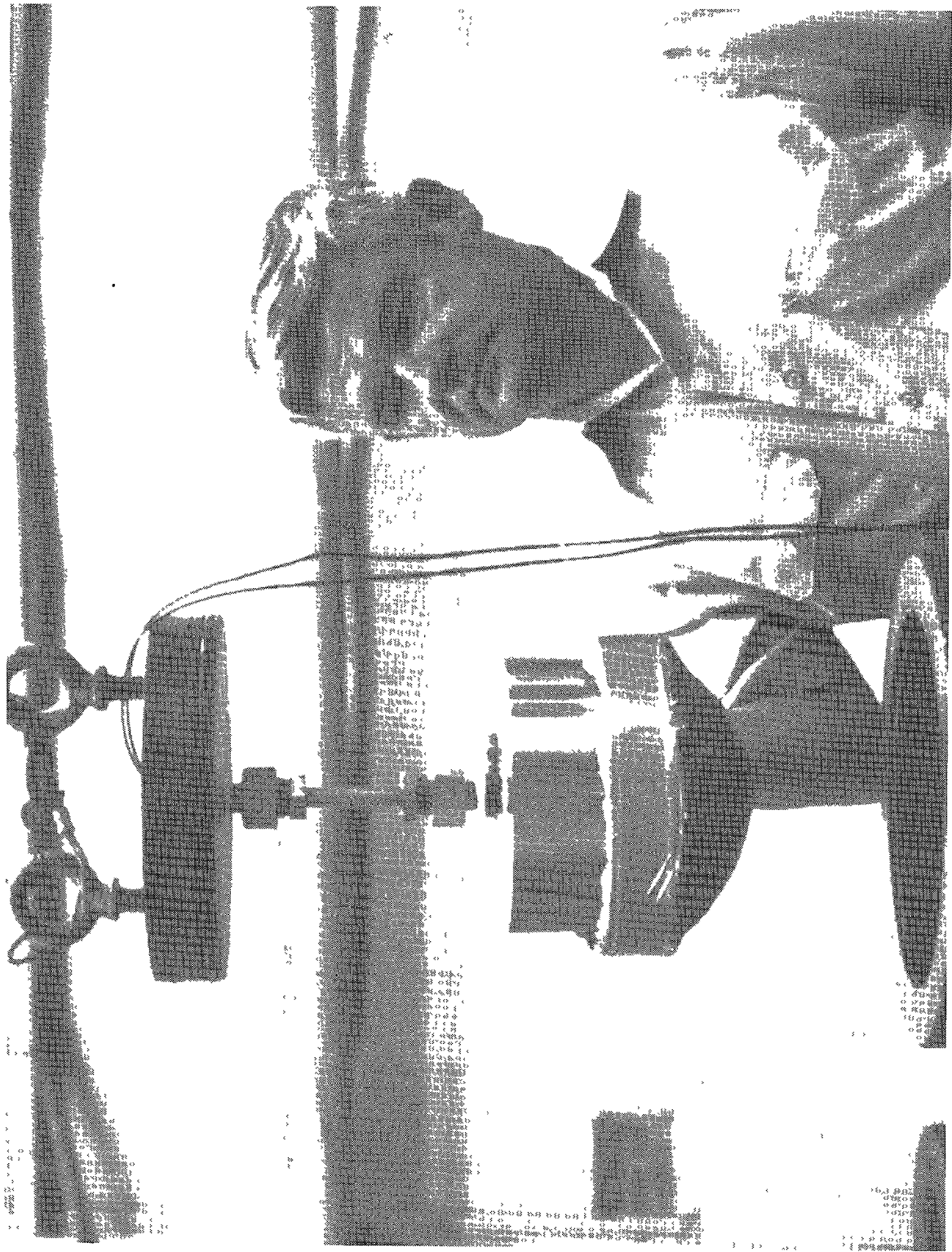


Figure 41. Window test assembly attached to a heavy steel bulkhead, which in turn is suspended by a pipe from the pressure vessel end closure.

Test Procedure

The test procedure for evaluation of germanium windows consisted of the following.

1. Hydrostatic Pressurization. The pressure vessel end closure with the attached window test fixture was placed in a 10-inch-diameter pressure vessel filled with tap water (figure 41) and an air-operated pump with pressure cycling capability was connected to the vessel. The pump was programmed to pressurize the vessel at a 1000-psi/minute rate, maintain the preset maximum pressure for 4 hours, depressurize the vessel at a 10 000-psi/minute rate, and allow the vessel to relax at 0 psi for 4 hours.

Four different cycling schedules, differing only in the magnitude of the maximum pressure, were applied to four separate window test assemblies. The cycling schedules were as follows:

- 0-4500 psi, 100 cycles, on Fairprene gasket; acoustic emissions were measured during the 1st, 2nd, and 100th cycle.
- 0-9000 psi, 100 cycles, on Fairprene gasket.
- 0-13 500 psi, 100 cycles, on Fairprene gasket.
- 0-20 000 psi, 100 cycles, on Fairprene/Kevlar-49 epoxy gasket combination.

At the conclusion of each pressure-cycling schedule, the test fixture was taken apart and the window and gasket inspected visually for wear and presence of cracks.

2. Dynamic Pressurization. The window test fixture was placed in a specially prepared framework which held the upward facing germanium window at a preset distance from an explosive charge above (figure 42). Only nylon-reinforced neoprene gaskets were used on the window seats since no particular benefit was to be derived from using the Kevlar-49-reinforced epoxy/nylon-reinforced neoprene gasket combination under the extremely short bearing pressure application. The window test fixture was covered with a heavy cloth to prevent metallic fragments emitted by the charge detonator from impacting the window and possibly chipping it. The framework, with the window test fixture and a 1.1-gm explosive charge mounted in place, was lowered into a 30-inch-diameter pressure vessel with a 13 500-psi pressure rating.

The test procedure consisted of (a) pressurizing with a pump the interior of the pressure vessel to 450 psi; (b) exploding the charge; (c) dropping the pressure to 0 psi; (d) removing the window test fixture from the framework; (e) disassembling the window test fixture and inspecting the window for damage; (f) reassembling the window test fixture; (g) attaching a new charge to the framework at a closer distance to the window; (h) inserting the framework into the pressure vessel; (i) pressurizing the vessel to 450 psi; and (j) setting the charge off again. The standoff distances for the explosive charges were 4, 3, 2, and 1 feet.

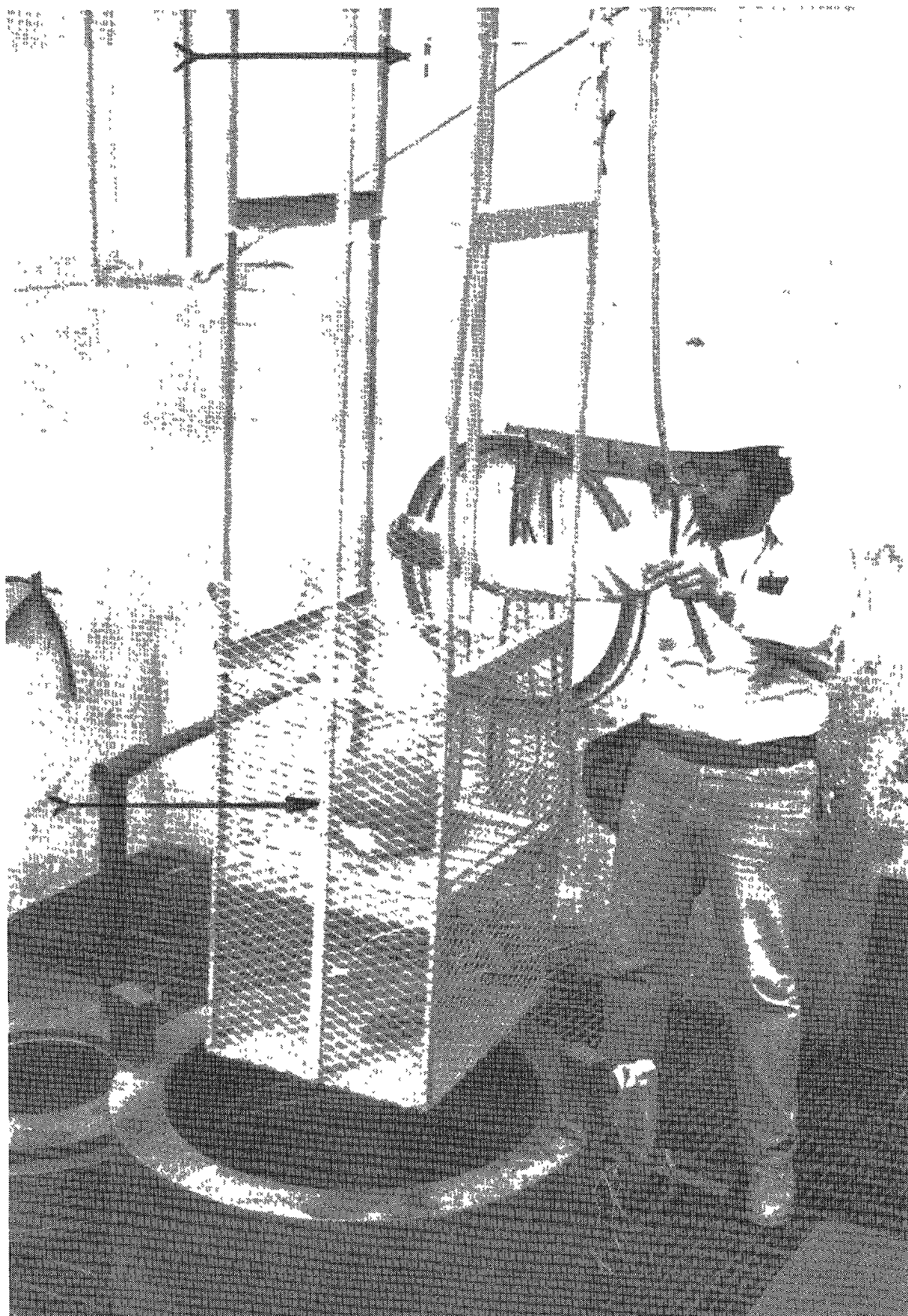


Figure 42. Framework for securing the window test assembly during dynamic pressure testing. Note that the explosive charge is suspended from a wire 4 feet above the window test assembly.

MATERIAL TEST SPECIMENS

Instrumentation

The only instrumentation utilized in the testing of material test specimens were load cells which accurately indicated the magnitude of force applied during testing.

Test Fixtures

Standard load application fixtures were utilized in the short-term flexure and compression testing (figures 43 and 44). The sole component which was custom made for the test fixtures consisted of conical steel anvils whose minor diameter matched the diameter of germanium cylinders utilized in compression testing (figure 44). Both the 20° included angle and the Rockwell C 60 hardness of the anvil were based on experience with compression testing of glass, ceramic, and other brittle material specimens. It was found that this anvil configuration, anvil material, quality of bearing surfaces, and absence of gaskets were conducive to the generation of high test values during compression testing.

A special load application fixture was designed and utilized for long-term flexure testing in room temperature and seawater environments (figure 45). The test fixture consisted of an acrylic plastic tank with integral specimen holders and removable Monel rods. The removable rods served as sliding surfaces for nylon strings which were used for suspension of dead weights. By half-filling the tank with water, only one-half of the test specimen was submerged in seawater during the test while the other half was kept dry. In this manner, the comparison of test data from the wet and dry portions of the test specimen would not be contaminated by other test variables, such as differences in temperature, load application procedure, and specimen holder design.

Test Procedure

Short-term compression testing was performed by carefully centering the compression test specimen on the bare anvils and applying compression at 0.05 inch per minute cross-head speed until fracture of the specimen took place. There were some deviations to this standard test procedure.

For some of the tests, nylon-reinforced neoprene or Kevlar-49-reinforced epoxy gaskets were placed on top of the anvils to determine the effect of such gaskets on the compressive-strength test values. During some other tests, the application of compressive load was terminated prior to failure of the specimen so that the incipient fractures present in the material could be inspected. In still other tests, the specimens were loaded repeatedly to approximately 93 percent of the average ultimate compression strength value to get an indication of the low cycle fatigue life under compression loading.

Short-term flexure testing was performed with a three-point load application fixture bearing directly against the test specimens (figure 43). The load was applied at a 0.02-inch-per-minute rate until fracture of the specimens took place.

Long-term flexure testing was performed by placing the test specimens inside the acrylic plastic test fixture and filling the fixture with sufficient seawater to cover one-half of the test specimens (figure 45). Dead weights were used to apply bending moments to the individual test specimens with a three-point loading arrangement. The dead weights were chosen to apply maximum flexure stress in the range of 6000 to 11 000 psi.

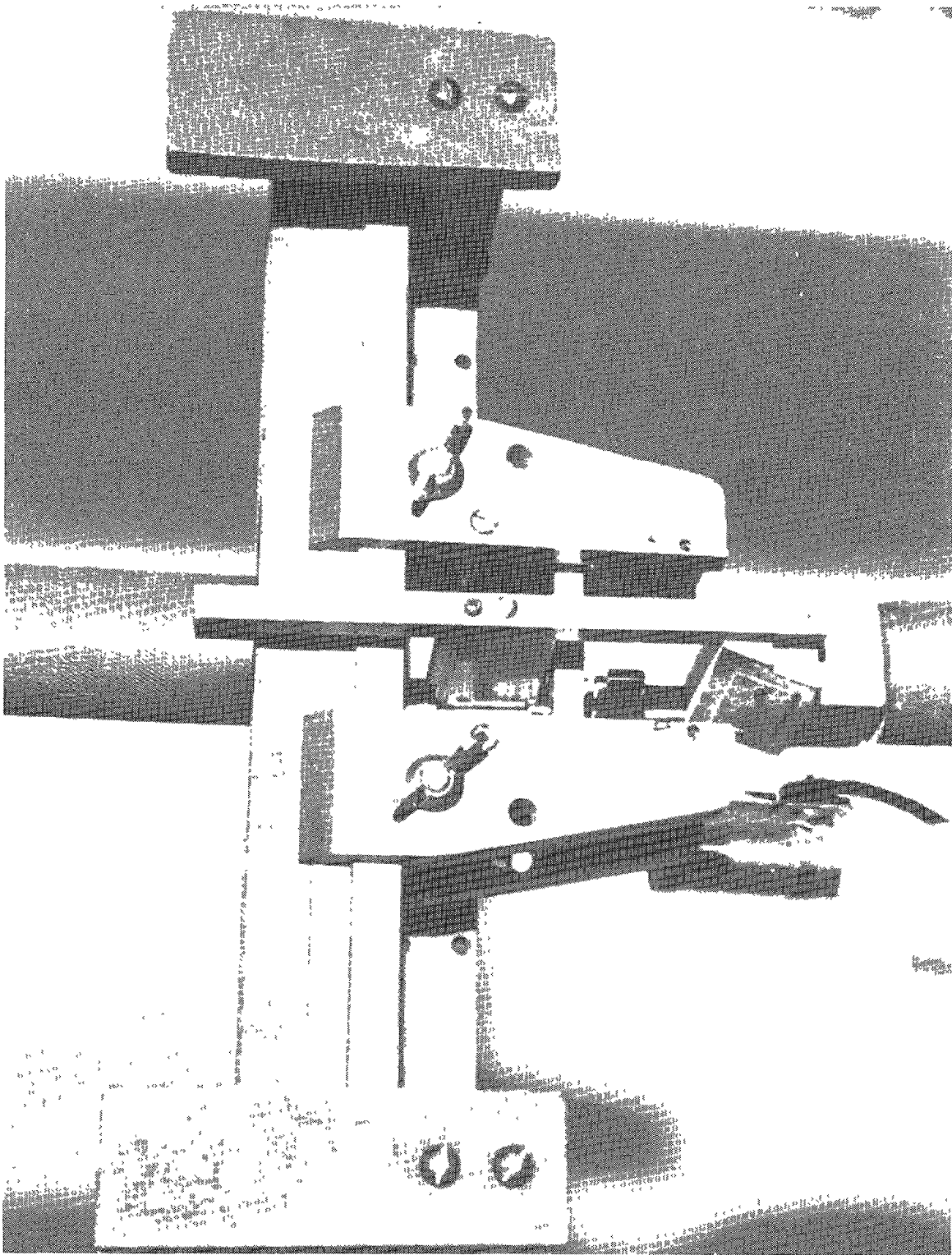


Figure 43. Test fixture for applying three-point bending moment to the germanium test specimens.

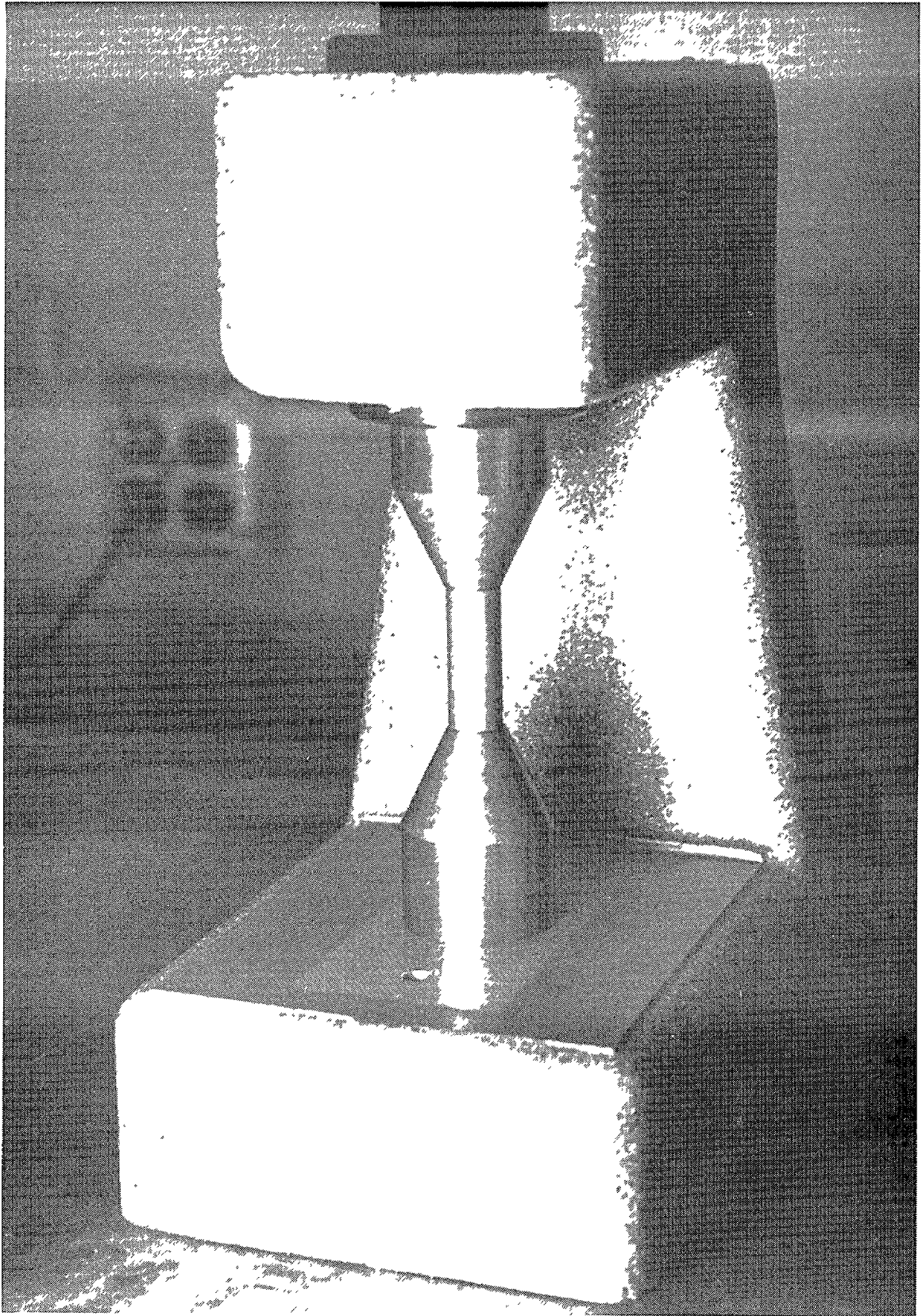


Figure 44. Test fixture for applying compressive load to the germanium test specimens. Note that the diameter of the anvils matches the diameter of the germanium cylinder.

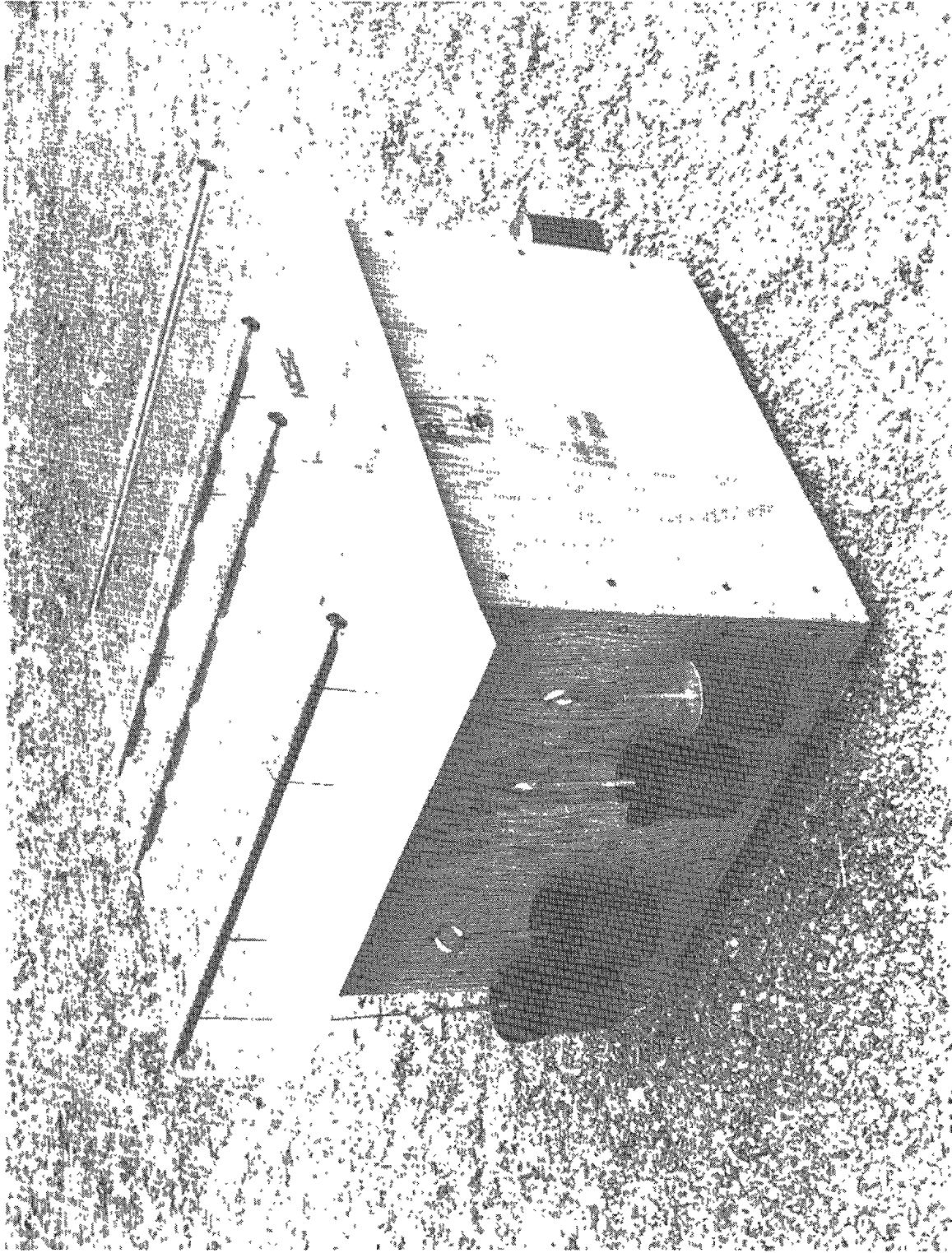


Figure 45. Test fixture for long-term flexure testing of germanium test specimens. Provision is made for keeping some of the specimens submerged in seawater while others remain dry.

The reasons for selecting this particular range of maximum flexure stress levels were twofold. By selecting a long-term stress level which was approximately 50 to 15 percent lower than the average value of short-term flexure strength, the premature failure of test specimens during the application of dead loads could be minimized, while at the same time the effect of static fatigue would become apparent in a matter of days rather than months.

TEST RESULTS

WINDOWS

Hydrostatic loading of spherical sector windows did not generate any fractures, even after 100 pressure cycles to 20 000 psi. Some of the gaskets, however, exhibited signs of wear and tear, particularly the nylon-reinforced neoprene composite gasket.

Inspection of gaskets removed from each of the window test assemblies that had completed their cyclic pressurization schedules disclosed the following levels of gasket wear:

1. Nylon-reinforced neoprene gasket—
 - #1 Test Assembly; 1 cycle 0 to 20 000 psi, 99 cycles 0 to 4500 psi; no wear.
 - #2 Test Assembly; 100 cycles 0 to 9000 psi; moderate wear.
 - #3 Test Assembly; 100 cycles 0 to 13 500 psi; severe wear (figures 46 and 47).
2. Kevlar-49-reinforced epoxy gasket bonded to the nylon-reinforced neoprene gasket—
 - #4 Test Assembly; 100 cycles 0 to 20 000 psi; moderate wear (figures 48 and 49).

Recording of acoustic events during the pressure cycling of #1 Test Assembly disclosed that germanium, although not very acoustically active, does exhibit the classical Kaiser effect (figure 50).

Dynamic loading of spherical sector windows resulted in fracturing of all the windows (figures 51 and 52). The dynamic overpressures which generated fractures are shown in table 7. It appears that a minimum peak dynamic overpressure of 1100 psi is required to initiate fracture in the germanium spherical sector under 450-psi hydrostatic pressure.

TEST SPECIMENS

Short-term flexure testing of polycrystalline germanium test specimens in a standard laboratory atmosphere generated maximum stress values in the 7500 to 15 000-psi range (tables 8, 9, and 10). The average value of the maximum flexure stress at the moment of fracture was calculated to be 11 512 psi, approximately midway between the high and low limits of recorded values

The fracture surfaces on failed specimens exhibited all the characteristics of brittle failure (figure 53). In many cases, the fracture surface seemed to follow the intergranular boundaries. Very little, if any, secondary cracking took place during failure, as evidenced by a total absence of fragmentation.



Figure 46. Fairprene 5722A bearing gasket after 100 pressure cycles; 0 to 13 500 psi, 8-hour cycle length. Detail of surface in contact with the metallic window seat.

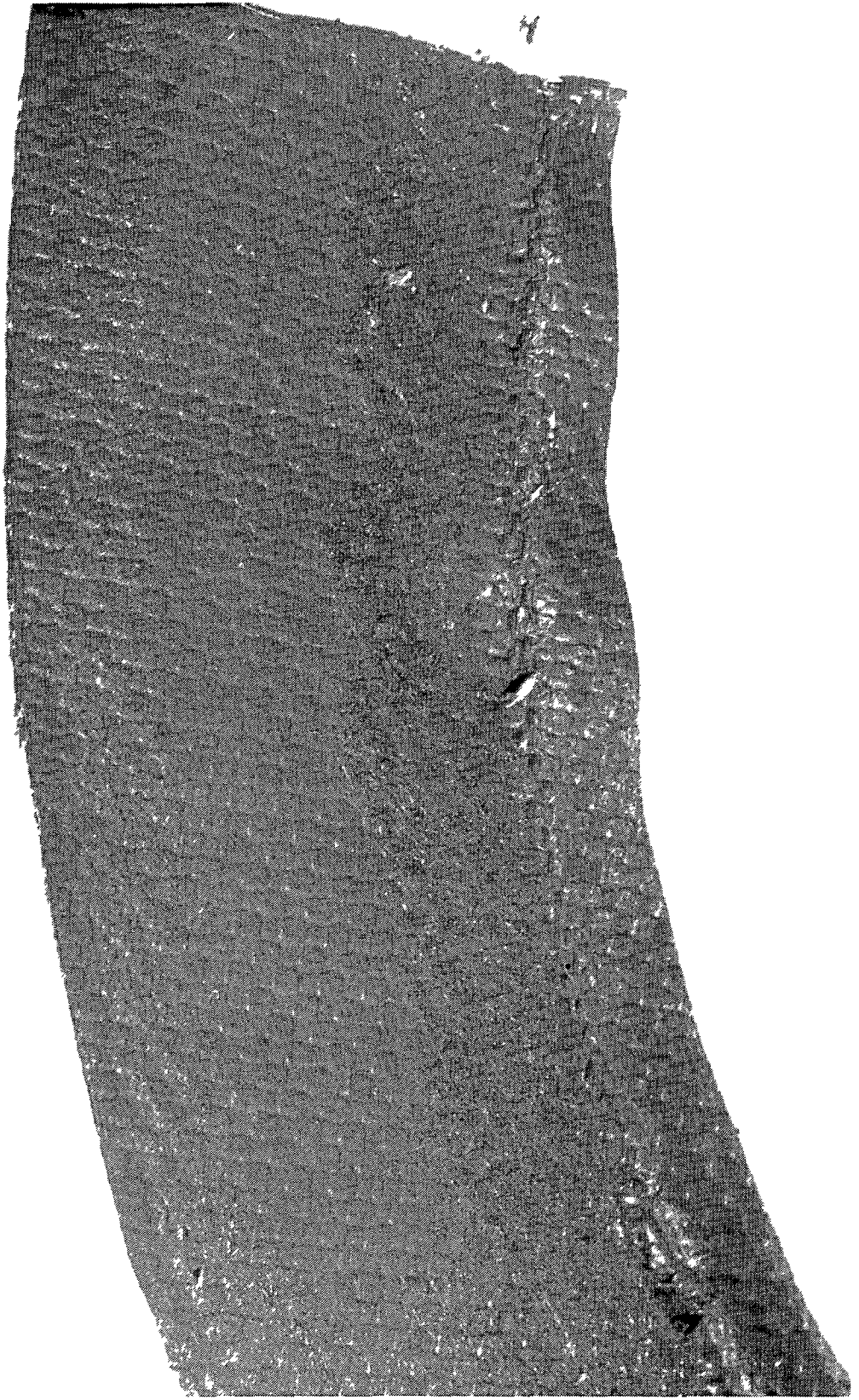


Figure 47. Same gasket as in figure 46. Detail of surface in contact with the window's bearing surface.

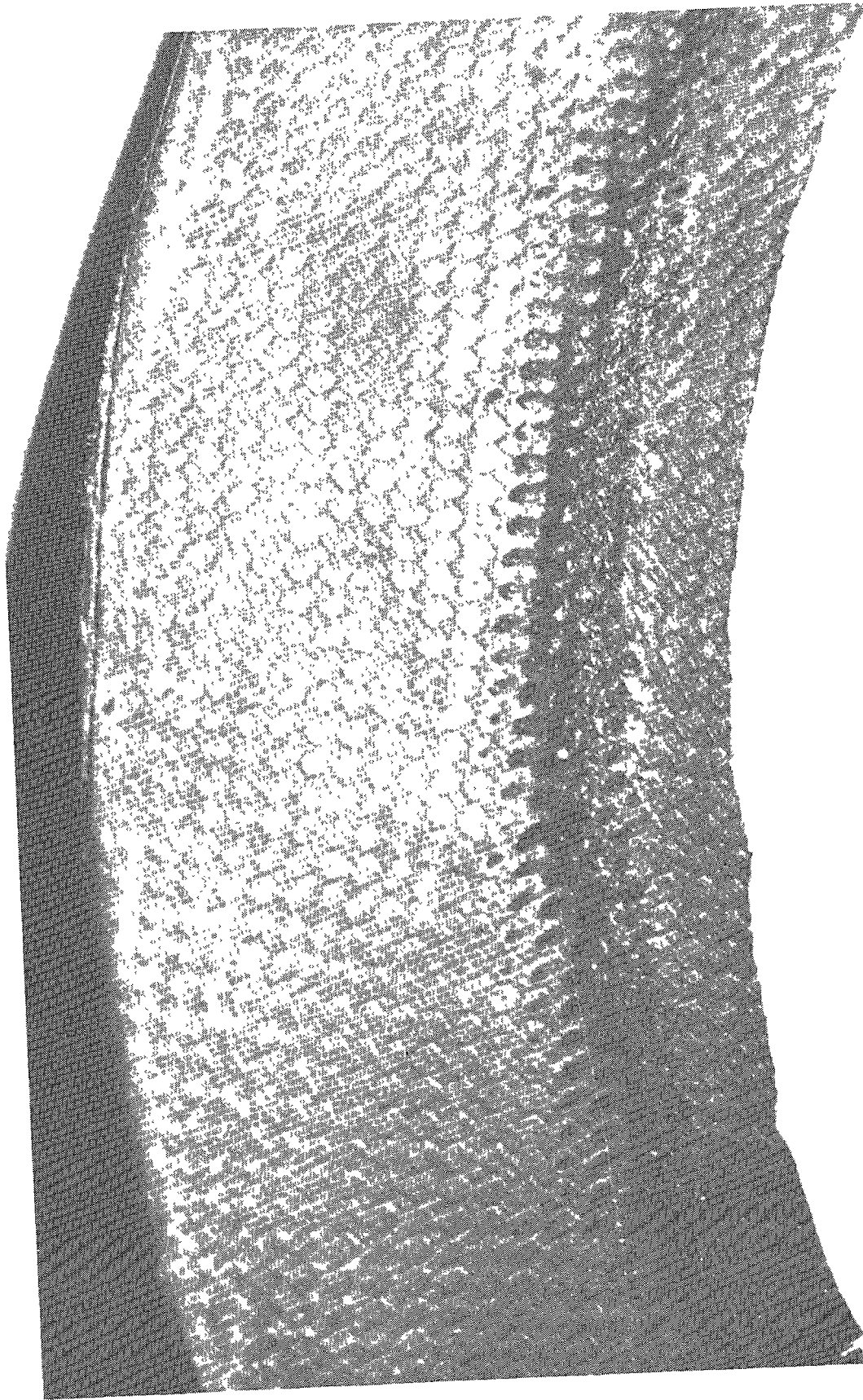


Figure 48. Composite bearing gasket (Fairprene 5722A bonded to KEVLAR-49 cloth-reinforced epoxy) after 100 pressure cycles; 0 to 20 000 psi, 8-hour cycle length. Detail of surface on Fairprene 5722A in contact with the metallic window seat.

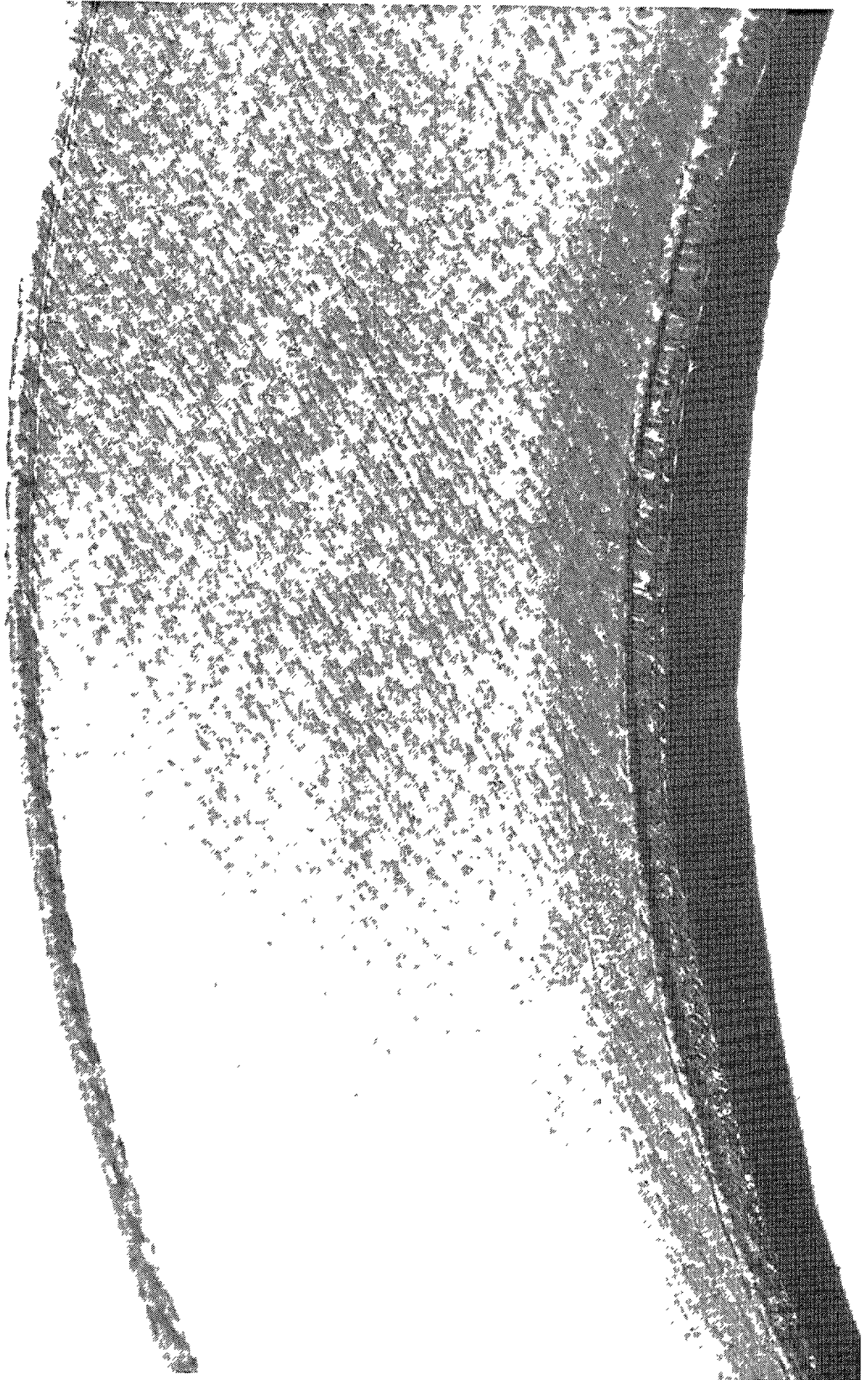


Figure 49. Same gasket as in figure 48. Detail of surface on Kevlar-49-reinforced epoxy gasket in contact with the window's bearing surface.

ACOUSTIC EMISSIONS FROM GERMANIUM WINDOW

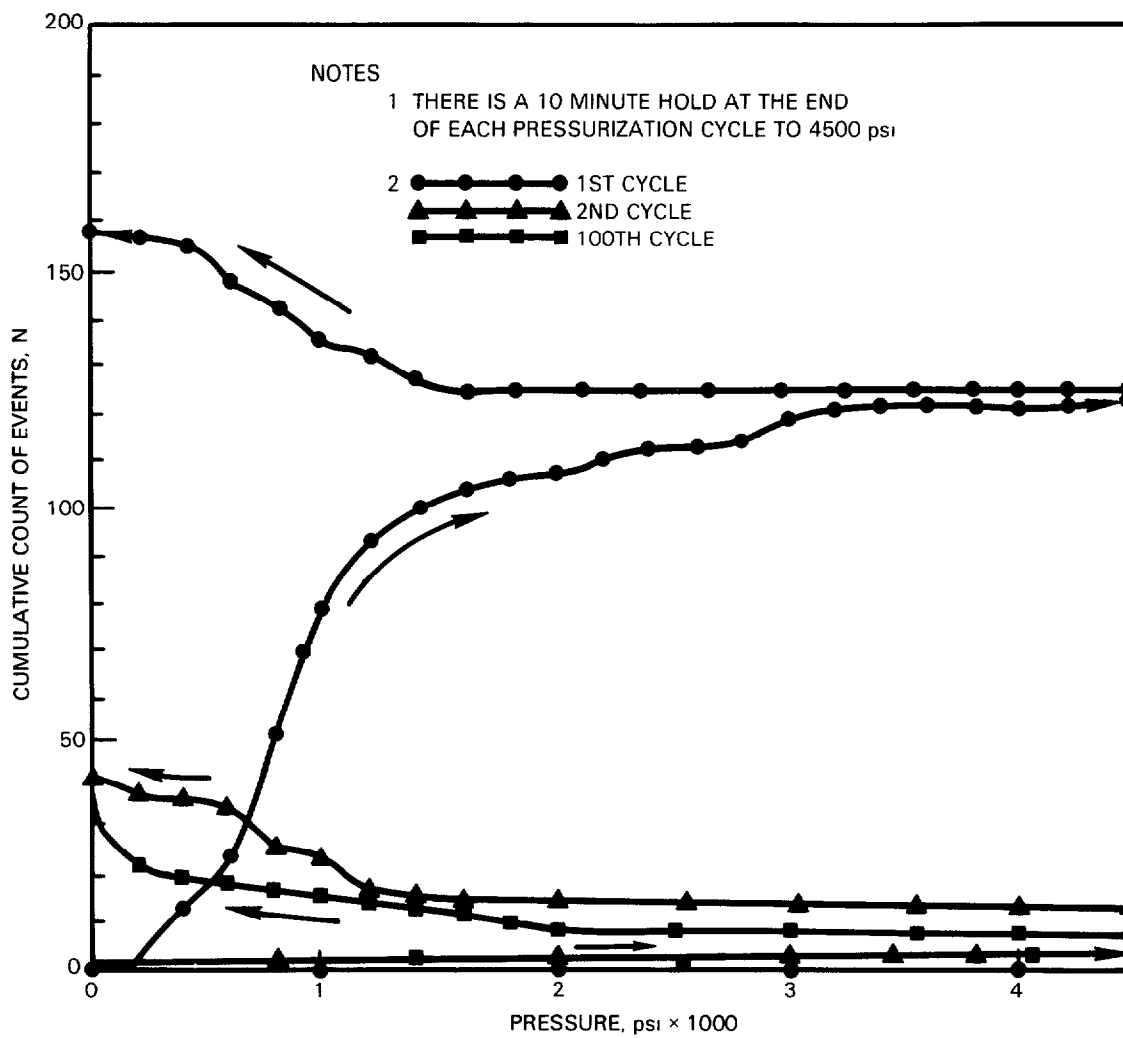


Figure 50. Acoustic emissions recorded during pressure cycling of the germanium spherical sector from 0 to 4500 psi. Note that the acoustic activity significantly decreased after the first pressure cycle, indicating the presence of Kaiser effect.

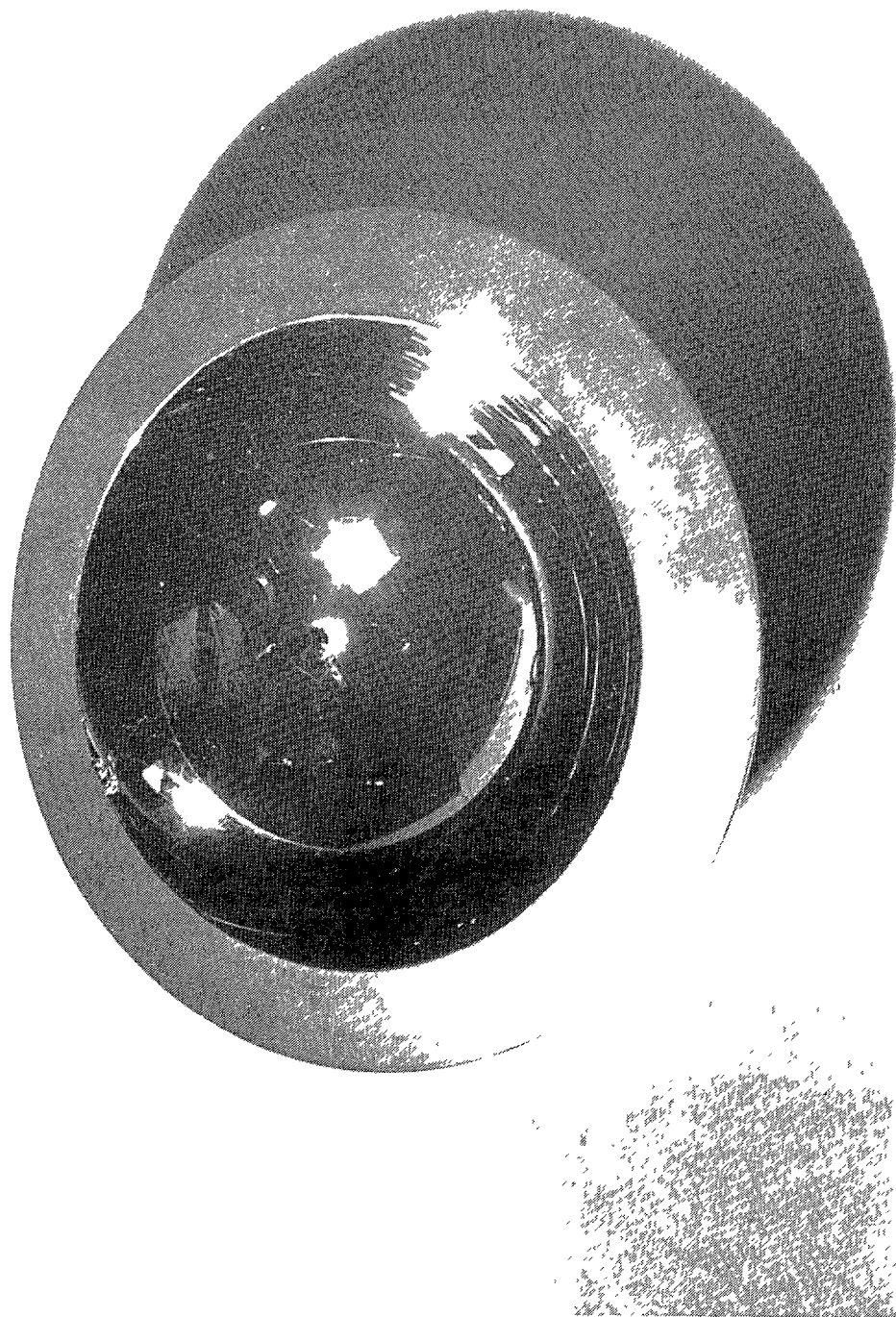


Figure 51. Germanium spherical sector after exposure to dynamic pressure pulse with 2250-psi peak pressure. The sector is still in one piece and no leakage was observed; however, the concave surface exhibits a multitude of fine cracks with meridional orientation.



Figure 52. Closeup of the germanium spherical sector in figure 51. Note that some spalling has already taken place at the inner edge of the sector.

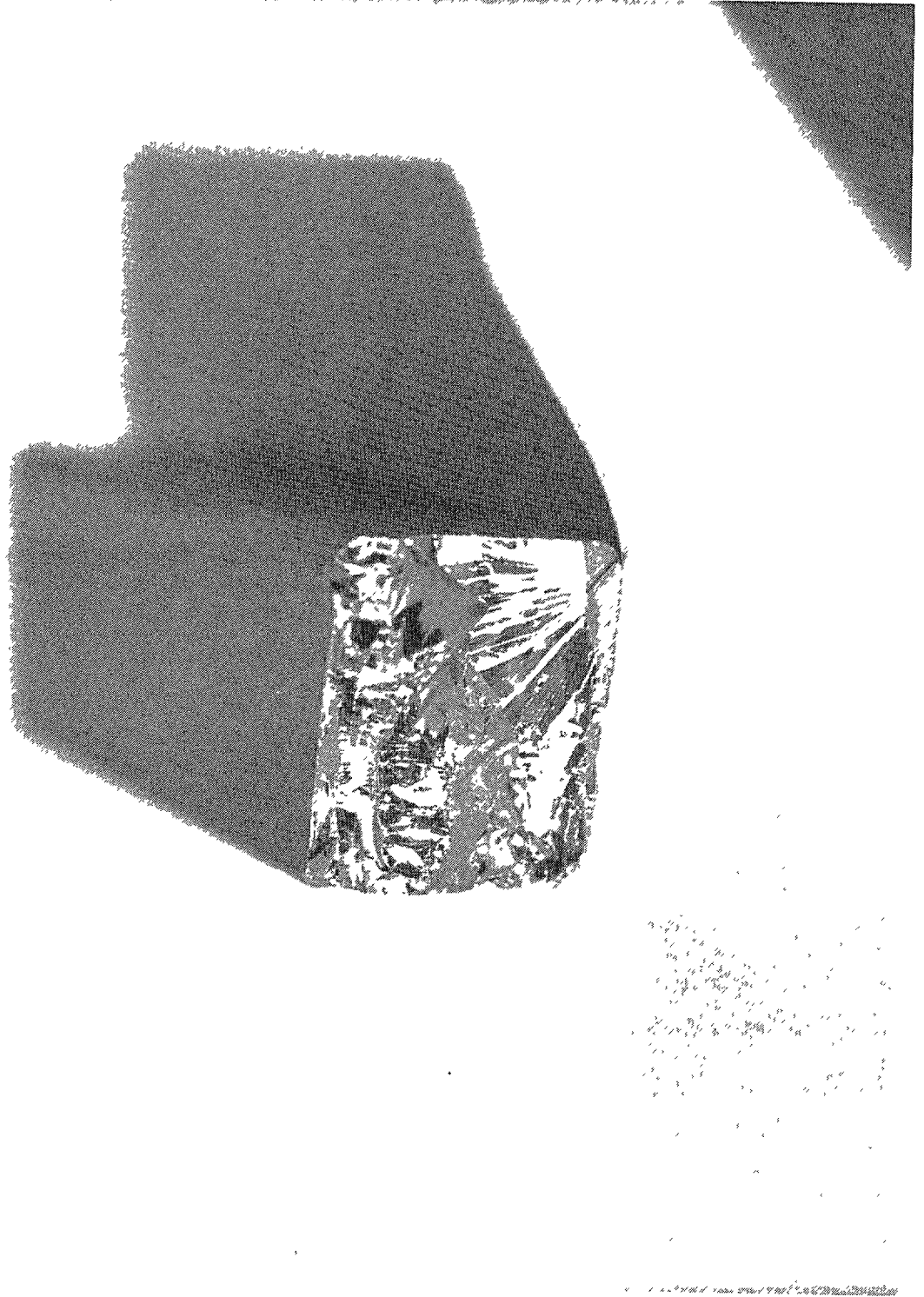


Figure 53. Spalling of the exterior surface on germanium test cylinders that occurred at approximately 70 percent of the ultimate load.

Specimens: $R_o = 4.0$ inches; $R_i = 30$ inches; $\alpha = 150^\circ$.

	Test Assembly #1	Test Assembly #2	Test Assembly #3	Test Assembly #4	Test Assembly #5
Standoff Distances, ft	4	4	4	4	4
	3	3	3	3	3
	2	2	2	2	2
	1	(1100 psi)	1	(1150 psi)	(1200 psi)
	(2300 psi)	—	(2250 psi)	—	—

Notes:

1. Explosions were generated by commercial detonators containing 1.1 gm of explosive.
2. The standoff distances were measured from the apex of the spherical sector to the center of the charge.
3. Static pressure at the moment of explosion was always 450 psi.
4. The dynamic peak pressure at the apex of the window was measured by piezoelectric transducers and recorded photographically on an oscilloscope.

Table 7. Resistance of germanium sector windows to underwater explosions.

Short-term compression testing of polycrystalline germanium test specimens on bare steel anvils in a standard laboratory atmosphere generated maximum stress values in the 26 500-to-89 215-psi range (tables 8, 9, and 10). The average value of the maximum compression stress in test specimens with 0.5 and 1.0-inch diameters at the moment of catastrophic failure was calculated to be 63 870 psi, approximately two thirds up between the high and low limits of recorded values.

The average compressive strengths of 0.5 and 1.0-inch-diameter specimens were 66 031 and 55 222 psi, respectively. Since the 10 809-psi difference between the average compression strengths of 0.5 and 1.0-inch-diameter test specimens is not statistically significant, it can be tentatively concluded that the volume of material contained within the test specimen had little influence on the stress level at which catastrophic failure of the specimen took place.

Audible cracking and spalling preceded catastrophic fracture in every case during short-term compression testing (figure 54). The interval between the initiation of cracking and catastrophic failure varied widely from one specimen to another. In some cases, audible cracking preceded catastrophic failure by less than 5000 psi, while in other cases it preceded it by more than 30 000 psi. Cracking produced, in all cases, vertical shear planes that caused spalling from the vertical surface on the cylinder. As spalling progressed, the cross-sectional area of the cylinder carrying the compressive load decreased until finally, at the moment of catastrophic failure, it was probably less than 60 percent of the original cross section.

Audible cracking and spalling was also noted during the single long-term compression test at a 61 538-psi stress level (figure 55). Since the test was terminated after only 24 hours

Flexural Strength*			
Specimen Number		Flexural Strength, psi**	Flexural Modulus, psi × 10 ⁶ **
1		7 490	13.5
2		10 640	14.0
3		9 030	13.8
4		12 500	13.5
5		8 160	12.8
	Maximum	12 500	14.0
	Average	9 564	13.5
	Minimum	7 490	12.8

Compression Strength†			
Specimen Number	Bearing Surfaces on Anvils	Compression Strength, psi**	Crack Initiation, psi**
1	Steel	71 258	46 720
2	Steel	47 530	42 050
3	Steel	76 391	43 150
4	Steel	34 578	28 050
5	Steel	26 502	20 000
	Maximum	71 258	46 720
	Average	51 251	35 994
	Minimum	26 502	20 000

*Test specimen: 0.3 inch (0.76 centimeter) thick by 0.5 inch (1.27 centimeters) wide by 3 inches (7.62 centimeters) long.

Rate of testing: 0.02 inch per minute (0.05 centimeter per minute) at 75°F (24°C).

Specimen surfaces: Finished with 220-micron grinding compound; edges beveled 0.02 inch (0.05 centimeter).

**To convert pounds per square inch to pascals multiply by 6.894 757 E+03.

†Test specimen: 0.5 inch (1.27 centimeters) in diameter by 1.5 inches (3.81 centimeters) in length.

Rate of testing: 0.05 inch per minute (0.13 centimeter per minute) at 75°F (24°C).

Specimen surfaces: Finished with 220-micron grinding compound, edges beveled 0.02 inch (0.05 centimeter).

Table 8. Mechanical properties of optical grade polycrystalline germanium. (Boule 1 supplied by Exotic Materials.)

Flexural Strength*		
Specimen Number	Flexural Strength, psi**	Flexural Modulus, psi X 10 ⁶ ***
1	9750	10.8
2	13 900	12.8
3	14 600	11.0
4	14 000	10.7
5	15 100	10.7
Maximum	15 100	10.7
Average	13 470	11.2
Minimum	9750	12.8

Compression Strength***			
Specimen Number	Bearing Surfaces on Anvils	Crack Initiation, psi**	Compression Strength, psi**
1	Steel	38 461	61 538 NF [†]
2	Steel	51 020	71 428
3	GRP	51 282	56 410
4	Fairprene	31 282	31 282
5	Steel	51 282	60 256
6	Steel	46 153	64 103 NF ^{††}
7	Steel	64 102	76 923 NF ^{††}
8	Steel	60 730	70 153
9	Steel	45 320	62 820
10	Steel	61 538	61 538 NF ^{††} , CYC ^{†††}
Maximum [†]		64 102	76 923
Average [†]		52 258	66 094
Minimum [†]		38 461	60 256

*Test Specimen: 0.3 inch (0.76 centimeter) thick by 0.5 inch (1.27 centimeters) wide by 3 inches (7.62 centimeters) long.
Rate of testing: 0.02 inch per minute (0.05 centimeter per minute) at 75°F (24°C).
Specimen surfaces: Finished with 220-micron grinding compound and etched; edges beveled 0.02 inch (0.05 centimeter).

**To convert pounds per square inch to pascals multiply by 6.894 757 E+03.

***Test specimen: 0.05 inch (1.27 centimeters) in diameter by 1.5 inches (3.81 centimeters) in length.
Rate of testing: 0.05 inch per minute (0.13 centimeter per minute) at 75°F (24°C).
Specimen surfaces: Finished with 220-micron grinding compound and etched; edges beveled 0.02 inch (0.05 centimeter) and polished.

†Specimens tested on Fairprene and glass-reinforced plastic were not considered.

††NF: Testing terminated without catastrophic failure.

†††CYC: Cycled rapidly nine times from 0 to 61 538 pounds per square inch (424.3 megapascals) without generation of cracks; spalling occurred during tenth cycle of 24-hour duration.

Table 9. Mechanical properties of optical grade polycrystalline germanium. (Boule 2 supplied by Exotic Materials.)

Compression Strength*

Specimen Number	Bearing Surfaces On Anvils	Crack Initiation	Failure
1	Bare	78 431 psi	89 215 psi
2	Bare	75 980 psi	81 862 psi
3	Bare	63 725 psi	73 529 psi
4	Bare	63 725 psi	74 509 psi
5	Bare	78 431 psi	84 313 psi
	Maximum	78 431 psi	89 215 psi
	Average	72 058 psi	80 685 psi
	Minimum	63 725 psi	73 529 psi

*Test Specimens: 0.510 diameter X 1.500 inches long; ends pitch polished

Test Speed: 1000 psi/second

Compression Strength**

Specimen Number	Bearing Surfaces On Anvils	Crack Initiation	Failure
6	Bare	44 585 psi	57 961 psi
7	Bare	47 770 psi	53 184 psi
8	Bare	57 324 psi	60 509 psi
9	Bare	52 229 psi	54 777 psi
10	Bare	40 764 psi	49 681 psi
	Maximum	57 324 psi	60 509 psi
	Average	48 534 psi	55 222 psi
	Minimum	40 764 psi	49 681 psi

**Test Specimen: 1.010 diameter X 2.010 inches long; ends pitch polished

Test Speed: 1000 psi/second

Table 10. Mechanical strength of optical grade polycrystalline germanium. (Boule 3 supplied by Exotic Materials).

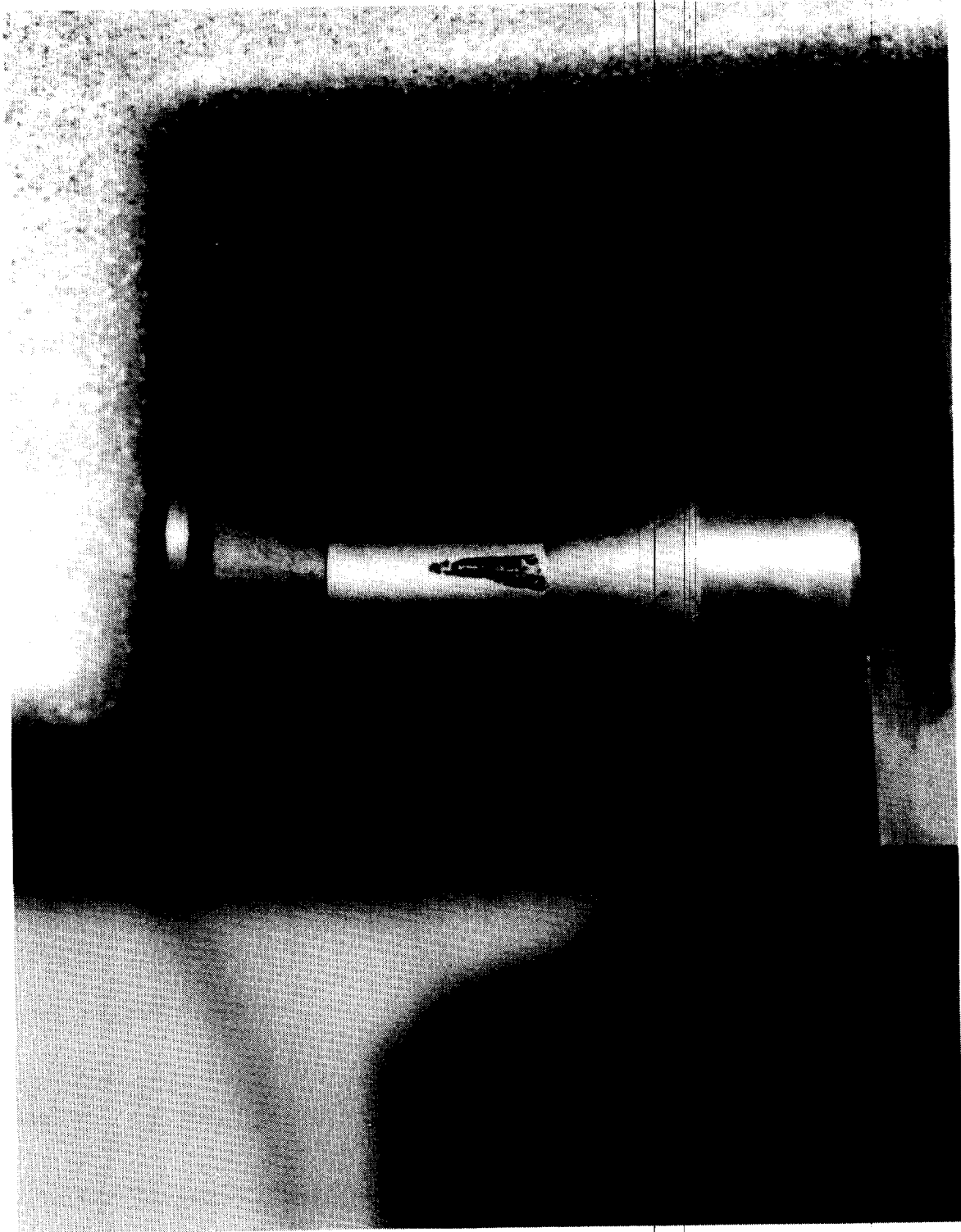


Figure 54. Spalling observed after 24-hour-long application of 61 538-psi compression stress.

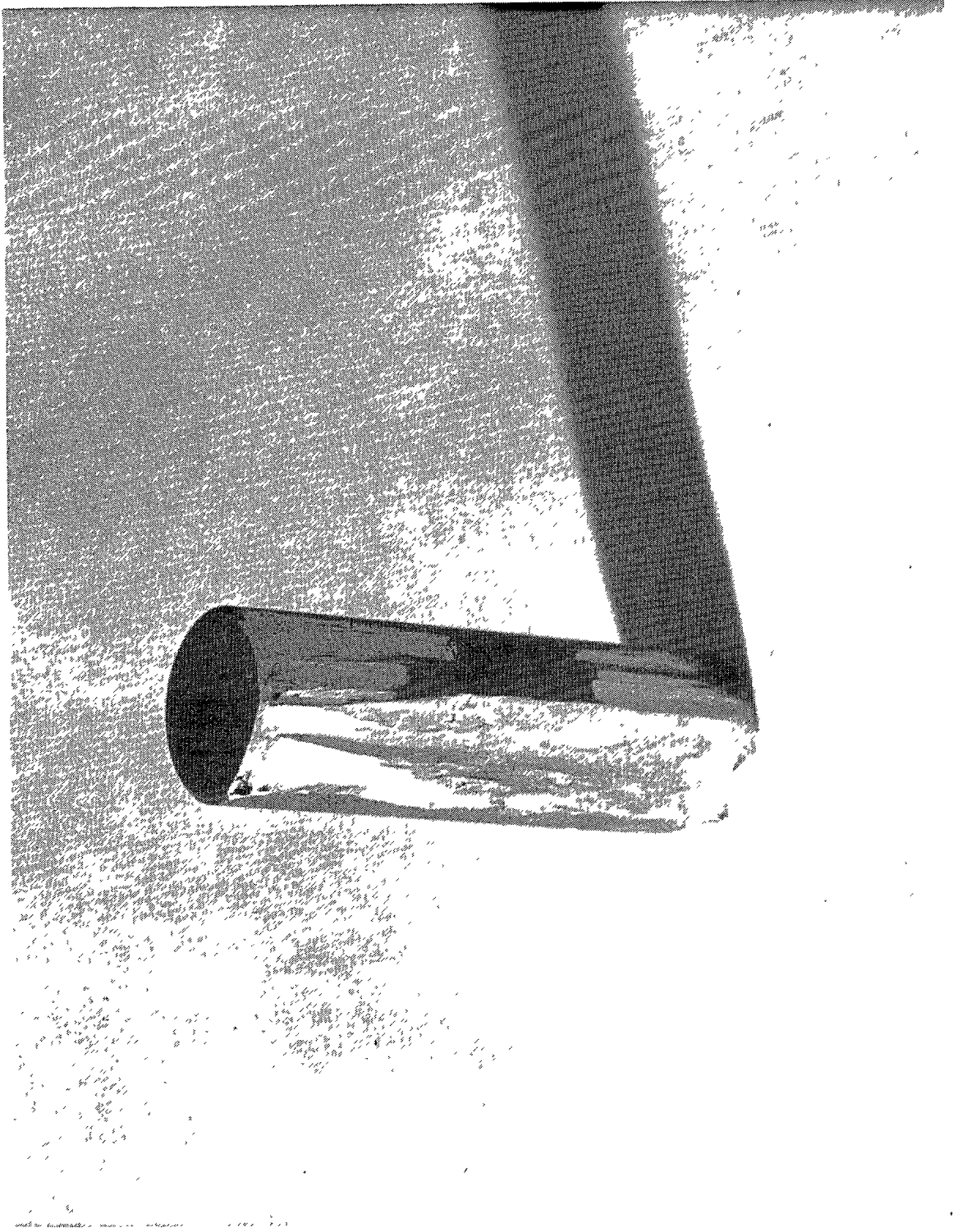


Figure 55. Typical fracture surface on specimens subjected to short-term flexure loading.

of sustained loading, it is not known how long the test specimen would have carried the sustained load prior to catastrophic failure.

Long-term flexure testing at the preselected stress levels resulted in the fracture of only some test specimens. The duration of sustained loading prior to catastrophic loading was found to be a function of sustained flexural stress and ambient atmosphere. High stress levels and seawater environment produced fracture sooner than low stress levels and standard laboratory atmosphere environment (table 11). When the results are plotted on semilog coordinates, a straight line can be drawn through the average values of test data. With the aid of this graph, the static fatigue strength of germanium in water or air environments can be extrapolated with confidence to loading durations in excess of 1000 hours (figure 56).

DISCUSSION

PHYSICAL PROPERTIES OF GERMANIUM

The physical properties of germanium, like those of glass, appear to be adequate for utilization of this material in IR optical elements subjected to high dynamic or static loads by operational environment.

The short-term flexure strength at standard laboratory temperature and environment is of the same magnitude, or slightly higher than that of glass with similar fine-ground surfaces (germanium: 11 500 psi average; glass: 8000 psi average). Surprisingly, comparison with data generated by polished test specimens shows that there is no significant difference between the short-term flexural strengths of samples with ground or polished surfaces (tables 12, 13, and 14). This would seem to indicate that fine microcracks present on the ground surface of germanium generate peak tensile stresses during flexure testing whose magnitude is significantly less than the tensile peak stresses in the body of the material resulting from grain boundaries, inclusions, and other discontinuities.

Comparison of short-term flexure strengths generated at standard laboratory and elevated temperature environments indicates that raising the ambient temperature has little effect on the flexure strength in the 25 to 400°C range (table 14). For this reason, the effect of temperature on the structural performance of germanium optics at maximum ambient temperature encountered during operation at sea can be disregarded, since that temperature rarely exceeds 50°C.

The short-term compression strength of germanium is significantly less than that of glass (germanium: 63 870 psi average; glass: 135 000 psi average). No significant difference was found between the ultimate compressive strengths of (1) specimens with ground or polished bearing surfaces, or (2) specimens of different diameters and length. Similarly, the presence or absence of a gasket did not appear to have a statistically significant effect on the ultimate strength of the specimens.

This latter finding differs from the findings of other studies where glass or ceramic specimens were crushed in steel anvils that were identical in size and material to those utilized in this study for compression testing of germanium specimens to failure under short-term compression loading. It was found that the use of nonmetallic and/or lead gaskets significantly decreased the ultimate load carried by the specimens prior to failure (bare anvils: 173 000 psi average; gaskets on anvils: 81 000 psi).

SPECIMEN	MAXIMUM FLEXURE STRESS (psi)	DURATION OF LOADING (minutes)	TEST RESULT
Atmospheric Environment			
1	10 746	112 320	} Test terminated without fracture
2	11 180	112 320	
3	10 565	112 320	
4	10 873	112 320	
5	11 189	112 320	
6	12 759	1.0	} Test terminated by fracture
7	16 693	0.01	
8	14 135	20.0	
9	13 427	300.0	
10	14 400	0.5	
11	13 588	1.0	
12	14 982	0.1	
Marine Environment			
13	10 063	181	Test terminated by fracture
14	9 386	112 320	} Test terminated without fracture
15	8 956	112 320	
16	11 174	112 320	
17	8 818	112 320	
18	11 337	1 200	
19	9 295	5 340	} Test terminated by fracture
20	11 526	10.0	
21	11 526	1.0	
22	10 292	0.5	
23	11 273	0.5	
24	11 148	2.0	
25	11 128	0.25	
26	9 978	120 000	Test terminated without fracture

Notes.

1. Temperature and relative humidity of ambient air environment fluctuated from 50 to 100°F and 30 to 70 percent, respectively
2. Temperature of ambient air environment fluctuated from 50 to 100°F, while the relative humidity was maintained at 100 percent by spraying seawater intermittently upon the surfaces of the test specimens.
3. The flexure moment was applied by 3-point loading.
4. The edges of the test specimens rested on acrylic plastic supports while the dead load was applied to the center of the rectangular test specimen by a nylon line with 0.06 inch diameter.
5. The test specimens were 0.250 x 0.500 x 6.00 inches, fine ground with 9-micrometer abrasive on all surfaces, including bevels, and subsequently etched.

Table 11. Static fatigue of optical-grade polycrystalline germanium in flexure.

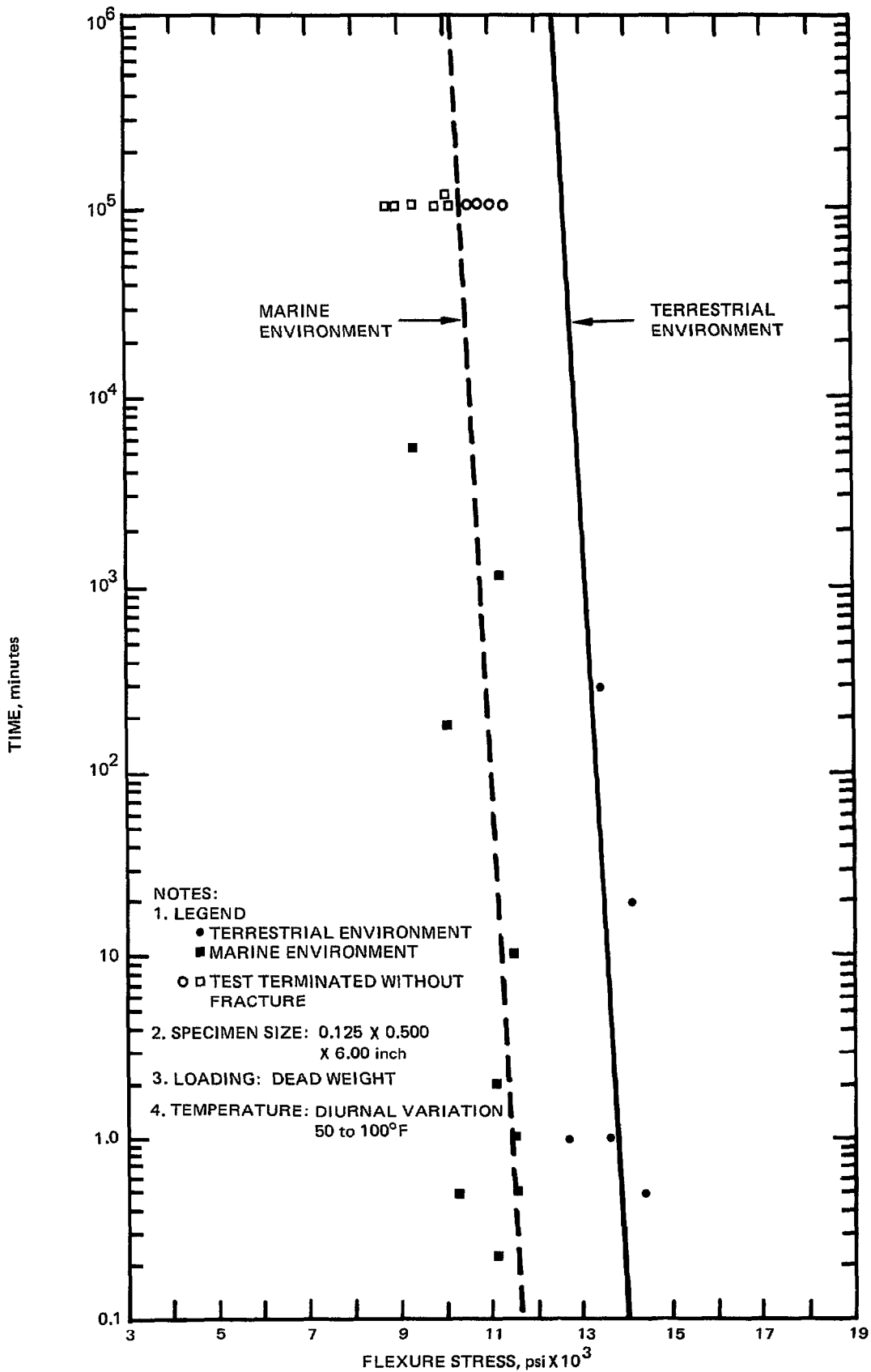


Figure 56. Static fatigue life of germanium.

Flexural Strength*			
Specimen	Surface Condition	Flexural Strength, psi**	Flexural Modulus, psi X 10 ⁶ **
C752-1	Polished	8300	
C752-2		8200	
C752-3		7100	
C752-4		9800	
C752-5		7900	
Maximum		9800	
Average	8300		
Minimum	7100		
C752-6	Etched	16 400	
C752-7		15 300	
Maximum	16 400		
Average	15 900		
Minimum	15 000		
C760-1	Abraded		
C760-2		7000	12.1
Maximum		7000	12.1
Average		7000	12.1
Minimum		7000	12.1
C760-3	Optically polished	7900	12.1
C760-4		13 900	13.4
C760-5		10 500	13.3
C760-7		10 300	12.9
C760-8		10 500	13.0
Maximum		13 900	13.4
Average		10 600	10.6
Minimum		7900	12.1

*Test specimen: 0.25 inch thick by 1.5 inches wide by 10 inches long (0.64 by 3.81 by 25.4 centimeters).

Rate of testing: 0.02 inch per minute (0.05 centimeter per minute) at 75°F (24°C).

Specimen surfaces: Optical polish required; 80-50 scratch and dig finish.

Test conducted by: Boeing Aircraft Company (June 1969).

**To convert pounds per square inch to pascals multiply by 6.894 757 E+03.

Table 12. Mechanical strength of optical grade polycrystalline germanium.
(Lots 3 and 4 supplied by Eagle Picher Industries.)

Compression Strength*			Flexural Strength**			
Orientation	Surface Finish	Compression Strength, psi [†]	Orientation	Surface Finish	Flexural Strength, psi [†]	Modulus, psi X 100 [†]
100	Ground	26 100	100	Polished	12 000	17.6
		21 700			11 000	12.9
		27 600	110	Polished	14 800	13.5
		33 700			13 300	13.0
		57 500	111	Polished	11 100	12.2
		Maximum			57 500	15 800
Average	33 320					
Minimum	21 700					
110	Ground	15 500	Poly-crystalline	Ground	13 600	13.7
		61 000			9 090	14.3
		88 700			10 700	19.5
		54 300			8 150	15.2
		55 100	10 000	16.1		
		Maximum	88 700	Maximum	13 600	19.5
Average	54 920	Average	10 410	15.8		
Minimum	15 500	Minimum	8 150	13.7		
111	Ground	83 400	Poly-crystalline	Polished	6 650	
		61 600			10 300	9.4
		83 400			13 900	11.0
		72 500			9 160	11.0
		61 600	11 100	7.6		
		Maximum	83 400	Maximum	13 900	
Average	72 500	Average	8 873			
Minimum	61 600	Minimum	6 650			
Poly-crystalline	Ground	22 700				
		44 800				
		49 400				
		45 700				
		31 500				
		Maximum	49 400			
Average	38 820					
Minimum	22 700					

*Test specimen: 0.750 inch (1.9 centimeters) diameter by 1.250 inches (3.18 centimeters) long.
Rate of testing: 63 844 pounds per square inch per minute (440 megapascals) at 75°F (24°C).
Specimen surfaces: Finished with 220-micron grinding compound.
Test conducted by: Hughes Aircraft Company (July 1974).

**Test specimen: 0.25 inch thick by 1.5 inches wide by 10 inches long (0.64 by 3.81 by 25.4 centimeters)
Rate of testing: 0.02 inch per minute (0.05 centimeter per minute) at 75°F (24°C).
Specimen surfaces: Optical polish required; 80-50 scratch and dig finish.
Test conducted by: Boeing Aircraft Company (June 1969).

†To convert pounds per square inch to pascals multiply by 6.894 757 E+03.

Table 13. Mechanical strength of optical grade germanium in various lots.

Material	Test Temperature	Flexural Strength, psi	Modulus, psi $\times 10^{-6}$
Germanium Polished	Room	6650	
		10 300	9.41
		13 900	11.0
		9160	11.0
		11 100	6.63
	Maximum Average Minimum	13 900	11.0
		10 222	9.76
		6650	7.63
	150°C	14 900	14.3
		12 800	13.3
		15 300	11.7
		4790	7.04
		4600	8.45
	Maximum Average Minimum	15 300	14.3
		10 478	10.95
		4600	7.04
	260°C	17 200	17.9
		12 100	19.5
		4960	10.0
		12 100	10.5
14 100		7.59	
Maximum Average Minimum	17 200	19.5	
	12 092	13.1	
	4960	7.59	
400°C	10 400	3.47	
	11 900	3.67	
	6180	3.36	
	12 300		
	11 600	2.97	
Maximum Average Minimum	12 300	3.67	
	10 476	3.37	
	6180	2.97	

NOTE: All specimens had identical optical polish and were tested in identical manner to failure under 4-point loading.

Table 14. Effect of temperature on the flexural strength of optical grade polycrystalline germanium.

The probable reason for the large difference in test values between bare and gasketed glass specimens is that the intrinsic compressive strength of glass exceeds the bearing strength of nonmetallic gaskets, and thus the lower test values resulting from the use of gaskets on glass represent in actuality only the ultimate compressive strength of the gaskets themselves, and not of glass. This is not the case with germanium, whose intrinsic compressive strength is either less or at most equal to that of the nonmetallic gaskets. Thus the test values generated with gasketed or bare germanium specimens should be approximately the same. The same is probably true for thin lead gaskets under a single, short-term pressure loading (table 15).

The fact that the ultimate compressive strength of germanium is not decreased significantly by the use of nonmetallic gaskets represents a practical advantage for the designer since the use of gaskets eliminates the lapping of germanium windows in their metallic seats, which is performed to ensure that the bearing surfaces on the windows are able to withstand successfully high bearing stresses generated by hydrostatic loading.

The absence of significant difference between compressive strengths of small and large cylindrical test specimens indicates that the compressive strength of germanium is not a function of specimen volume. In this respect, it differs from glass and ceramics, whose compressive strength is a function of test specimen volume. For this reason, the designer need not discount the compressive strength of germanium listed in this report when applying it to the design of large germanium windows with spherical sector shape.

The long-term flexural strength of germanium appears to be a function of loading duration and ambient atmosphere; ie, germanium exhibits static fatigue. Since only a few discrete stress levels and a total of 26 samples were used to generate the data, the resulting plot of fatigue strength can be considered only an approximation (figure 56). Still, it is pretty apparent that (a) the seawater environment decreases the static fatigue life; and (b) decreasing the value of maximum flexural stress increases the static fatigue life. Based on the plotted data, it appears that for sustained loadings of less than 1000-hour duration the maximum flexural stress on a germanium window in the air environment must be less than 10 000 psi to prevent catastrophic failure of the window under sustained load.

The stress corrosion introduced by contact with seawater appears to reduce the static fatigue life by approximately 20 percent, and for this reason steps must be taken to protect the surface of germanium from seawater corrosion (figures 57 and 58).

Protection against corrosion by seawater can be accomplished by employing the following two approaches:

1. Apply to all surfaces of the germanium window a single or multilayer anti-reflective coating which is also highly resistant to seawater attack.
2. Apply to the nonwetted surface of the window a single or multilayer anti-reflective coating with excellent antireflection characteristics but only fair resistance to seawater; apply to the wetted surface a thick coating, which has been selected on the basis of its superior resistance to seawater rather than its antireflection characteristics.

Extensive evaluation of antireflective coatings on germanium windows conducted by NOSC in San Diego Bay (ref 6) has shown that the majority of AR coatings display signs of deterioration after only 1000 hours of intermittent submersion; after 6000 hours

Specimen Number	Bearing Surfaces on Anvils	Compression Strength, psi**
2013-1	Lead tape on massive steel blocks whose diameters are significantly bigger than that of test specimen	46 185
2045-1		38 034
2047-1		18 474
2047-2		39 823
2013-2		42 953
2045-2		46 728
2045-3		39 251
2013-3		50 532
2013-4		36 540
2047-3		37 355
30-118-1		11 410
30-118-2		37 582
30-118-3		33 620
30-118-4		35 318
30-117-1		31 786
30-117-2		34 774
30-117-3		43 558
30-116-1		34 095
30-116-2		35 861
30-116-3		49 807
Maximum		50 532
Average		37 184
Minimum		11 410

*Test specimen: 0.750 inch (1.9 centimeters) diameter by 1.250 inches (3.18 centimeters) long.

Rate of testing: 63 844 pounds per square inch per minute (440 megapascals) at 75°F (24°C).

Specimen surfaces: Finished with 220-micron grinding compound.

Test conducted by: Hughes Aircraft Company (July 1974).

**To convert pounds per square inch to pascals multiply by 6.894 757 E +03.

Table 15. Mechanical strength of optical-grade polycrystalline germanium. (Lots 1 and 2 supplied by Exotic Materials and Eagle Picher Industries.)

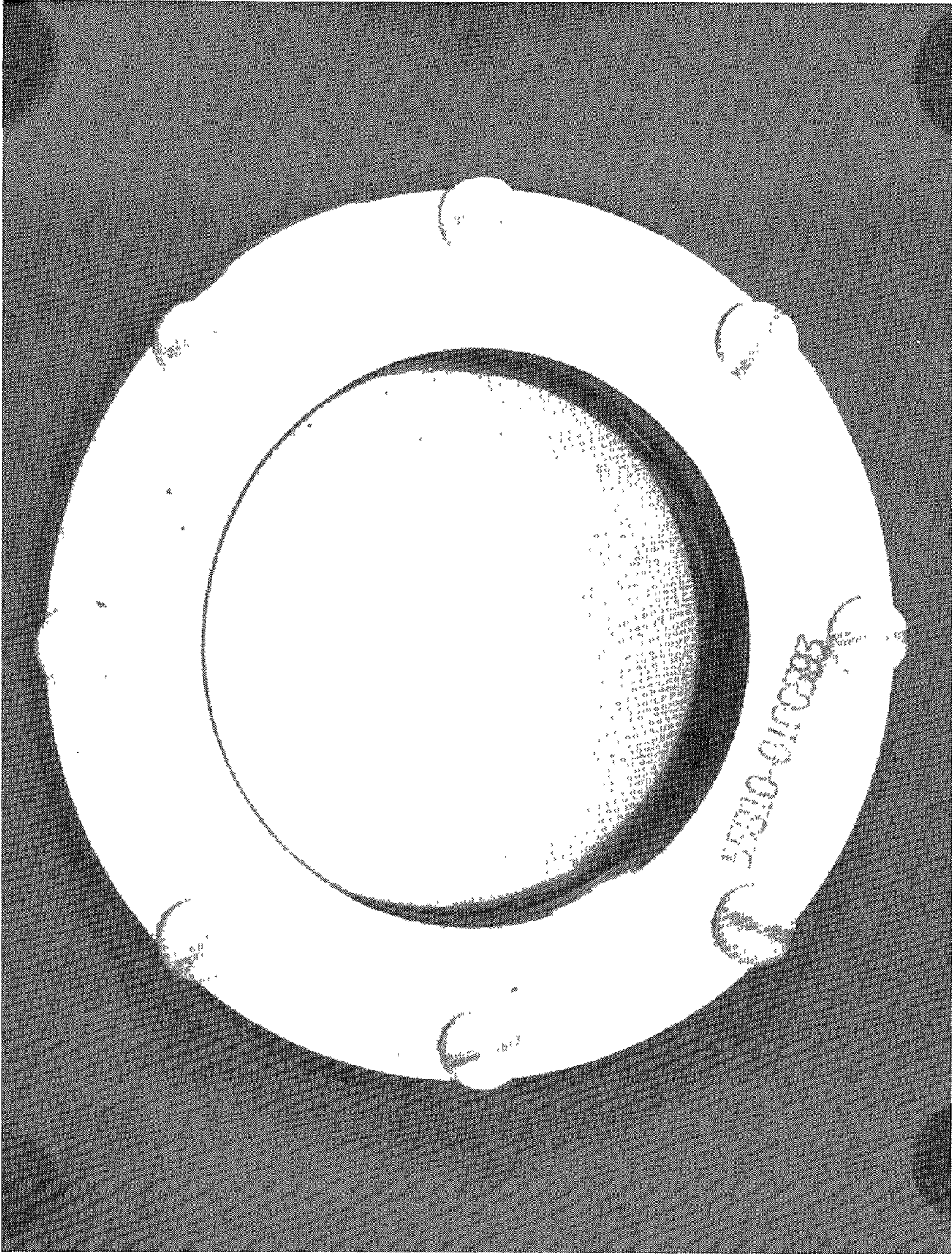
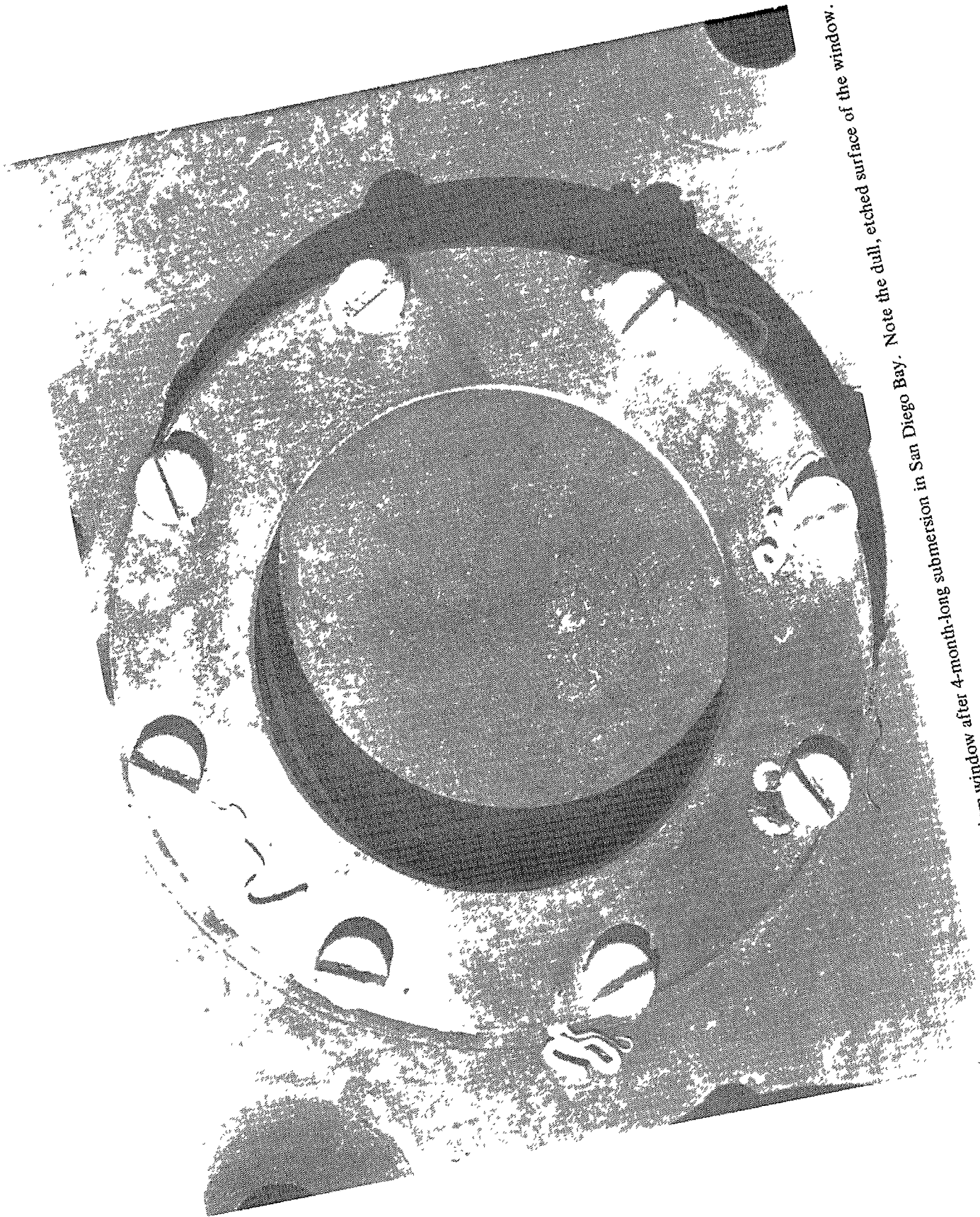


Figure 57. Uncoated germanium window prior to immersion in San Diego Bay.



... window after 4-month-long submersion in San Diego Bay. Note the dull, etched surface of the window.



Figure 58b. Closeup of the etched germanium surface.

they disintegrate completely (figure 59). Only a single multilayer antireflective coating* that was tested did not display signs of serious deterioration after 3000 hours of intermittent submersion, and probably would have protected the germanium window adequately for an additional 1000 to 2000 hours.

Thus it appears that, using the present state of AR coating technology, germanium windows can be protected against seawater corrosion for only half a year at the most. After that time, the deteriorated coating must be stripped, the germanium surface refinished until all pits and craters are removed, and then recoated. The cost of applying a durable, multilayer AR coating free of pinholes to a germanium window is high, particularly to a window with spherical surfaces, as the allowable variation in thickness of individual layers in the AR coating is very small.

The other approach to providing protection against corrosion, by covering the exterior surface of the window with a single thick coating of material excellent in durability but poor in AR characteristics, has until lately been very unsuccessful. The plastic coating either separated in a short time from the germanium substrata because of adhesion loss or permitted the water to seep through small pinholes in the plastic. The plastics utilized were polyethylene, polypropylene, and polyolefin in the thickness range of 0.006 to 0.010 inch.

The breakthrough in the application of thick, seawater-resistant coatings on germanium windows came in the form of the vapor-deposited chalcogenide glass composition AMTIR-I. This glass composition, developed by Amorphous Materials, Inc., Dallas, Texas, has not only uniform transparency in the 1-to-14- μm range (figure 60), but also excellent resistance to corrosion by seawater. Windows fabricated from solid chalcogenide glass (composition AMTIR #1) have shown no deterioration even after 4000 hours of intermittent submersion in stagnant or fast-flowing seawater. Obviously, the ideal solution would be to make all IR windows for marine service from the chalcogenide glass, but the current state of chalcogenide glass technology precludes that.

This obstacle was resolved by utilizing germanium as substrata and chalcogenide glass as coating. The use of germanium as structural substrata allowed the designer to utilize the high level of germanium fabrication technology in the design and fabrication of very large pressure-resistant windows with excellent optical properties in the 7-to-12- μm IR region, while the application of chalcogenide coating to the exterior surface of the window endowed it with the corrosion resistance of a solid chalcogenide glass window (figure 61).

Germanium windows, covered on the internal surface with a standard high-performance AR coating, and on the exterior with a custom-tailored AR coating (to decrease reflection at the germanium/glass outerface) protected by a 0.001-inch-thick overcoat of chalcogenide glass, have been found to transmit at least 72 percent of incident IR energy in the 7-to-12- μm range. This compares rather well with 92 percent transmittance of germanium windows coated on both sides with AR coatings without a protective layer of chalcogenide glass. The reflectance loss at the outer surface of the chalcogenide glass layer could be substantially reduced by covering it with an AR coating, but this AR coating, like any other of its type, would deteriorate rapidly in seawater and thus nullify any cost benefits derived from the application of a chalcogenide glass overcoating.

*Multilayer AR Coating, Exotic Materials #40,100; minimum transmission through 1-mm-thick germanium coated on both sides is 94 percent in the 8-to-11.7- μm range.

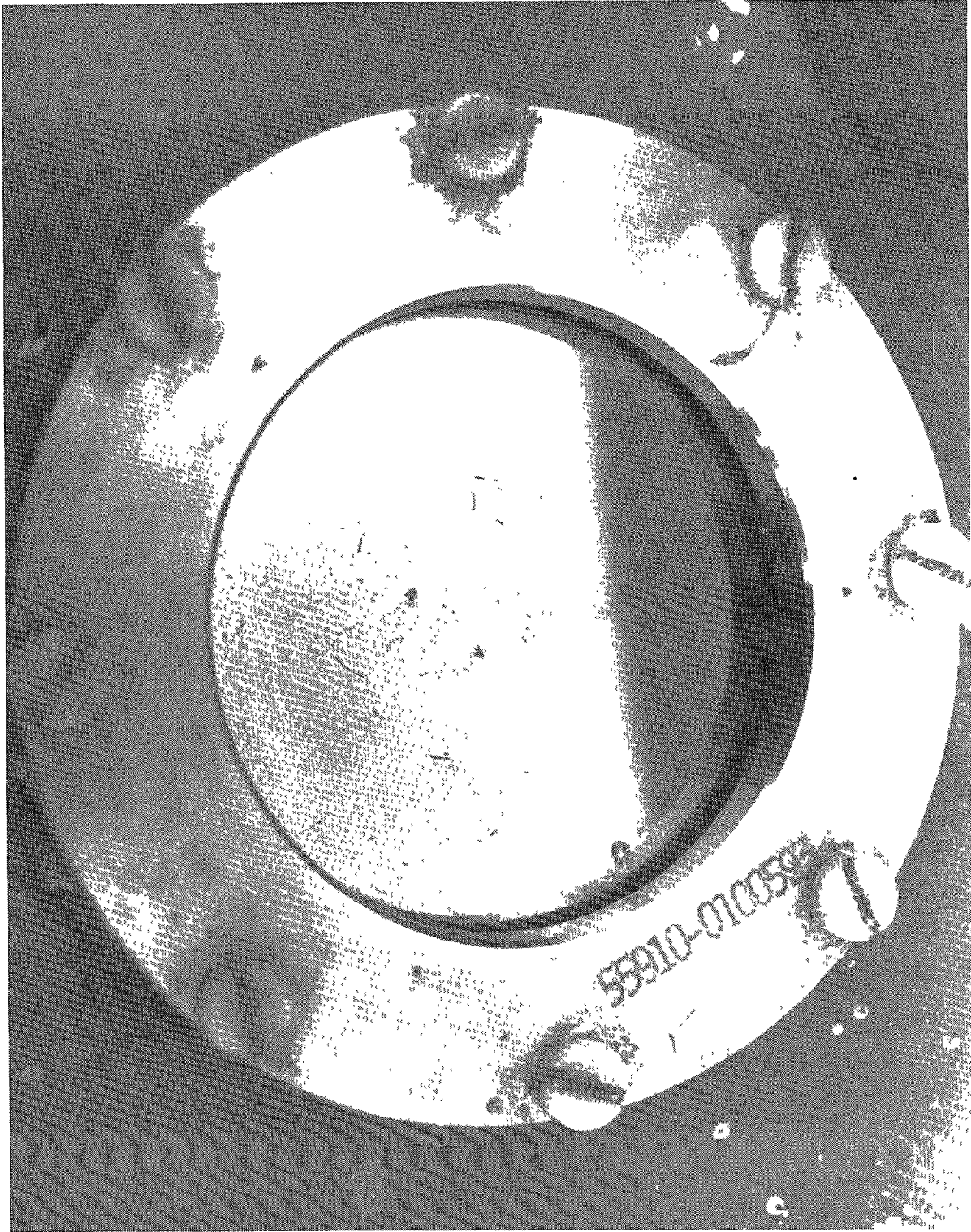


Figure 59a. Typical monolayer AR coating after 4 months of submersion. Note the presence of many fine pits.

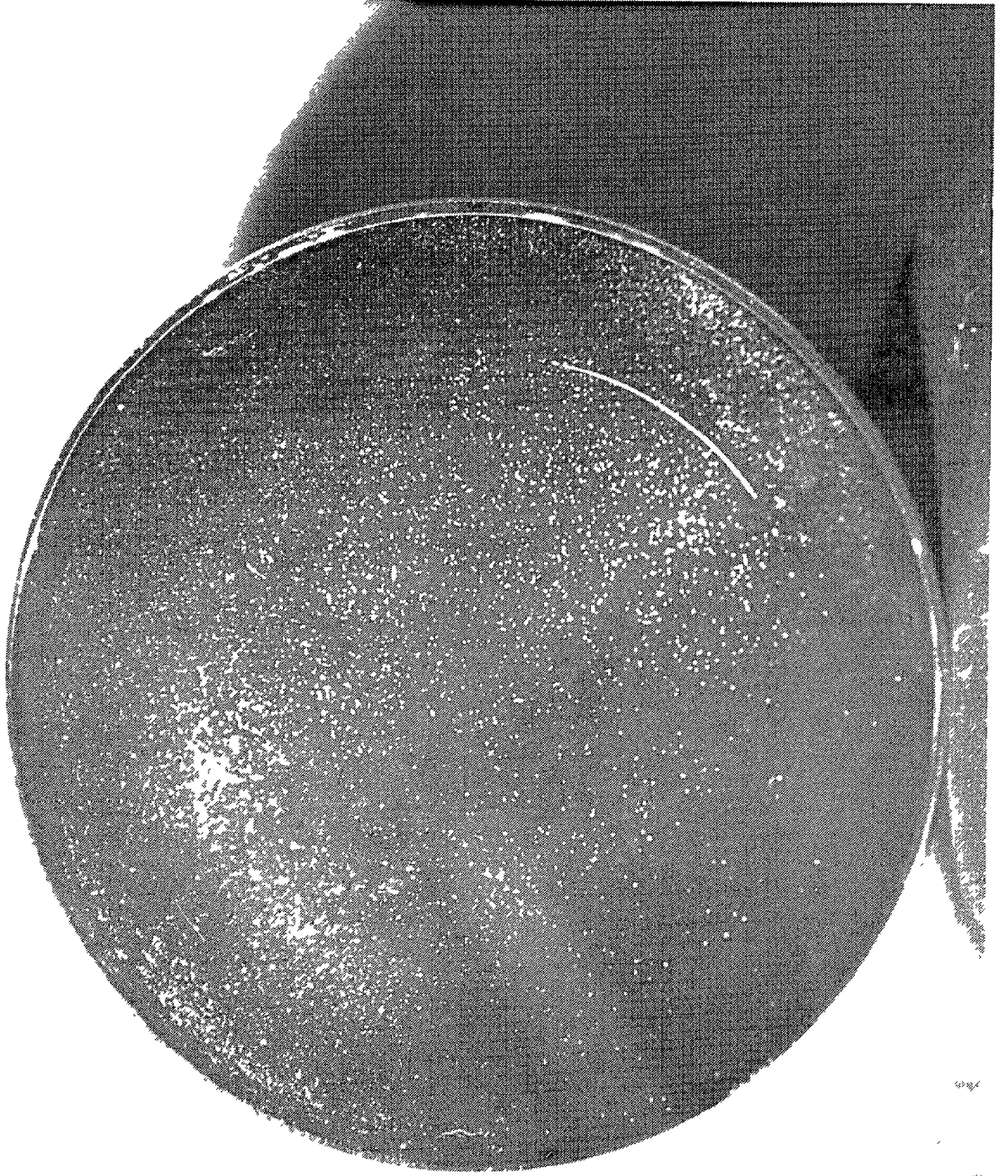


Figure 59b. Closeup of the pitted surface on coated germanium.

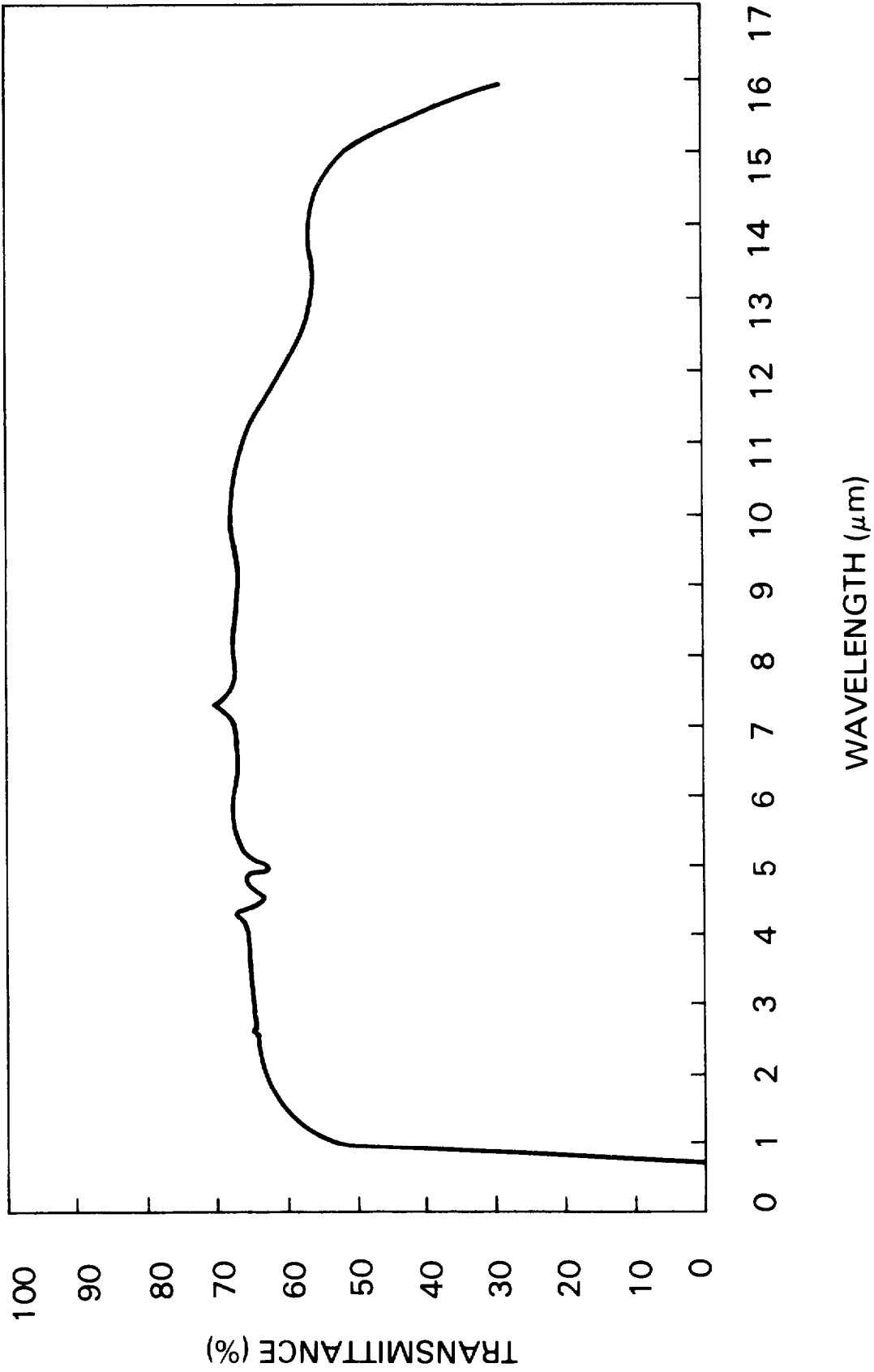


Figure 60. Transmittance of solid AMTIR-1 chalcogenide glass, 0.25 inch thick, uncoated.

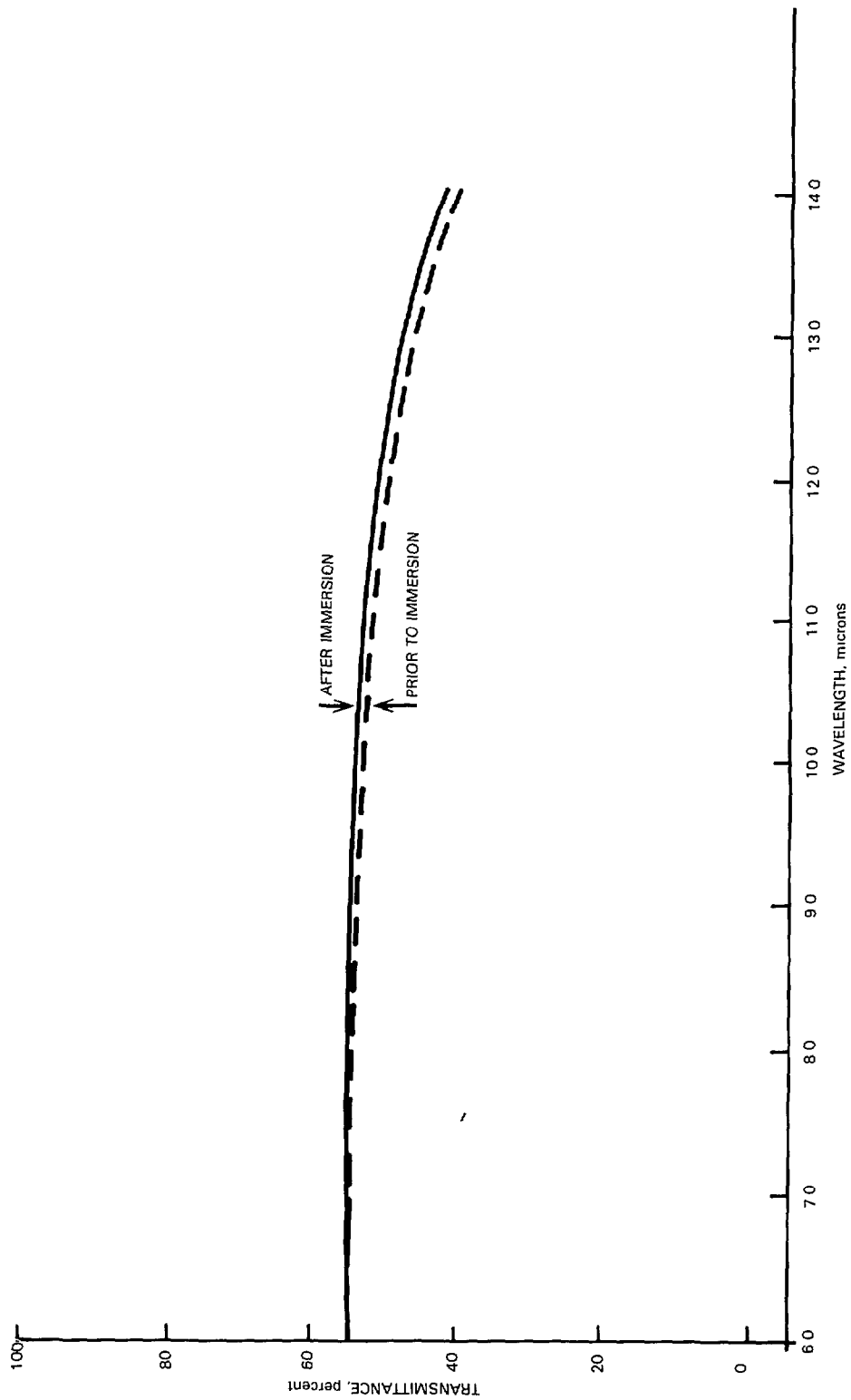


Figure 61. Transmittance of 0.25-inch-thick germanium window, coated on a single surface with 0.001-inch-thick AMTIR 1 chalcogenide glass. The coated surface was exposed to seawater for 2500 hours in San Diego Bay.

STRUCTURAL PERFORMANCE OF GERMANIUM WINDOWS

Spherical sectors are ideal shapes for germanium windows subjected to static or dynamic pressure loading as the curved shape either eliminates totally, or minimizes, the magnitude of tensile stresses in the window. Since germanium's compressive strength surpasses its tensile strength by a factor of at least three, the elimination of tensile stresses allows germanium sectors to be subjected to significantly higher pressures than they could be otherwise.

Static pressurizations of 150° spherical sector windows with $t/R_i = 0.333$ did not generate any incipient or catastrophic failures in germanium even though the peak compressive stress in the windows was in excess of 62 000 psi. The absence of cracks after cyclic application of 62 000-psi compressive stress indicates that the low-cycle compressive fatigue strength is in excess of 50 000 psi. The actual magnitude of cyclic fatigue strength for a life of 100 cycles is not known since none of the windows failed. Based on the short-term compression strength data, however, one can make a conservative estimate of this value, which in all probability is in the range of 60 000 to 70 000 psi for 100 cycles, and 50 000 to 60 000 psi for 200 cycles.

Since other studies (ref 20) conducted by the author show that the cyclic fatigue life of spherical sectors with identical dimensions fabricated from glass is approximately the same as that of spherical sectors made from germanium, inexpensive glass windows may be substituted for expensive germanium windows in test programs that have as their objective the structural evaluation of IR window designs under static pressure loading. The only drawback of using glass instead of germanium in the structural models is that because of the difference in moduli of elasticity between glass and germanium (9×10^6 versus 13.5×10^6), the deflections and displacements of glass windows will be somewhat larger than of germanium windows.

This difference in displacements may influence the magnitude of stresses in the bearing surfaces of the window during pressure testing, as the metallic seat would have been designed to match the displacements of the operational germanium window and not of the structural glass model. In those cases where the displacements of the structural test model must match those of the operational germanium window, glass ceramic should be substituted for glass as the moduli of elasticity for glass ceramic and germanium are approximately the same. Tests with structural models of windows fabricated from Cervit C-101® have confirmed that the strains and displacements measured on the glass ceramic window correspond closely to those measured on germanium.

There are, of course, other glass ceramic compositions besides Cervit C-101 with moduli of elasticity in the 13-to-15 $\times 10^6$ -psi range; however, their moduli of rupture (flexural strength) and compressive strength may be significantly higher than those of germanium. Testing of structural models fabricated from glass ceramics with higher moduli of rupture and/or compressive strengths than germanium tends, in general, to generate data which mislead the designer into thinking that the structural performance of the germanium window will equal that of the glass ceramic model, while in reality it will not. For this reason, it is preferable to use glass instead of glass ceramic in the fabrication of structural models. The deviation in magnitude of displacements generated by structural models

®Registered trademark, Owens-Illinois Glass Co.

fabricated from lower-modulus glass are less critical to the experimental evaluation of the window design than the deviation in cyclic fatigue life displayed by structural models fabricated from higher-strength glass ceramic.

Dynamic pressurizations of the 150° spherical sector windows with $t/D_1 = 0.333$ resulted in the fracture of all windows tested. The magnitude of dynamic overpressure which causes the window to fracture at 450 psi ambient static pressure varied from 1100 to 2250 psi. The magnitude of critical dynamic overpressure represents only a 5 to 10-percent fraction of the estimated critical static pressure. Although the ratio between the critical dynamic and static pressures of germanium windows in the shape of spherical sectors is rather low, it is typical of all windows fabricated from brittle materials with intrinsic low tensile strength.

Test data from other studies, for example, show that the critical dynamic pressures of spherical sectors with dimensions identical to the ones used in this study, but fabricated from BK-7 borosilicate crown glass, represent also only 10 percent of their static critical pressure (ref 6). The fact that the critical dynamic pressures of germanium windows are approximately of the same magnitude as those of glass windows of identical dimensions is a very valuable finding, as it allows substitution of the much less expensive glass windows for germanium windows also in the test programs where the resistance of germanium windows to dynamic overpressures is being investigated. Some of the glass ceramics also could be used for construction of structural models; however, the test results would be misleading, as the critical dynamic pressures of most windows made from glass ceramic compositions would be higher than if they were made from glass or germanium, since the modulus of rupture for most glass ceramics is significantly higher than that of glass or germanium.

DESIGN RECOMMENDATIONS

DESIGN STRESSES

Although the measured average short-term flexure strength in tension for germanium is 11 500 psi, the effects of surface scratches, chips, and corrosion pits and of static or cyclic fatigue can lower it to the 5000–6000-psi level. For this reason, it is considered prudent to have the magnitude of maximum tensile design stress in a germanium window not exceed 1000 psi. The value of maximum tensile stress may be increased to 2000 psi if the window is not subjected to constant loading of long duration, or a high number of load cycles; and if the surface in tension is protected from scratches or corrosive attack of seawater by appropriate coatings. In applications where the window has to survive only a single loading of short duration (for example, in a missile), the maximum tensile stress may be increased to 4000 psi.

Because the measured short-term compressive strength of germanium is in the 40 000 -to-80 000-psi range, and because the static and cyclic fatigue as well as the surface scratches do not exert as large an effect on the strength as in flexure, the maximum design stress in compression can be significantly higher than in flexure. For windows which will see extended sustained loading and/or a large number of loading cycles at maximum design stress, the value of this stress should not exceed 10 000 psi. For applications where the windows will not see extended sustained loadings and/or a large number of cyclic loadings at maximum design stress level, the value of maximum design stress can be safely increased to 20 000 psi. In applications where the window has to survive only a single loading of short duration,

(for example, in a missile), the maximum compressive design stress may be increased to 40 000 psi.

That such high design stress values are feasible was proven by the testing of spherical sectors in this study; no failure took place even though the peak compressive stress was approximately 60 000 psi and the 100 cyclic load applications were each of 4-hour duration. However, this was made feasible only by meticulous attention to bearing surface finish, dimensional and angular tolerances, and proper seat design.

WINDOW DESIGN

Unless operational requirements absolutely forbid it, the windows should always assume the shape of a spherical sector with the included spherical angle in the 30-to-330° range. In cases where the thickness of the window is to be optimized, the spherical included angle must be limited to only the 140–160° range as experiments with glass and plastic spherical sectors have shown that sectors with included angles in that range can withstand higher bearing stresses without cracking than sectors with any other angle.

The bearing surfaces on spherical sectors must be normal to the spherical surfaces. The edges of the bearing surface shall terminate in large, smooth chamfers (0.020–0.040 inch), since it is known that the inner edge of the sector is never under high compressive stress, and is sometimes even under low tensile stress. Unless the chipped and nicked sharp corner on brittle germanium is eliminated by chamfering prior to loading, the nicks and chips will act as stress risers that may, even at a very low tensile stress level at that location, initiate fracture of the bearing surface.

The dimensional, angular, and surface-finish tolerances imposed on the bearing surface of the window must of necessity be tight to preclude the presence of stress risers in the form of point or line contacts between the mating bearing surfaces on the window and the seat. Special attention must be paid to the finish on the bearing surface, as the radial component of stress on that surface is generally of tensile nature. Besides grinding this surface with progressively finer compounds, the final operation following grinding with a 9-micron compound is chemical etching. The etching ensures that the tips of microcracks generated by grinding are rounded out, thus significantly decreasing their stress riser effect.

MOUNTINGS

Mountings for IR windows under external pressure must meet the same design criteria as mountings developed successfully in the past for glass or ceramic structural components under external pressure loading (ref 17). These criteria are rather straightforward, but failure to heed them invariably leads to premature fracture of any brittle window. The criteria can be summarized in two statements:

1. The radial dilation, or contraction of the seat on the mounting under the combined actions of the pressurized window, the hydrostatic pressure, and the pressurized housing, should be uniform all around its circumference.
2. The radial dilation or contraction of the window circumference and the rotation of the window's bearing surface should be matched by the radial dilation or contraction and the angular rotation of the seat on the mounting.

In practice, it is impossible to meet both criteria completely. Thus every mounting design is only an imperfect attempt to meet these ideal criteria. If compromises have to be

made, it is best that they be made in the realm of matching the radial contraction or dilation of the window to that of the mounting, and not in the realms of uniform radial displacement or excessive angular rotation of the mounting. Unless the design stresses are set excessively high, the compliant elastomeric gasket between the mating surfaces will take care of minor angular or diametrical displacements of the seat relative to the window's bearing surface under hydrostatic loading.

There are additional requirements placed on mountings when they are subject to hydrodynamic forces and shock forces such as drag, lift, or wave slap. Thus the mountings must be rigid enough to prevent the window from shifting or being detached by these nonuniform forces, and yet must not generate significant tensile stresses in the windows under these conditions as well as under hydrostatic loads.

There are two practical techniques currently in use to satisfy these requirements. These are: (1) semirigid mounting and (2) compliant mounting. In the first case, the window is mechanically affixed to the sensor housing, so that the window and housing are rigidly connected. The common method is to place the window in a prepared oversized recess in the housing and to fill the space between the window and the mounting with casting epoxy or silicone rubber. This method is acceptable for simple shapes, such as flat or cylindrical windows exposed to low hydrostatic pressure. A major shortcoming is the difficulty experienced in removing the window for refurbishment or replacement.

The second technique is based on a compliant mounting and is more satisfactory for higher pressures, more complex window shapes (eg, hyperhemispheres), and for window refurbishment. As the term 'compliant' implies, the mounting allows the window and housing to deform independently while maintaining a watertight seal and minimizing tensile stresses. The mating bearing surfaces of the window and mounting are allowed to slide with respect to one another, with a compliant gasket distributing the bearing loads. Figure 62 illustrates one method for achieving the desired compliance, in this case for a hyperhemispherical window (ref 21). The mounting employs a conical seat and elastomeric O-rings to both seal and retain the window in place. Because highly compressed elastomeric O-rings exert considerable, but uniform, bearing pressure against the exterior and interior surfaces of the window, it is held securely against the seat of the mounting without the generation of local stress concentrations in the window. In addition, the compliance of the O-rings and bearing gasket allows for differential expansion or contraction between the window and the mounting as the result of static pressure, hydrodynamic drag, wave slap, or temperature variations, without generation of stresses in the window. The presence of compliant barriers in the form of O-rings and bearing gaskets between the window and the mounting also serves as a shock absorber against high-frequency vibration of the housing generated by vortex shedding, wave slap, or ship's engines. It should be noted that even in a compliant mounting with a conical seat, the magnitude of compressive stresses across the bearing surface of the window varies significantly. However, without the conical seat and compliant mounting, the peak stress would be significantly higher and probably cause the window to fail at a much lower hydrostatic loading. Figure 16 illustrates a compliant mounting, but in this case for a spherical sector window. The basic difference between this mounting and the one for hyperhemispheres is that the retaining ring is located on the exterior instead of the interior of the window. Because of its exterior location, the retaining ring generates only compressive stresses in the window and thus can be clamped down tighter than the interior retaining ring in hyperhemispheres, where tensile stresses are generated in the window during tightening of the retaining ring. The compliant mountings shown in figures 16 and 61 already have been successfully used with plastic, glass, and germanium windows.

SEALING

The marine environment imposes one condition more extreme than that experienced by IR sensors in aerospace applications—exposure to moisture. It is well known that optical systems are very intolerant of even minor amounts of moisture. Moisture can fog lenses, corrode precision parts, and eventually make a sensor inoperable. IR systems are equally vulnerable, so that the window and housing must be completely sealed from the external seawater. All sealing configurations for marine applications must be compliant. Only in this manner can the seal be maintained during differential expansions and contractions resulting from pressure, temperature changes, or external forces. The three major categories of seals are cast-in-place seals, compressed gaskets, and O-rings. The cast-in-place seal can be an epoxy or a silicone rubber compound which is poured into the bearing interface area and allowed to cure. This type of seal depends primarily on adhesion to the window and housing surfaces and is therefore useful only for relatively low external pressure.

Compressed gaskets are fabricated from cured elastomeric materials, usually synthetic rubber. The gasket is cut so as to conform to the two mating surfaces and is subsequently clamped in place by mechanical means. The advantages over cast-in-place seals include resistance to higher pressures, the ability to remove and refurbish the window, and relative ease of duplicating performance with identically designed gaskets. The primary drawback of a gasket seal is that, for the seal to function properly, the retaining ring must be clamped very tightly. Otherwise, the gasket will not be properly precompressed.

The O-ring seal is widely recognized as a modern, cost-effective, and reliable sealing technique for a wide range of pressures. A large variety of O-ring thicknesses and materials is commercially available. For the O-ring seal to function properly, the IR system designer must match the size of the O-rings to the grooves in the mounting and use a clamping arrangement which retains the window against the housing. As can be seen in the mounting for hyperhemispherical windows (figures 62 and 63), this may involve O-rings which are sandwiched between the clamp and the window as well as between the window and the housing. Such a seal design eliminates high point loading and resultant tensile stresses which might fracture the window during tightening of the retaining ring. In the design of the grooves for O-rings, care must be taken in providing adequate restraint for the window without the generation of unacceptable tensile stresses in the window. The peak stresses generated on the interior surface in the meridional direction by tightening the split retaining ring against the internal O-ring seal should be kept below 500 psi so that no opportunity is presented for microcracks to grow larger. The advantages of O-ring seals include improved repeatability of performance, tolerance to higher pressure, and commercial availability of replacement seals.

CONCLUSION

A number of thermal imaging systems are currently being operated successfully in the marine environment. In designing such systems, it is necessary to select a window material that has the proper mechanical characteristics so that it can protect the thermal imager components from a hostile external environment and also satisfy the optical criteria of IR transmittance, high refractive index, and thermal stability. Polycrystalline germanium and chalcogenide glass are two materials which meet these criteria (ref 14). Of these two,

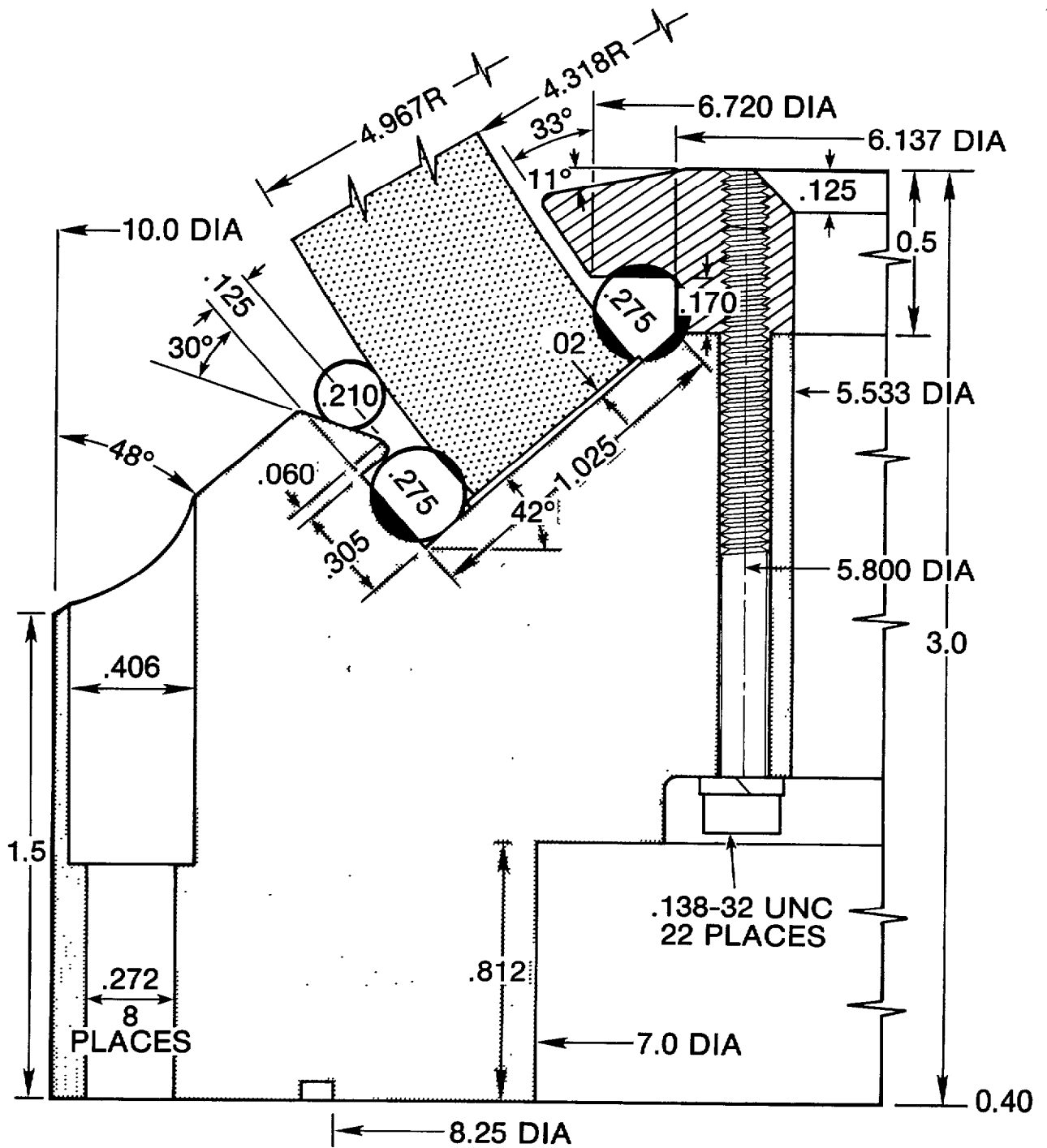


Figure 62. Compliant mounting design for brittle windows of hyperhemispherical shape subjected to (1) static and dynamic pressure loading; (2) vertical and transverse vibration; and (3) lateral impact; rated for 10 000-psi service when fabricated from Ti-6Al-4V alloy.

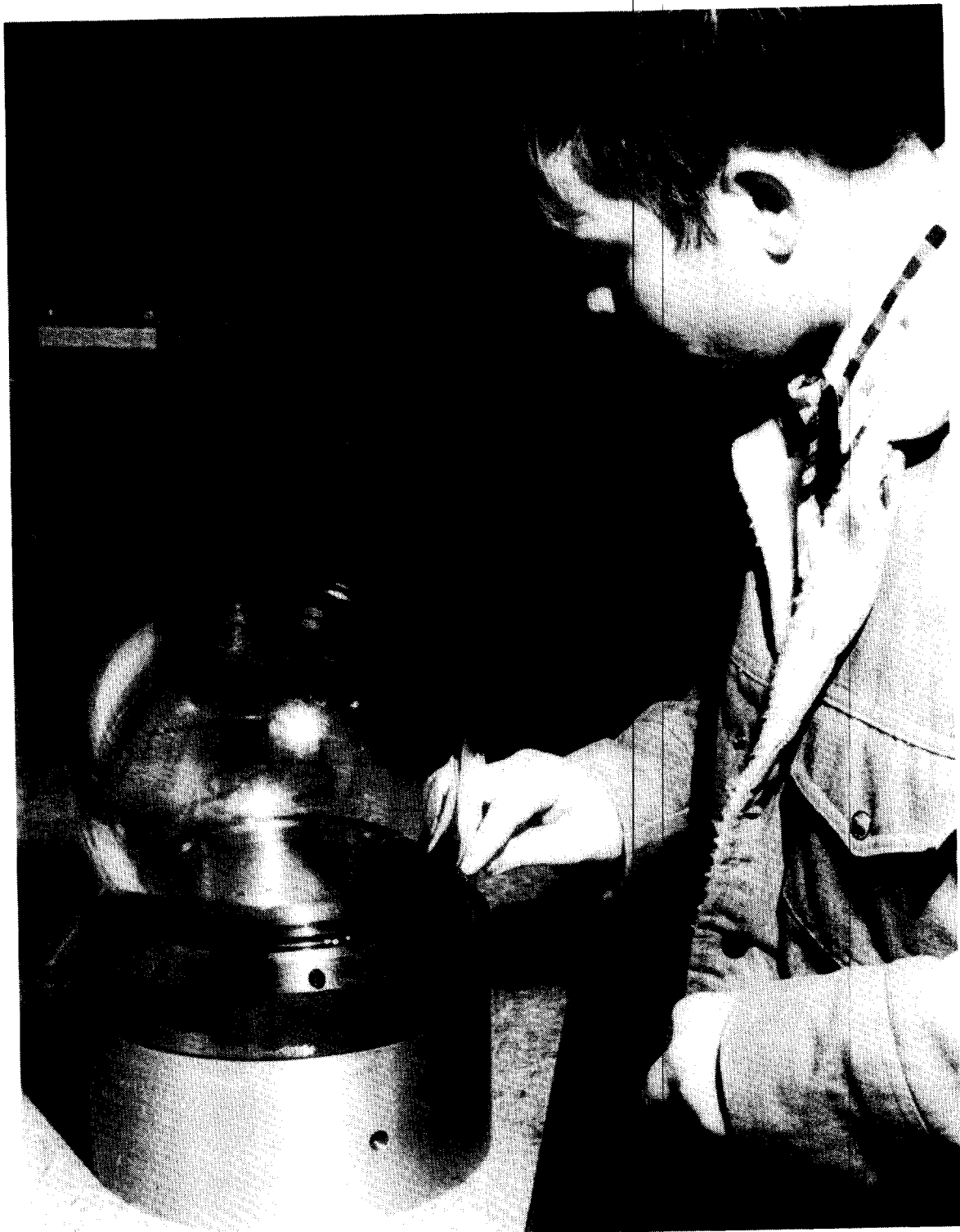


Figure 63. Hyperhemispherical window in a compliant mounting. The mounting has been tested with a glass window to 10 000-psi hydrostatic pressure.

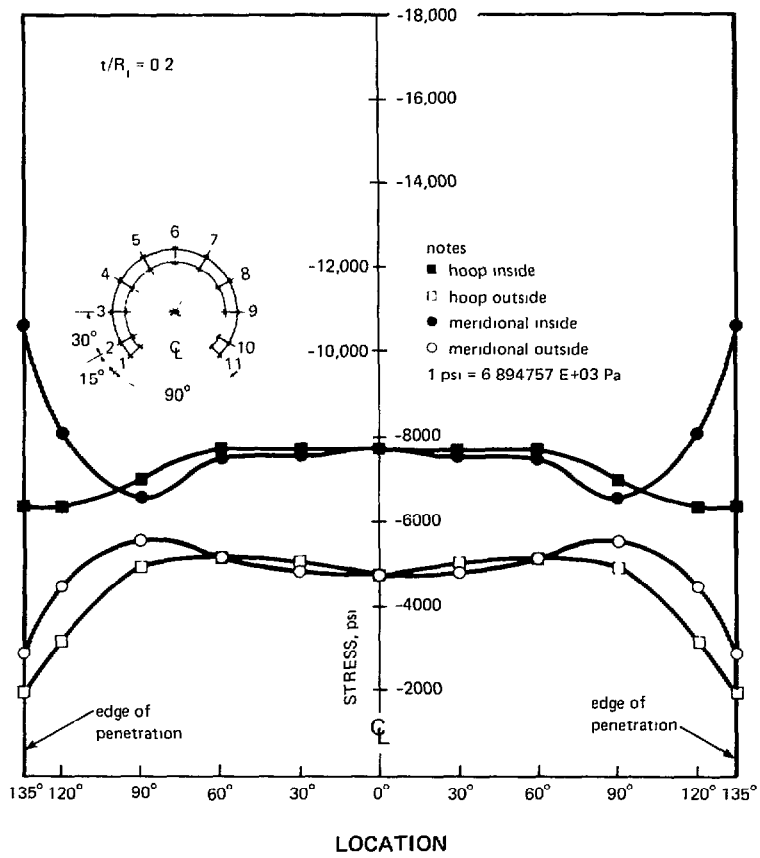


Figure 64. Distribution of stresses on the interior surface of the hyper-hemisphere shown in figure 62 under short-term pressurization of 2000 pounds per square inch (13.7 mPa) at ambient room temperature.

germanium is the most frequently selected window material, partially as a result of fabrication experience developed by IR window manufacturers. Once the material has been selected, care must be taken in designing an IR window mounting which minimizes tensile stresses as well as seals the imager from the surrounding seawater when the system is subjected to hydrostatic pressure and wave impact. Coating materials and application techniques must also be selected which will reduce the reflectance of the window and which will provide protection against chemical corrosion in seawater. If the imaging system is to be subjected to arctic marine conditions, provision must also be made to heat the window and prevent icing up. Otherwise, even a thin layer of ice can seriously impair the optical performance. However, if proper design procedures are followed, germanium windows can be designed and fabricated that will successfully perform in the marine environment from the ocean surface to abyssal depths.

To date, the only part of the IR window assembly for ocean environment that is less than satisfactory is the optical coating on the exterior surface. Durable antireflection coatings, as exemplified by Exotic Materials multilayer 40100, provide germanium with transmission of 92 percent in 8-to-10-micron-wavelength range, but even they deteriorate under continuous submersion in excess of 6 months duration. Furthermore, it is doubtful whether a multilayer AR coating may ever be developed that will extend the length of protection against corrosive action of seawater past 6 months.

There are, however, two new exciting developments that may provide a significant improvement in coating durability. The new coatings are chalcogenide glass and carbon. Either of those coatings, if properly applied, may provide protection in excess of a year. It is hoped that their development will proceed at a rapid pace and will culminate in a series of reliable coatings with proven long-term durability in the marine environment under continuous or intermittent wetting by seawater.